GA Technologies

GA-A17842

Final Report

INERTIAL CONFINEMENT FUSION REACTION CHAMBER AND POWER CONVERSION SYSTEM STUDY

by
I. MAYA, K. R. SCHULTZ, and PROJECT STAFF

Work supported by
Lawrence Livermore National Laboratory
Subcontract 2632605 under
Department of Energy Contract No. W-7405-ENG-48

OCTOBER 1985

GA Technologies

UCRL--15750

DE86 006725

Final Report

INERTIAL CONFINEMENT FUSION REACTION CHAMBER AND POWER CONVERSION SYSTEM STUDY

by

I. MAYA
K.R. SCHULTZ
R.F. BOURQUE
E.T. CHENG
R.L. CREEDON
J.H. NORMAN
R.J. PRICE
J. PORTER
H.L. SCHUSTER
M.T. SIMNAD*
D.L. SONN
ING TANG
R.K. WISE

Work supported by
Lawrence Livermore National Laboratory
Subcontract 2632605 under
Department of Energy Contract No. W-7405-ENG-48

*University of California, San Diego

GA PROJECT 3400
OCTOBER 1985

DISCLAIMER

Abstract

This report summarizes the results of the second year of a two-year study on the design and evaluation of the Cascade concept as a commercial inertial confinement fusion (ICF) reactor. We developed a reactor design based on the Cascade reaction chamber concept that would be competitive in terms of both capital and operating costs, safe and environmentally acceptable in terms of hazard to the public, occupational exposure and radioactive waste production, and highly efficient. The Cascade reaction chamber is a double-cone-shaped rotating drum. The granulated solid blanket materials inside the rotating chamber are held against the walls by centrifugal force. The fusion energy is captured in a blanket of solid carbon, BeO, and $LiAlO_2$ granules. These granules are circulated to the primary side of a ceramic heat exchanger. Primary-side granule temperatures range from 1285 K at the $LiAlO_2$ granule heat exchanger outlet to 1600 K at the carbon granule heat exchanger inlet. The secondary side consists of a closed-cycle gas turbine power conversion system with helium working fluid, operating at 1300 K peak outlet temperature and achieving a thermal power conversion efficiency of 55%. The net plant efficiency is 49%. The reference design is a plant producing 1500 MW of D-T fusion power and delivering 815 MW of electrical power for sale to the utility grid.

The Cascade plant possesses many inherent (passive) safety features which may avoid the need for nuclear-grade systems and components and dedicated safety systems, may allow use of conventional construction methods, and may prevent public exposure doses above regulatory limits or reactor damage during postulated accident events. The capital cost of the Cascade plant with conventional construction is \$1500M (\$1800/kWe), resulting in a Cost-of-Electricity (COE) of 34 mills/kWe-hr. The capital cost of the Cascade plant with nuclear-grade construction and component qualification would be \$1900M (\$2400/kWe), resulting in a COE of 41 mills/kWe-hr. In either case, these costs are competitive with the 37, 40, and 49 mills/kWe-hr costs for LWR, HTGR, and coal plants calculated using the same economic groundrules.

Contents

Figures

1. EXECUTIVE SUMMARY

1.1. INTRODUCTION

This report summarizes the results of the second year of a two-year study on the design and evaluation of the Cascade concept as a commercial inertial confinement fusion (ICF) reactor. (Ref. 1-1, 1-2) The Cascade concept involves the use of a rotating reaction chamber within which the ICF pellet blasts occur. Granular solid blanket material, held against the walls by the centrifugal force of rotation, flows along the walls and captures and transports the fusion energy out of the chamber to the power conversion system. A conceptual design of the Cascade reaction chamber is shown in Fig. 1-1. The goal of this study was to develop a reactor design based on the Cascade reaction chamber concept that would be inexpensive in terms of both capital and operating costs, safe and environmentally acceptable in terms of hazard to the public, occupational exposure and radioactive waste production, and highly efficient. Specifically, GA Technologies Inc. (GA) accomplished the following tasks:

- Developed a number of high-temperature solid breeder blanket concepts, evaluated the thermodynamic performance of each and recommended a reference blanket.
- Explored power conversion system options available to Cascade, examined the tradeoffs of efficiency versus simplicity and cost, and developed in detail the most suitable secondary system design.
- Developed the conceptual design of a ceramic heat exchanger capable of operating at temperatures consistent with the high temperature potential of ceramic blanket materials.
- Evaluated the tritium inventory and permeation associated with the reference

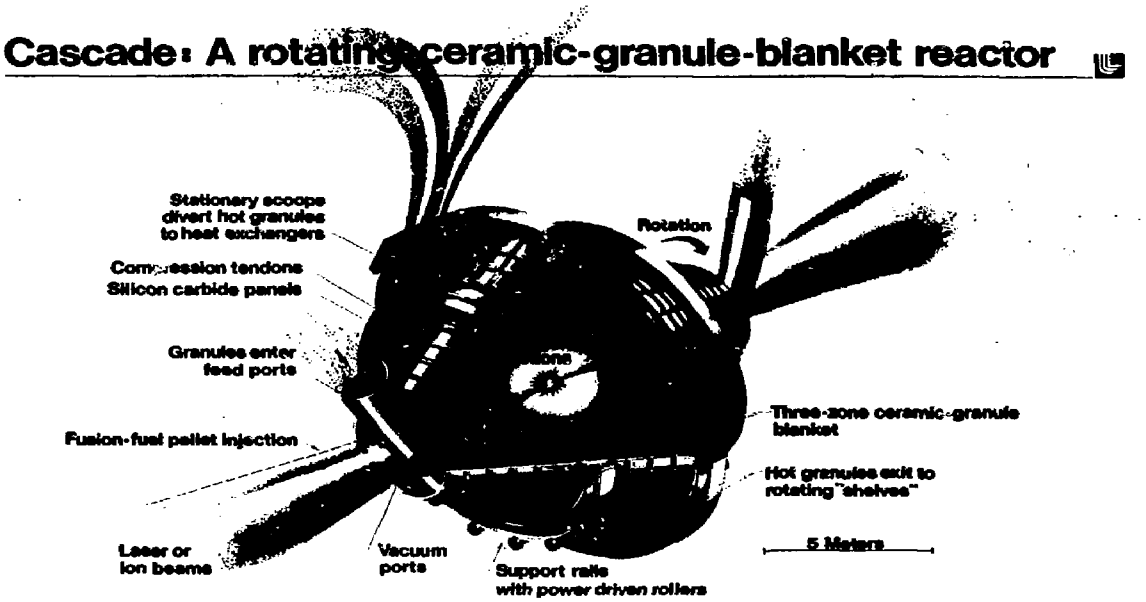

Fig. 1-1. Cascade: A rotating ceramic-granule-blanket reactor.

solid breeder ($LiAlO_2$) blanket, and recommended a tritium recovery system.

- Performed activation analysis of the Cascade plant.
- Performed Balance-of-Plant studies consisting of component and system specifications, safety assessments, and plant capital and operating costs estimates.

The results of this effort are summarized below.

1.2. SUMMARY AND CONCLUSIONS

Cascade ICF Power Plant Design Summary

An overall power flow diagram for the Cascade ICF power plant is shown in Fig. 1-2. The reference design parameters are summarized in Table 1-1. The reference design is a plant producing 1500 MW of D-T fusion power and delivering 815 MW of electrical power for sale to the utility grid. The fusion energy yield is captured in a blanket of solid carbon, BeO, and $LiAlO_2$ granules. These granules are circulated to the primary side of a ceramic heat exchanger. Primary-side granule temperatures range from 1285 K at the $LiAlO_2$ granule heat exchanger outlet to 1600 K at the carbon granule heat exchanger inlet. The secondary side consists of a closed-cycle gas turbine power conversion system with helium working fluid, operating at 1300 K peak outlet temperature and achieving a net thermal power conversion efficiency of 55%. The net plant efficiency is 49%.

The Cascade plant possesses many inherent (passive) safety features (see subsection below) which may avoid the need for nuclear-grade systems and components and dedicated safety systems, and may allow conventional (fossil plant) construction methods. The capital cost of the Cascade plant with conventional construction is \$1500M (\$1800/kWe), resulting in a Cost-of-Electricity (COE) of 34 mills/kWe-hr. It is possible that future safety analysis of the Cascade plant or more stringent licensing guidelines may result in additional safety requirements or nuclear qualification of

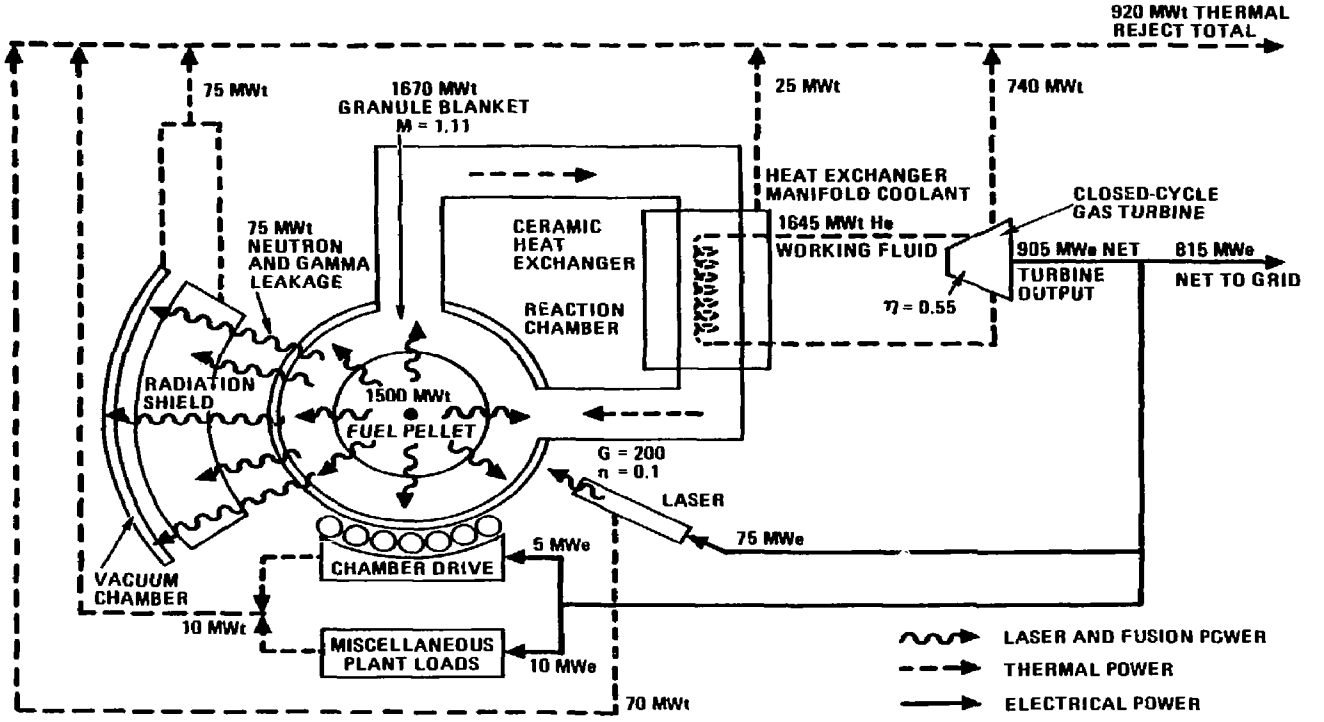

Fig. 1-2. Schematic of fusion-to-electrical power flow.

TABLE 1-1
CASCADE ICF POWER PLANT
REFERENCE DESIGN PARAMETERS

Power Balance	
Fusion Power	1500 MWf
Thermal Power	
Blanket Thermal Power	1670 MWt
Turbine Thermal Power Input	1645 MWt
Electrical Power	
Net Turbine Electrical Output	905 MWe
Total Station Electrical Demand	90 MWe
Net Electrical Output	815 MWe
Net Plant Efficiency	49%
Primary Granule Loop	
Surface Layer	
Material	C
Thermal Power	460 MWt (28%)
Inlet Temperature	1500 K
Outlet Temperature	1600 K
Front Zone	
Material	BeO
Thermal Power	220 MWt (13%)
Inlet Temperature	1410 K
Outlet Temperature	1505 K
Breeder (Back) Zone	
Material	$LiAlO_2$
Thermal Power	990 MWt (59%)
Inlet Temperature	1285 K
Outlet Temperature	1355 K
Power Conversion System	
Type	Closed Cycle Gas Turbine
Coolant	Helium
Number of Loops	1
Pressure	5.0 MPa
Inlet Temperature	960 K
Outlet Temperature	1300 K
Net Thermal Conversion Efficiency	55%
Capital Cost	
Conventional	\$1500M (\$1800/kWe)
Nuclear+Conventional	\$1900M (\$2400/kWe)
Operating Cost	
Conventional	34 mills/kWe-hr
Nuclear+Conventional	41 mills/kWe-hr

Cascade equipment. The capital cost of the Cascade plant with nuclear-grade construction and component qualification would be $1900M ($2400/kWe), resulting in a COE of 41 mills/kWe-hr. In either case, these costs are competitive with the 37, 40, and 49 mills/kWe-hr costs for LWR, HTGR, and coal plants calculated using the same economic groundrules. Individual features of the Cascade plant are summarized in the following subsections.

High-Temperature Blanket Design Options

A characteristic of deuterium-tritium inertial confinement fusion is that a large fraction of the energy, typically ~30%, is in the form charged particles, reflected laser light, and x rays which results in an intense surface heat flux. The balance of the energy is in the form of neutrons and results in volumetric heating. The Cascade reaction chamber concept is ideally suited to couple with this characteristic in that a thin, fast-moving surface layer of high-temperature (>1500K) material can be used to absorb and transport the surface heat flux, and a thicker, slower-moving blanket of high-temperature and/or tritium-breeding material can be used to absorb and transport the neutron energy. The high-temperature material can then be used to achieve very high power conversion efficiency (55%) while still allowing for adequate tritium breeding.

In this work, we developed a number of high-temperature blanket design options available to the Cascade concept. We surveyed the low activation, high-temperature material options for the surface layer in terms of mechanical properties for thermal stress resistance, irradiation stability and fabricability into granules suitable for Cascade, and selected carbon, beryllium oxide, beryllium carbide and silicon carbide as the most suitable materials. Additional considerations of surface layer evaporation and recondensation indicated that the surface layer may have to be composed strictly of elemental material, most notably carbon, for adequate chamber evacuation between fusion shots. We determined material temperature limits based on compatibility of the surface layer with Li_2O and $LiAlO_2$ tritium breeder, and with the chamber and heat

exchanger materials. We then coupled the results of these analyses with the nucleonic performance of candidate material combinations to calculate the power-producing potential of selected blanket designs. The analysis indicated that a high-temperature material front zone between the surface layer and the tritium breeder would act as a buffer zone between the two materials, allowing higher surface layer temperatures, higher [illegible] conversion efficiency, and thus further improvment in blanket performance. Thus, we selected the BeO/BeO/$LiAlO_2$ and C/BeO/$LiAlO_2$ blankets, where the notation here refers to the surface layer/front zone/tritium breeder materials, as reference designs in subsequent secondary system design and tritium analyses. These blankets offer comparable performance. Their design parameters are shown in Table 1-2.

Other prime blanket material combinations available to Cascade are:

- C or BeO surface layer, BeO front zone, $LiAlO_2$ tritium-breeder,
- C or SiC surface layer, SiC front zone, Li_2O tritium-breeder, and
- C or SiC-coated Be_2C surface layer, SiC-coated Be_2C front zone, $LiAlO_2$ tritium-breeder.

These blankets are described in Chapter 2.

Power Conversion System Design

The objectives of the power conversion system design effort were to maximize net power conversion efficiency (gross plant efficiency) while maintaining simplicity and low cost. Two power cycles were explored for application to Cascade: the regenerative Brayton cycle using helium, and the Field cycle using steam. We found that with the Cascade blanket delivery temperatures, a simple once-through Brayton cycle with no reheats gives an efficiency of 55%. Furthermore, this efficiency is achieved with 1300 K peak helium temperature. The low helium temperature relative to the ceramic granule primary side temperature also eases heat exchanger design by allowing large driving temperature differentials.

TABLE 1-2
REFERENCE DESIGNS OF THE
BeO/BeO/$LiAlO_2$ AND C/BeO/$LiAlO_2$ BLANKETS

	BeO/BeO/$LiAlO_2$	C/BeO/$LiAlO_2$
Fusion power, MW	1500	1500
Blanket power, MW(t)	1670	1670
Total $\dot{m}$, m^3/s	10.6	10.7
Surface Layer		
Power fraction	0.29	0.28
T_{inlet}, K	2100	1500
$T_{avg\ outlet}$, K	2300	1600
$\dot{m}$, m^3/s	1.0	2.2
Peak chamber exit velocity, m/s	1.9	4.4
Front Zone		
Power fraction	0.13	0.13
T_{inlet}, K	1435	1410
$T_{avg\ outlet}$, K	1505	1505
$\dot{m}$, m^3/s	1.3	1.0
Peak chamber exit velocity, m/s	0.25	0.22
Breeder Zone		
Power fraction	0.58	0.59
T_{inlet}, K	1325	1285
$T_{avg\ outlet}$, K	1385	1355
$\dot{m}$, m^3/s	8.4	7.5
Peak chamber exit velocity, m/s	0.25	0.22

With the Field cycle, we adopted a modified version with dry compression, one reheat, and one extraction. It appears to have features that are worth further inquiry. Net efficiencies of 56% are achieved, also with peak steam temperatures of 1300 K. The Brayton and Field cycles match closely in terms of performance, equipment requirements and developmental needs. On the basis of perceived advantages in tritium recovery and potential for higher temperature operation, the Brayton cycle was chosen as the reference design for Cascade. Other power cycles, such as dissociating gas Brayton, supercritical CO_2 Brayton, and topping and bottoming cycles show no advantage over the Brayton and Field cycles. The Rankine cycle still is best at temperatures below 850 K, and is considered as a fallback option.

Ceramic Heat Exchanger Design

The ceramic primary heat exchanger transfers the fusion energy deposited in the high temperature granules to the helium working fluid of the closed-cycle gas turbine power conversion system. At the operating temperatures of the present blanket materials (up to 1600 K), the only functional materials for the heat exchange surface are ceramics such as SiC or Si_3N_4. To accommodate these high temperatures, the heat exchanger design of Ref. 1-2 was modified to incorporate SiC tubes. The heat exchanger design parameters for the three blanket zones are shown in Table 1-3.

The solid granules comprising the blanket flow across the ceramic tube array in a vacuum (1 Pa), in a direction cross-countercurrent to the multipass helium working fluid contained within the tubes. With the selection of a closed-cycle gas turbine for power conversion, the secondary-side working fluid pressure is 5 MPa. Thus, though the tubes are in hoop tension due to the internal helium pressure, the tensile stresses are modest (e.g., ~50 MPa in 4 cm o.d. tubes with 2 mm wall thickness) and can be accommodated while allowing adequate reserve for thermal stresses. The state-of-the-art in proof-testing of ceramic components has advanced significantly in recent years, and the small size and low stress levels in this design make this a suitable application for SiC tubes.

TABLE 1-3
CERAMIC HEAT EXCHANGER
REFERENCE DESIGN PARAMETERS

Blanket Material	C	BeO	$LiAlO_2$
Power Rating, MWt	460	220	990
PRIMARY SIDE			
Gas pressure, Pa	1	1	1
Average gas temperature, K	1550	1460	1320
Granule diameter, mm	1	1	1
Granule inlet temperature, K	1600	1510	1355
Granule outlet temperature, K	1500	1410	1285
Bed porosity	0.5	0.4	0.5
Overall granule-to-tube heat transfer coefficient, W/m^2 K	790	660	490
Log-mean temperature difference, K	220	220	220
SECONDARY SIDE			
Helium pressure, MPa	5.0	5.0	5.0
Helium inlet temperature, K	1200	1155	945
Helium outlet temperature, K	1300	1200	1155
Helium velocity, m/s	90	82	69
Total helium mass flow rate, kg/s	910	920	910
Reynolds number	1.5×10^5	1.5×10^5	7.0×10^4
Fractional pressure drop	0.0045	0.0022	0.0088
Pumping power fraction	0.023	0.022	0.018
Heat transfer coefficient, W/m^2 K	2600	2500	3000
Log-mean temperature difference (film drop), K	70	60	40
OVERALL HEAT EXCHANGER DIMENSIONS			
Heat exchange area, m^2	2600	1600	9000
Active height, m	5.1	5.5	5.7
Active width, m	15	15	20
Active tube length, m	1.0	0.5	1.5
Total number of tubes	1.8×10^4	1.9×10^4	8.2×10^4
Number of working fluid passes	6	6	5
Tube pitch, cm	7.0	7.0	4.0
Tube outside diameter, cm	5.0	5.0	2.5
Tube inside diameter, cm	4.6	4.6	2.1
Tube wall temperature difference, K	7	6	4
Granule flow area, m^2	4.3	2.1	11
Overall heat transfer coefficient, W/m^2 K	590	510	420
Overall log-mean temperature difference, K	300	280	260

The design of the heat exchanger considers that the structure must eventually revert to metal. Thus, the high pressure headers are insulated and actively cooled metal, and incorporate a practical metal-to-ceramic joint. Metal wall temperatures are 700 K, allowing the use of low cost carbon steels, and the seal temperature is below 500 K, allowing a seal life of 30 years. A low-stress ceramic boundary wall separates the granules from the metallic wall and protects the structural members from abrasion and heat. This configuration avoids extremely complex or highly stressed ceramic components, enhancing manufacturability. The cooled, straightforward polymeric seal at the joint appears practical. The end of the tube is ground to accept the O-ring seal. The venturi serves to reduce the structural and seal cooling load by providing a region for insulating material. The total heat loss rate into the heat exchanger manifold coolants is 25 MW.

Capital and Operating Costs

Capital cost estimates for the Cascade ICF power plant are presented in the two digit summary format on Table 1-4. Capital costs are dependent on the classification of the construction and equipment used in the plant design as dictated by regulatory guidelines. The capital cost estimates are presented for an "All Conventional" Cascade, constructed using well established, conventional fossil power plant construction methods, and requiring no nuclear-classified equipment or systems, and for a "Nuclear+Conventional" Cascade design constructed using a combination of fossil and fission reactor plant methods and standards, which includes a combination of nuclear and non-nuclear grade systems similar to that found in modern fission reactor plants. The total capital requirements for the "All Conventional" construction plant were estimated to be \$1490M, or \$1820/kWe. The "Nuclear+Conventional" construction plant was estimated to be \$1940M, or \$2380/kWe. The resultant savings of \$450M (\$560/kWe) represents strictly the difference between a Cascade ICF power plant designed and constructed to include equipment and systems that are nuclear safety-rated versus a plant whose equipment and systems are all non-nuclear

TABLE 1-4
Preliminary Capital Cost Summary
Equilibrium Cascade Plant
($M, 1/85 Constant Dollars)

Acc. No.	Description	COST			
		Nuclear + Conventional			
		Nuclear	Conv.	Total	All Conv.
20	Land & Land Rights	(included in Owner's Cost)			
21	Structures & Improvements	65	19	84	37
22	Reactor Plant Equipment	283		283	254
23	Turbine Plant Equipment	184		184	156
24	Electric Plant Equipment	44	26	71	47
25	Reactor Maint. Plant Equip.	7	9	16	12
26	Heat Rejection System		22	22	22
27	Laser Plant Bldg. & Equip.		275	275	275
28	Fuel Pellet Fabrication Plant	100		100	100
	TOTAL DIRECT COST	683	351	1034	903
	Constr. Serv. & Field Engr.	171	53	223	135
	Home Office Engr. & Services	128	32	160	83
	Owner's Cost	98	44	142	112
	TOTAL PLANT INVESTMENT	1080	480	1560	1233
	Contingency	162	48	210	123
	AFUDC	119	51	170	130
	TOTAL CAPITAL REQUIREMENT	1361	578	1940	1486
	$/kWe net			2380	1824

safety-rated. These higher capital costs are generally associated with the increased quality control and assurance, documentation and verification requirements on nuclear safety-rated equipment.

An economic evaluation of the levelized busbar cost of electricity (COE) for the ICF power plant is presented in Table 1-5. Also presented in Table 1-5 is the levelized busbar cost of electricity for a High Temperature Gas-Cooled Reactor (HTGR), a Pressurized Water Reactor (PWR) and a Coal Plant, (Ref. 1-4) all estimated using the same economic ground rules and data base. The results of the economic evaluation provide an indication of the potential competitiveness of the Cascade ICF plant. The COE for the ICF was estimated to be 34 Mills/kWe-hr for the All Conventional and 41 for the Nuclear+Conventional plant. The estimated COE for the Coal Plant was 49 Mills/kWe-hr and the PWR and HTGR were 37 and 40 Mills/kWe-hr respectively. The economic ground rules of Ref. 1-3 were used for the economic comparison of COE. These results show that Cascade will be able to compete well with current power plant alternatives. If full advantage can be taken of Cascade's safety features to eliminate the need for nuclear safety related equipment, Cascade has an economic advantage over these alternative power plants.

Safety and Tritium Issues

The Cascade approach to fusion power offers some very attractive safety features. First, tritium inventory and routine permeation release rates are very low. Second, the use of low activation materials brings the benefits of minimum radioactive inventory and decay heat production. Third, the use of a solid breeder avoids the potential for a large uncontrolled chemical energy release. Cascade minimizes both the radioactive source term as well as the mechanism for its release and thus approaches the ultimate inherent safety and environmental potential of fusion. These inherent advantages can be translated into an economic advantage by exploiting the cost savings of conventional versus nuclear classification of plant components and equipment and by avoiding unnecessary safety systems. By providing safety design

TABLE 1-5
ICF FUSION PLANT ECONOMIC COMPARISON
LEVELIZED BUSBAR COST OF PRODUCT
(Millions of 1-1-85 $, 2005 Operation Date)

	ICF PLANT				
	CONVENTIONAL CONSTRUCTION	NUC/CONVT. CONSTRUCTION	2240MWT HTGR-SC/E	2400MWT PWR	2300MWT P-COAL
PLANT CHARACTERISTICS					
THERMAL INPUT (MWT)	1670.0	1670.0	2240.0	2400.0	2285.0
NET ELECTRICAL RATING (MWE)	815.0	815.0	855.0	800.0	800.0
CAPACITY FACTOR	0.75	0.75	0.75	0.70	0.75
ANNUAL ELECTRICITY PROD. (KW-HRxE6)	5354.5	5354.5	5617.4	4905.6	5258.0
FIXED CHARGES					
TOTAL PLANT INVESTMENT ($xE6)	1356.3	1769.8	1411.0	1129.0	836.0
CONSTRUCTION PERIOD (MONTHS)	72.0	72.0	72.0	72.0	48.0
AFUDC ANNUAL RATE (%)	3.1	3.1	3.1	3.1	3.1
TOTAL CAPITAL REQUIRMENT ($xE6)	1486.4	1939.5	1546.3	1237.3	888.6
FIXED CHARGE RATE	8.7	8.7	8.7	8.7	9.0
ANNUAL FIXED CHARGES ($xE6)	129.3	168.7	134.5	107.8	80.0
O&M					
FIXED ($xE6)	50.0	50.0	35.0	38.0	20.0
VARIABLE: RATE (MILLS/KW-HR)	0.1	0.1	0.1	0.1	0.5
AMOUNT ($xE6)	1.5	1.5	2.0	1.8	7.5
TOTAL ANNUAL O&M ($xE6)	51.5	51.5	37.9	39.8	27.5
FUEL					
UNIT COST ($/MMBTU)	-	-	1.07	0.71	2.54
LEVELIZING FACTOR	-	-	1.00	1.03	1.14
ANNUAL FUEL COST ($xE6)	(small)	(small)	53.7	35.7	148.4
BUSBAR COST SUMMARY (MILLS/KW-HR)					
FIXED CHARGES	24.2	31.5	23.9	21.9	15.2
O&M	9.6	9.6	6.6	8.1	5.2
FUEL			9.6	7.3	28.2
TOTAL	33.8	41.1	40.1	37.3	48.7
RELATIVE COST (1200MWT P-COAL REF.)	0.69	0.84	0.82	0.77	1.00

guidance early in the design stage, we can minimize safety-related costs. In this study, we reviewed the fission-industry's licensing criteria on accidental and routine releases of radioactivity and waste disposal and their applicability to Cascade. We determined the appropriate licensing boundary classifications and developed the system design requirements which maximize Cascade's advantages and minimize the need for dedicated safety systems.

At present, classification systems for safety (structural/mechanical/electrical), seismic, and quality assurance level have been developed. (Ref. 1-5 and 1-6) These classification systems were developed for the fission-nuclear industry, and their applicability to fusion in general has not been determined. For Cascade in particular, much of the safety classification system would appear to be inappropriate due to the absence of a pressure retaining primary coolant boundary. Although the accident scenarios and classification systems developed by the fission industry may not apply, the dose guidelines used by the fission industry will probably either be directly applicable or serve as as useful references in defining the radiological safety requirements. The current Nuclear Regulatory Commission (NRC) regulations covering fission reactors are described in the code of Federal Regulations in Sections:

- 10CFR20 – Standards for Protection Against Radiation
- 10CFR50 – Domestic Licensing of Production and Utilization Facilities
- 10CFR100 – Reactor Site Criteria

These NRC regulations define the maximum dose limits and releases of radioactivity during routine and anticipated operations (10CFR20 and 10CFR50) and during severe hypothetical accidents (10CFR100). In general, these guidelines were established based on the biological effect of a radioactive release and are thus independent of the source of the release. Therefore, even though the regulations frequently reference nuclides of importance to nuclear fission which will have no significance in fusion, e.g., thyroid dose from iodine-131, the intent of the guidelines remains valid.

By applying the established and applicable safety analysis and licensing methodology to Cascade, we obtain design guidance that can be used to design Cascade such that the numerical dose limits are inherently satisfied to the greatest extent possible. In the activation analysis, we determined that the major contributor to decay heat is the ^{24}Na produced from (n,α) captures in ^{27}Al. This is a threshold-type reaction, and the level of ^{24}Na in the $LiAlO_2$ can be controlled by moderating the neutron flux entering the $LiAlO_2$ zone below the (n,α) reaction threshold energy. This can be accomplished by adjusting the thickness of the BeO front zone. We found that, conservatively considering only the heat capacity of the blanket materials, a BeO zone thickness of 5 cm will keep the total decay energy below the 710 GJ heat capacity of the blanket that will preclude melting of the blanket. Thus, the reference blanket, with a 9 cm BeO front zone thickness will not melt. Furthermore, for the reference blanket, the radiation shield provides a massive ultimate heat sink which can absorb passively the total amount of decay energy produced with a temperature rise of only 100 K. An active ultimate heat sink is not necessary. This analysis indicates that the Cascade blanket will be inherently safe from meltdown and accidental radioactivity release. These results form the foundation for the following design decisions: eliminating dedicated active safety cooling systems from the baseline reactor design, reducing the containment requirements imposed on the reactor building, and also reducing the costs of system components by specifying conventional construction and qualification rather than "nuclear safety" grade.

Considering tritium events, we compared the maximum routine tritium leakage rate which will satisfy 10CFR50 and the maximum accidental tritium release which will satisfy the requirements of 10CFR100 with the Cascade values. The tritium leakage rate which will meet the 5 mrem/y 10CFR50 limit is 100 Ci/d from all sources through a 100 m stack. The allowed leakages from a 10 m stack and ground level would be 10 and 1 Ci/d. The design limits would be lower than these values to account for nontritium contributions to dose and uncertainties. The main Cascade tritium loss rate is 25 Ci/d into the helium secondary coolant, which has a tritium recovery system within its own containment. Virtually negligible tritium permeation

rates into the environment are thus expected.

We then calculated the maximum tritium release which will meet current accident guidelines. The results shows that the maximum inventory is a function of the building containment characteristics and release height. Of greatest interest to Cascade is the result that a tritium inventory of 210 g releasable over 12 h will meet the 25 rem regulatory guideline of 10CFR100 (170 g to satisfy 80% guideline during design stage) without requiring containment leak-rate or seismic qualification of the reactor building, or an effluent release stack. Cascade's total tritium inventory, including all components within the reactor building, secondary loop and tritium recovery system, is 140 g releasable over 30 days, and an additional 120 g releasable in a time scale on the order of 100 years. This does not include the tritium in the Fuel Pellet Fabrication Plant (also containing the tritium storage vault), which is well protected and secured independently of the balance of the Cascade plant. Based on these findings, Cascade's tritium inventory and leakage rate will meet current regulatory guidelines without requiring safety classification of equipment or dedicated safety systems. Thus, with respect to tritium events, Cascade is inherently safe.

Activation Analysis

The Cascade reactor design incorporates low activation materials in all the regions of high neutron fluence. The result is relatively low activation (700 MCi one minute after shutdown after 30 full power continuous years of operation versus 3000 MCi for a MARS tandem mirror reactor of comparable power, Ref. 1-7, after 2 years operation,) and reduced safety, waste management and maintenance dose rate concerns caused by radioactivity. The waste disposal characteristics of Cascade are dominated by the inherent constituents of the reactor materials (oxygen and aluminum). Shallow land disposal as low level waste under 10CFR61 is possible, but will require dilution of the reactor materials with inert materials by a factor of 10 to 100, depending on the exposure lifetime.

A 2.0 m thick radiation shield of borated water is used outside the reaction chamber to reduce the operating neutron fluence to low enough levels to allow conventional iron and nickel alloys to be used in the heat exchanger region and outside the vacuum boundary. Contact maintenance of these components is possible 1 day after reactor shutdown. Only very limited access will be possible inside the radiation shield, and at least 3 weeks of cooldown time would be needed prior to this very limited access. A 2.5 m thick concrete biological shield is employed exterior to the radiation shield, heat exchangers and vacuum vessel. The dose rate exterior to this biological shield is less than 1 mrem/h during reactor operation, permitting unrestricted occupational access.

References for Chapter 1

1-1. J. H. Pitts, "Cascade: A Centrifugal-Action Solid-Breeder Reaction Chamber," *Nuclear Technology/Fusion*, Vol. 4, No. 2, part 3, September 1983, p. 967.

1-2. I. Maya, K. R. Schultz, et al., "Inertial Confinement Fusion Reaction Chamber and Power Conversion System Study," GA Technologies Report, GA-A17267, September 1984; also Lawrence Livermore National Laboratory Report, UCRL-15642.

1-3. J. E. Russ III, "Economic Ground Rules for the HTGR Program," Gas-Cooled Reactor Associates (GCRA) Document HP-20702, Revision 5, January 7, 1985.

1-4. United Engineers and Constructors, "The HTGR for Electric Power Generation – Design and Cost Evaluation," GCRA/AE/78-1, Revision 1, August 1981.

1-5. American Nuclear Society, "Nuclear Safety Criteria for the Design of Stationary Boiling Water Reactor Plants," ANSI/ANS - 52.1, 1983.

1-6. GA Technologies, "Nuclear Safety Plant Specifications for the HTGR SC/C, 2240 MWt," Report 905842, June 1983.

1-7. B. G. Logan *et al.*., "Mirror Advanced Reactor Study, Final Report," Lawrence Livermore National Laboratory Report UCRL-53480, July 1984.

2. HIGH-TEMPERATURE BLANKET DESIGN OPTIONS

2.1. INTRODUCTION

A unique characteristic of deuterium-tritium inertial confinement fusion is that a large fraction of the energy yield, typically ~30%, is in the form of a surface heat flux from charged particles, reflected laser light, and x-rays. The balance of the energy yield is in the form of volumetric heating from neutron absorption. The Cascade reaction chamber concept (Refs. 2-1 and 2-2) is ideally suited to accommodate this characteristic in that a thin, fast-moving surface layer of high-temperature (>1500K) material is used to absorb and transport the surface heat flux, and a thicker, slower-moving zone of high-temperature and/or tritium-breeding material can be used to absorb and transport the neutron energy. The high-temperature material can then be used to achieve very high power conversion efficiency (55%) while still allowing for adequate tritium breeding.

This chapter presents a number of high-temperature blanket design options available to the Cascade concept. Section 2.2 examines the high-temperature material options for the surface layer. It includes analyses of mechanical properties for thermal stress resistance, irradiation stability and fabricability into granules suitable for Cascade. In Section 2.3, material temperature limits are suggested based on compatibility of the surface layer with the tritium breeder and chamber and heat exchanger materials. In the last section we couple the results of the previous sections with nucleonic performance of candidate material combinations to calculate the overall thermodynamic, and thus power-producing, potential of selected blanket designs. A reference design is selected for subsequent secondary system design and tritium analysis.

2.2. HIGH-TEMPERATURE MATERIAL OPTIONS

2.2.1. Introduction

Ceramic materials, such as SiC and BeO, are usable at temperatures into the range of ~2000 K and higher. A high-temperature surface layer of ceramic material can significantly enhance the power conversion efficiency of a Cascade reactor by permitting higher temperatures than the typical 1400 K to 1500 K maximum of solid ceramic tritium breeders such as Li_2O and $LiAlO_2$. In this section we examine the candidate materials for the surface layer. We present mechanical properties at elevated temperatures, evaluate granule resistance to the thermal stress induced by the surface heat flux, and estimate irradiation lifetimes. Preliminary issues of fabricability are also presented. The survey was restricted to low-activation materials which would maintain the safety and environmental attractiveness of Cascade.

2.2.2. High-Temperature Material Properties

Typical properties of ceramic material candidates for the surface layer are shown in Table 2-1. Data for metallic Be-compounds, Li_2O and $LiAlO_2$ are shown for comparison. Data from Ref. 2-3 are for high-density polycrystalline materials prepared by hot pressing, except for SiC and carbon, where they refer to chemical vapor deposited (CVD) β-SiC and pyrolytic carbon. The thermal stress parameter shown in Table 2-1 is calculated according to (Ref. 2-4)

$$R = \frac{S(1-\nu)}{\alpha E}$$

where R is the thermal stress parameter, a measure of the material strength relative to the thermal stress, S is the flexural strength, ν is Poisson's ratio, α is the coefficient of thermal expansion, and E is Young's modulus. For materials for which Poisson's ratio is not available, the value for Li_2O was used in the calculation of R.

TABLE 2–1
TYPICAL PROPERTIES OF CERAMIC MATERIALS[a]

Material	Melting Point (K)	Density (Mg/m^3)	Thermal Expansivity (10^{-6} K^{-1})	Thermal Conductivity (W/mK)	Young's Modulus (GPa)	Poisson's Ratio	Flexural Strength (MPa)	Specific Heat (J/kg K)	Thermal Stress Parameter	Ref.
Al_2O_3	2320	3.99	9.0	7	340	>0.45[d]	300	(b)	54	2-3
$MgAl_2O_4$	2408	3.59	9.0	6	206	(b)	250	(b)	100	2-3
MgO	3100	3.58	15.7	9	275	(b)	250	(b)	43	2-3
PyC, ∥[d,e]	3800	2.10	1.3	280	26	-0.15[f]	100	2000	3400	2-4
PyC, ⊥[d,e]	3800	2.10	26.0	1.4	11[f]	0.35[f]	3	2000	6.8	2-4
SiC	>3000[c]	3.21	4.9	50	360	0.2	500-1000	1300[d]	230-450	2-3
Neutron-Mutipliers										
Be[f]	1558	1.85	11.5	150	290	(b)	210-410[f,g]	1883	47-92	2-5
Be-38Al[f]	918	2.08	16.2	210	190	(b)	210-280[f,g]	(b)	51-68	2-5
Be_2C	>2400[c]	2.24	10.8	23[f]	214	0.1	100[h]	1400[f]	3 9	2-4
BeO	2890	2.90	9.1	29	360	0.22	390	2000	93	(i)
Tritium-Breeders										
$LiAlO_2$	1883	2.55[e]	12.4	2.2	(b)	(b)	(b)	1500	31[j]	2-6
Li_2O	1706	2.00	35.9	3.6	54	0.25	28	2890	11	2-2

(a) At 1270 K unless otherwise noted.

(b) Not available.

(c) Decomposes.

(d) At 1800 K, Ref. 2-4.

(e) Pyrolytic carbon: ∥ – parallel to deposition plane; ⊥ – perpendicular to deposition plane.

(f) At room temperature.

(g) Yield strength depends on form.

(h) Modulus of rupture at room temperature.

(i) See Table 2-2.

(j) Assuming flexural strength, Poisson's ratio and Young's modulus of Li_2O.

Inspection of Table 2-1 shows that, among candidate non-neutron-multipliers, SiC is clearly superior in terms of thermal stress resistance, followed by $MgAl_2O_4$ spinel. Pyrolitic carbon properties vary with deposition conditions and crystallographic orientation and are thus highly anisotropic. At the small sizes of interest for Cascade, pyrolytic carbons can be made near-isotropic. This material is of interest for the surface layer because it is the only ceramic material in elemental form. It is further discussed in Section 2.4.3. Among the Be neutron-multipliers, BeO exhibits the highest thermal stress resistance at elevated temperature, comparable to that of $MgAl_2O_4$. As is shown in the next section, Be_2C must be coated in the present application due to compatibility concerns and thus its thermal stress resistance is less important. In all cases, however, these high-temperature ceramics exhibit thermal stress resistances which are at least one order of magnitude higher than that of Li_2O. Thus, they are likely to survive the thermal shock induced by the surface heat load without experiencing the cracking and chipping predicted for Li_2O in Ref. 2-2.

As discused in Section 2.4, BeO is the preferred material for the surface layer. Thus, the thermal and mechanical property values for BeO at elevated temperatures were further reviewed. Typical values are shown in Table 2-2 at 1270 K and 1770 K, for unirradiated material and material irradiated to $\sim 10^{25}$ n/m^2. The high temperature strength is sensitive to the fabrication method, so typical data for hot-pressed and cold-pressed and sintered material are shown separately. High purity BeO produced via sol-gel can be assumed to have properties similar to the hot-pressed material. The thermal properties of BeO (specific heat, thermal expansivity, and thermal conductivity) are not very sensitive to the fabrication method, so data were obtained from a standard handbook (Ref. 2-9). The accuracy of the thermal expansivity was stated to be $\pm 3\%$ and that of the thermal conductivity was given as ± 8 to 15%.

The high temperature strength of BeO is very sensitive to the fabrication method, density and composition. Cold-pressing and sintering produces 95 to 98% dense materials with moderate strength at low temperatures, but the additives used to aid sintering or inhibit grain growth frequently result in poor strength at temperatures

above 1100 K to 1300 K because of grain boundary phase separation. Typical strength data for this type of material taken from Ref. 2-10 are shown in Table 2-2. In contrast, high purity BeO with essentially 100% density has been produced whose strength is much higher than that of cold-pressed BeO and which remains strong to at least 1800 K (Ref. 2-11). These data are also shown in Table 2-2.

The elastic constants of BeO decrease with decreasing density but are otherwise insensitive to fabrication variables. Table 2-2 shows typical data from Ref. 2-12. The 1770 K value for Young's modulus was obtained by extrapolation using a formula in Ref. 2-12 based on tests to 1670 K.

The stable form of BeO is a hexagonal α-phase. Above 2320 K, it undergoes a transition to a tetragonal β-phase with a large volume expansion (Ref. 2-4).

2.2.3. Irradiation Stability

The front zone of the Cascade blanket will experience the highest neutron fluence. We thus examined the irradiation stability of SiC, BeO, and Be_2C. The properties of single-phase β-SiC after neutron irradiation in a fission spectrum are documented in Ref. 2-7. In summary, at fluences up to 5×10^{26} n/m^2 at 823 K, specimens of β-SiC showed no structural deterioration and a linear expansion of 0.4%. At 1773 K, the same linear expansion of 0.4% was reached in a fluence of 10^{26} n/m^2. The unirradiated dimensions can be recovered by annealing. Due to the cyclic nature of ICF neutron loading, in addition to the recirculation of the blanket for energy transport, this annealing process may be inherent to the Cascade concept. In addition, SiC's flexural strength, Young's modulus and thermal expansivity are insensitive to irradiation up to 5×10^{26} n/m^2. The neutron fluence expected at the surface layer at a radius of 4 m for 3000 MW fusion is 1.5×10^{26} n/m^{2}y, and thus an irradiation lifetime of 4 to 5 years appears possible for surface granules of SiC.

TABLE 2-2
Typical Thermal and Mechanical Properties of BeO

Property	Fabrication (a)	Temperature (K)	Property Value: Unirrad.	Property Value: Irradiated (1×10^{25}n/m^2)	Reference
Density, g/cm^3	All	1270	2.93	2.90	2-8
		1770	2.87	2.84	2-8
Specific Heat, J/kg K	All	1270	2000	2000	2-9
		1770	2100	2100	2-9
Thermal Expansivity,[b] 10^{-6} K^{-1}	All	1270	9.1	9.1	2-9
		1770	10.2	10.2	2-9
Thermal Conductivity, W/m K	All	1270	29	28	2-9
		1770	17	16[c]	2-9
Flexural Strength, MPa	CPS	1270	110	110	2-10
		1770	28	28	2-10
	HP	1270	390	390	2-11
		1770	331	331	2-11
Young's Modulus, GPa	CPS	1270	322	317	2-12
		1770	296	292	2-12
	HP	1270	360	355	2-12
		1770	330[c]	325[c]	2-12
Poisson's Ratio	All	1270	0.22	0.22	2-8
		1770	0.22	0.22	2-8

[a] CPS = cold pressed and sintered, approximately 95% dense.

HP = hot pressed, high purity, 100% dense.

[b] Mean from 300 K to temperature.

[c] Extrapolated.

Radiation damage to BeO results from three processes:

(1) Accumulation of bubbles of helium in grain boundaries.

(2) Intergranular stresses caused by anisotropic crystal growth, which can cause microcracking.

(3) Accumulation of clusters of interstitial atoms and vacant lattice sites within the grains.

Processes (1) and (2) can result in volumetric expansion, grain boundary separation, loss of strength, and ultimately powdering. Process (3) does not affect the strength or integrity of the material, but it contributes to the volume expansion and reduces the thermal conductivity.

Some early data on radiation damage to BeO are available in Refs. 2-8 and 2-13 to 2-16. There are some inconsistencies in the data, but they can be used as a general basis for estimating the probable operational limits for the material. The test data come from specimens irradiated at steady neutron fluxes in test reactors; the damage produced by short, intense neutron pulses in an ICF reactor may be different.

The data on BeO volume expansion upon irradiation in Refs. 2-8 and 2-13 to 2-16 show the following trends:

(1) For a given neutron fluence, the volume expansion decreases with increasing irradiation temperature up to about 1300 K, then increases with temperature.

(2) Large grain size material expands more than small grain size material.

(3) Expansion initially increases progressively with fluence, and then saturates. Expansion may increase again at high fluences.

Data from Ref. 2-8 for sintered compacts from UOX-BeO powder with 0.5% MgO addition, with grain size of 20 μm and density of 2.9 g/cm^3, show volume expansion

saturating at less than 1% at a temperature of 1300 K for fluences up to 10^{25} n/m^2. Additional data from Refs. 2-14 and 2-15 at temperatures above 1300 K show saturation levels in the range of 1 to 2% at fluences up to 2×10^{25}n/m^2. Data for irradiation temperatures above 1300 K are quite scattered and expansion appears to depend on details of the material preparation, composition, and microstructure. Higher fluence data reported in Ref. 2-8 shows the 20 μm grain size UOX material expanding by 1.7% when irradiated to 4.4×10^25 n/m^2 (E>1 MeV), while materials with somewhat different compositions and grain size expand by up to 5%.

When microcracking becomes extensive, the flexural strength falls off sharply. Ultimately the specimen is reduced to powder. The fluence at which the strength is reduced increases with irradiation temperature and increasing grain size (Ref. 2-15). A number of models have been proposed for predicting the fluence at the onset of microcracking, but have not been consistently successful (Ref. 2-15). Collins (Ref. 2-13) noted that there appeared to be a correlation between strength loss and volume expansion for material irradiated at 400 K to 1300 K. His data for AOX-grade BeO with 20 μm grain size irradiated in this temperature range suggests that the critical volume change for the onset of strength loss is about 0.5% for irradiation temperatures up to 1100 K, and about 1% at higher temperatures. However, later high fluence data (Ref. 2-8) indicate that this limit may be unduly pessimistic. A number of specimens with grain sizes of 7 μm or less, irradiated to about 4.4×10^{25} n/m^2 (E>1 MeV) at 1300 K showed no strength loss at 1.5 to 2.4% expansion. Only large-grained material (29 μm), which expanded to 4.2% showed significant weakening.

In conclusion, for the best irradiation stability, BeO should have a small grain size ($\leq$ 10 μm). At irradiation temperatures above 1300 K, the volume expansion is likely to be less than 3% for fast neutron fluence up to 5×10^{25}n/m^2. Ultimately, microcracking will occur and the material will weaken. The limiting fluence is not well-defined, but some fine-grained specimens have been shown to retain their strength to these fast fluences at 1300 K. BeO surface granule lifetime would thus be on the order of 0.5 year. The effect of pulsed neutron bursts is unknown, but may reduce the

limiting fluence. If longer lifetimes are required, the granules could be coated with SiC as described below.

There is no significant data on irradiation effects on Be_2C, except for some transient pulsing exposures to very low fluences in a Sandia reactor (Ref. 2-17). The cubic crystal structure of Be_2C would indicate good resistance to irradiation damage. However, the formation of the transmutation products of helium, tritium, and lithium by neutron absorption in the Be will no doubt have a significant effect on the irradiation behavior of the Be_2C. Swelling may result from the agglomeration of the He in the Be_2C granules, unless the He can diffuse out at the high operating temperature. With coated Be_2C, the effects of irradiation on the Be_2C kernel could be accommodated with no significant damage to the particles. Coatings are discussed further below.

2.2.4. Granule Fabricability

Be_2C particles were produced at Los Alamos National Laboratory in the 1970's to fabricate a graphite-matrix dispersion fuel, containing uranium carbide and Be_2C particles, for the Sandia pulsed reactor (Ref. 2-17). No difficulties were reported in the fabrication of the fuel rods (2.5 cm dia. $\times$ 5.0 cm length) by hot pressing. The blending of the powders was carried out in an inert atmosphere because the carbides are hygroscopic. Earlier work in the fabrication of Be_2C bodies is described in Ref. 2-18.

As discussed in Section 2.4, coated Be_2C granules are preferred for the Cascade blanket. Spherical granules may be produced by carburizing spherical Be metal particles, either prior to or after coating, by providing sufficient carbon in the inner coating to carburize the Be kernel in-situ. Alternately, Be_2C granules may be spheroidized by the drop-melt technique used in the production of carbide fuel particles for the High Temperature Gas-Cooled Reactor.

2.3. COMPATIBILITY TEMPERATURE LIMITS

One of the strengths of Cascade is its ability to attain an adequate tritium breeding ratio of 1.05 or greater with a variety of material combinations. In this section, we examine the compatibility of candidate blanket material combinations and establish maximum use temperatures. The high-temperature materials considered are SiC, BeO, and Be_2C. The tritium-breeder materials considered are Li_2O and $LiAlO_2$ since these are the currently preferred breeders for fusion application (Ref. 2-19). The reaction chamber and heat exchanger material is SiC.

To establish the maximum temperature limits for the candidate materials, we performed a thermochemical assessment of all possible material interactions and examined the mass transport and overpressure that would result from vaporization, assuming thermodynamic equilibrium. The possible material reactions are listed in Table 2-3. The resultant temperature limits are summarized in Table 2-4. Mass transport was calculated assuming reactions proceed to completion and are very conservative, i.e., no credit is taken for possible kinetics effect. Postulated interactions were evaluated for overpressure by calculating the heats of reaction (ΔH) and standard free energies of reaction (ΔF) at 1800 K using JANAF data (Ref. 2-20). The standard entropy (ΔS) was then calculated from the second law,

$$\Delta F = \Delta H - T\Delta S.$$

Over a reasonable temperature range, it can be assumed that ΔH and ΔS are constant, and ΔF at other temperatures can be calculated using the ΔH and ΔS values at 1800 K. Since the processes of interest include gaseous species, the equilibrium constant, K, given by

$$K = e^{-\frac{\Delta F}{RT}}$$

is a measure of the overpressure. The background pressures of T_2 and T_2O used in the calculations are 13 and 1.3 Pa (Ref. 2-2).

TABLE 2–3
MATERIAL REACTIONS AND THERMODYNAMIC DATA AT 1800K

	Reaction	ΔH (kJ/mole)	ΔF (kJ/mole)	ΔS (kJ/mole K)	K (atm)
1.	$SiC \rightarrow Si(g) + C$	517	246	0.151	7.3×10^{-8}
2.	$SiC + T_2O(g) \rightarrow Si(g) + CO(g) + T_2(g)$	649	124	0.292	2.5×10^{-4}
3.	$SiC + 2T_2O(g) \rightarrow SiO(g) + CO(g) + 2T_2(g)$	345	-166	0.284	6.6×10^{4}
4.	$SiC + 3T_2O(g) \rightarrow SiO_2 + CO(g) + 3T_2(g)$	-188	-361	0.0961	3.0×10^{10}
5.	$SiC + 3Li_2O \rightarrow SiO_2 + CO(g) + 6Li(g)$	1525	185	0.744	4.3×10^{-6}
6.	$SiC + 6LiOT(g) \rightarrow SiO_2 + CO(g) + 3Li_2O + 3T_2(g)$	-908	-405	-0.279	5.7×10^{11}
7.	$SiC + 6LiAlO_2 \rightarrow SiO_2 + CO(g) + 6Li(g) + 3AlO_3$	2040	596	0.802	5.1×10^{-18}
8.	$SiC + BeO \rightarrow Be(g) + Si(g) + CO(g)$	1250	483	0.426	9.6×10^{-15}
9.	$BeO + 2LiAlO_2 \rightarrow BeO{\cdot}Al_2O_3 + LiO$	(a)	(a)	(a)	(a)
10.	$BeO + T_2O(g) \rightarrow Be(OT)_2(g)$	167(b)	95(b)	0.0360(b)	3.3×10^{-3}(b)
11.	$Be_2C \rightarrow 2Be(g) + C$	722(c)	329(c)	0.251(c)	1.1×10^{-11}(c)
12.	$Be_2C + 3T_2O(g) \rightarrow 2BeO + CO(g) + 3T_2(g)$	(a)	(a)	(a)	(a)

(a) Not required.
(b) 2000K
(c) 1566K

TABLE 2-4
MATERIAL COMPATIBILITY TEMPERATURE LIMITS FOR CASCADE

Material	Temperature Limit, K	Basis
SiC, bulk temperature	2100	Thermal decomposition overpressure of 1 Pa.[a]
SiC/T_2O interface	No limit	Acceptable material transport assuming complete reaction of all T_2O.
SiC/Li_2O interface:		
(a) Front surface	1100	Overpressure of 1 Pa.
	1200	Overpressure of 10 Pa.
(b) Within the blanket	1500	Stability of SiO_2 layer on SiC.
SiC/LiOT	No limit	Acceptable material transport, assuming complete reaction of all LiOT.
SiC/$LiAlO_2$ interface	1400	Overpressure of 1 Pa.
	1500	Stability of SiO_2 layer on SiC, overpressure of 4 Pa.
SiC/BeO interface	1700	Overpressure of 1 Pa.
BeO	2300	Material phase transition.
BeO/$LiAlO_2$	No limit	$LiAlO_2$ has much lower (more negative) free energy of formation than Be·Al_2O_3.
BeO/T_2O	No limit	Overpressures much less than 1 Pa at 2300K; Acceptable mass transport assuming complete reaction of T_2O.
Be_2C, bulk temperatures	1600	Thermal decomposition overpressure of 1 Pa.
Be_2C/T_2O	No limit	Acceptable mass transport assuming complete reaction of all T_2O.
Li_2O, bulk temperature	1200	LiOT mass transport. (Ref. 2-2)
$LiAlO_2$, bulk temperature	1500	0.8× melting temperature. (Ref. 2-6)

(a) Equal to background pressure.

SiC. We consider first the direct thermal decomposition of SiC, Reaction 1 in Table 2-3. The equilibrium constant in this case is equal to the overpressure due to Si evaporation, P_{Si}. A log plot of P_{Si} versus 1/T is presented in Fig. 2-1. The plot shows that to maintain a Si overpressure which is less than 1 Pa, i.e., comparable to the background pressure, the SiC temperature must be maintained below 2100 K.

We next examine the three reactions of SiC with water (T_2O), Reactions 2 to 4 in Table 2-3. For these reactions, the total partial pressure at equilibrium is given by $2\sqrt{K}$. Table 2-3 shows that this pressure would be unacceptable in the 1800 K temperature range. However, the T_2O source rate is only 1.25×10^{-6} kg-moles/s for 3000 MW of fusion power at a tritium breeding ratio of 1.4. Assuming the T_2O continually and fully reacts only with the SiC, the maximum resultant SiC loss rate is 5×10^{-5} kg-SiC/s, or 1.5×10^3 kg/y. These figures are to be compared with typical front zone flow rates of $\sim 10^4$ kg/s and a total available SiC mass of 6×10^4 kg. It is thus concluded that the reactions of SiC with T_2O do not impose operational temperature limits.

In the reaction of SiC with Li_2O, Reaction 5 in Table 2-3, the equilibrium constant has the form $K = P_{CO} \times (P_{Li})^6$. If the gas phase has the reaction stoichiometry of $P_{Li} = 6P_{CO}$, then the total overpressure for this reaction is given by $P_{Li_2O} = 1.51(K)^{1/7}$. A log plot of P_{Li_2O} versus 1/T is presented in Fig. 2-2, which shows that the temperature limit at a SiC-Li_2O interface is approximately 1100 K for a maximum overpressure of 1 Pa, and 1200 K for 10 Pa. The latter is assumed in the present application since these limits are particularly conservative in that they apply to a solid-solid reaction in which kinetics may limit the overpressure due to point-to-point contact limitations.

Examination of the products of Reaction 5 reflects the fact that SiC has "kinetic stability" in the presence of Li_2O due to the formation of a SiO_2 film. After formation of this film, further reaction is limited by diffusion of the reactants. The high temperature capability of SiC in the presence of Li_2O is thus limited by the stability of the SiO_2 protective layer, and the temperature at a SiC-Li_2O interface will be limited

to the protection temperature of the SiO_2 layer. The SiO_2 protective layer will be stable until the sum of the partial pressures of the SiO and CO produced via reaction of the SiC with the SiO_2 itself exceeds the ambient pressure, at which time the silica film detaches from the SiC. Ref. 2-21 indicates that at 1923 K, the total gas pressure at the SiC-SiO_2 interface reaches 10^5 Pa. The pressure decreases to about 6×10^3 Pa at 1673 K. The SiO_2 is amorphous below 1500 K and partly vitreous and partly crystalline cristobalite above this temperature, and diffusion of CO and SiO through the SiO_2 is suggested as the rate limiting mechanism (Ref. 2-21). On the basis of these data, a limit of 1500 K at a SiC-Li_2O interface within the blanket is extrapolated for the present application. For the surface layer, were the stability of the SiO_2 cannot be preserved due to the surface heat flux, the limits based on overpressure given above are applicable.

The impact of the reaction of SiC with LiOT can be analyzed on a mass transport basis similarly to that of the reactions of SiC with water. Assuming a bulk average Li_2O temperature of 1300 K, the LiOT production rate is 7×10^{-5} kg/s or 3×10^{-6} moles/s (Ref. 2-2). The corresponding SiC loss rate assuming complete reaction is 600 kg/y, which is quite acceptable, and thus no SiC temperature limit arises from LiOT considerations.

In the case of $LiAlO_2$, the reaction stoichiometry is the same as for Li_2O. The resultant total pressure, P_{LiAlO_2}, versus temperature is given in Fig. 2-2. A temperature limit of 1500 K can be established based on both overpressure and SiO_2 stability considerations.

BeO will contact the SiC reaction chamber and heat exchanger. Possibly, it may also be necessary to coat BeO granules with SiC to accommodate thermal stresses. The dominant reaction of these two materials is given by Reaction 8 in Table 2-3. Reaction stoichiometry dictates that the total product overpressure is given by $P_{BeO} = 3(K)^{1/3}$. The log plot of pressure versus temperature for this reaction is shown in Fig. 2-1. The figure shows that a temperature limit of 1700 K is necessary to limit overpressure to 1 Pa, one-tenth of background.

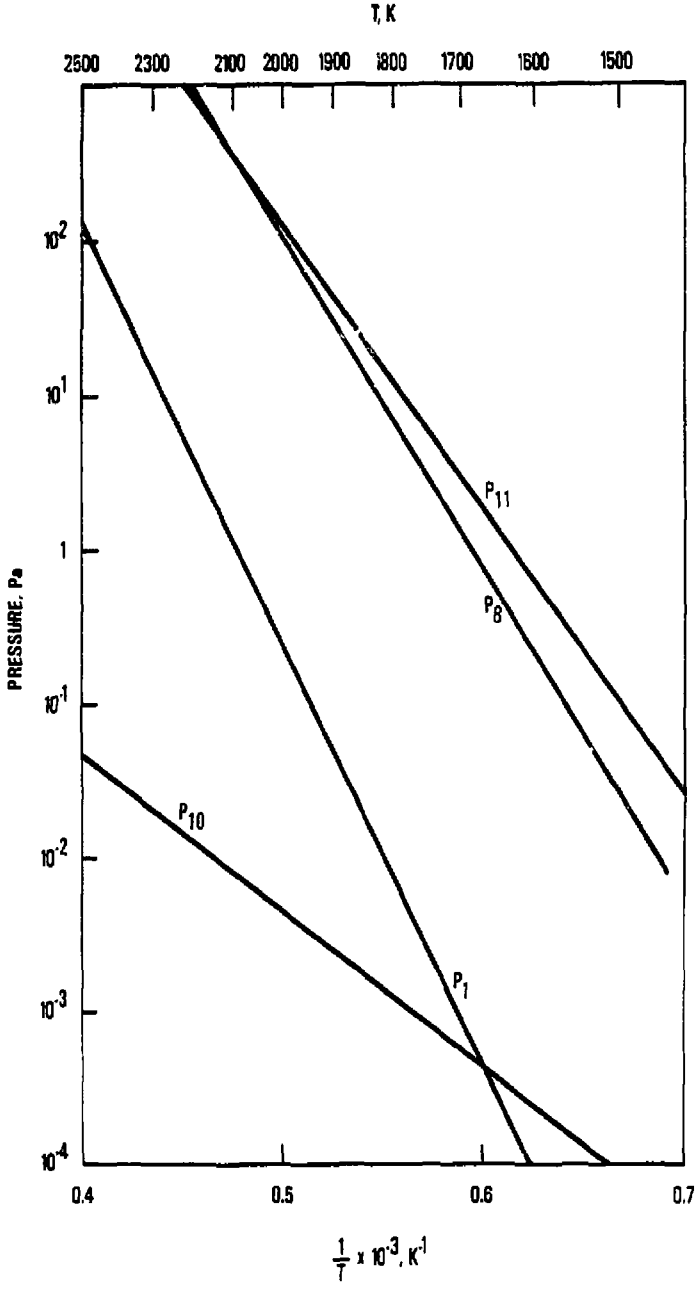

Fig. 2-1. Overpressure versus material temperature, Reactions 1, 8, 10 and 11 of Table 2-3.

BeO. In addition to the reaction of BeO with SiC considered above, the reactions of BeO with $LiAlO_2$ and T_2O also need to be considered. With respect to interaction with $LiAlO_2$, $Li_2O{\cdot}Al_2O_3$ has a much more negative free energy of formation than $BeO{\cdot}Al_2O_3$. There is thus no likelihood of Reaction 9. The possibility exists for a ternary composition melting below $Li_2O{\cdot}Al_2O_3$ but it is not likely. No ternary phase diagrams for the $Li_2O/BeO/Al_2O_3$ system were located.

In the reaction with water, the equilibrium constant has the form

$$K = \frac{P_{Be(OT)_2}}{P_{T_2O}}.$$

A plot of $P_{Be(OT)_2}$ versus temperature is shown in Fig. 2-1 for $P_{T_2O} = 1.3\ Pa$. The figure shows that the total overpressure is much lower than 1 Pa as high as 2300 K and thus does not present a limitation. In addition, assuming complete reaction of the BeO with the available T_2O, the BeO loss rate is 3×10^{-5} kg/s or 1000 kg/y. This is also acceptable compared to a typical front zone flow rate of 5×10^3 kg/s and total available BeO mass of $\sim 10^5$ kg. On cooling, the reaction is expected to reverse rather than condense the $Be(OT)_2$ since the total temperature range in the present application is far above the $Be(OT)_2$ stability range. Thus tritium trapping in this form is not expected. The BeO temperature limit is thus not set on compatibility considerations, but rather mechanical properties as discussed above.

Be_2C. For the thermal decomposition of Be_2C, the experimental results of Ref. 2-22 were taken directly. The Be overpressure is given in this case by $P_{Be} = \sqrt{K}$ and is shown in Fig. 2-2. The figure shows that a temperature limit of 1600 K would maintain the overpressure due to decomposition below 1 Pa. This temperature is relatively low and would suggest that a SiC coating be applied to the Be_2C which would contain the overpressure, allowing the limiting temperature to be that of the SiC, 2100 K. With a coating, reactions of Be_2C with T_2O are precluded. Nonetheless, as in the case of BeO, mass transport via reaction of uncoated Be_2C with T_2O would not present a temperature limitation. Finally, it is noted that though Be_2C hydrolyses to methane at low temperatures, it does not do so at the temperatures of present interest.

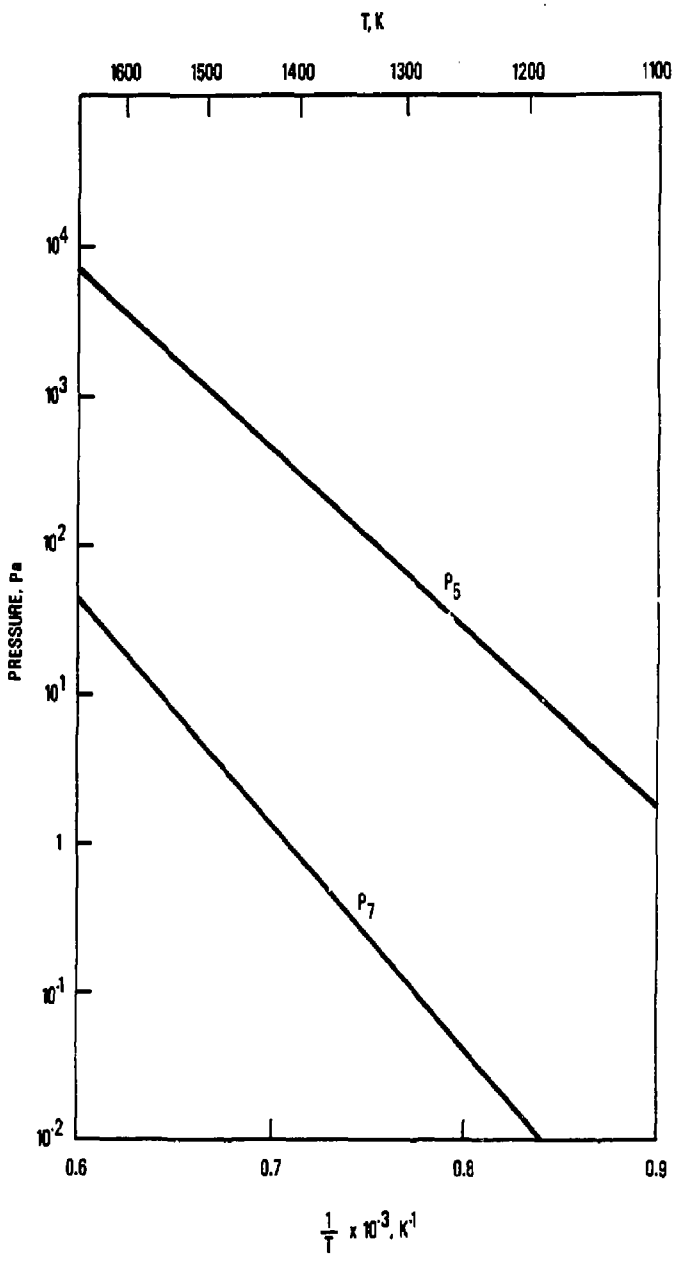

Figure 2-2. Overpressure versus material temperature, Reactions 5 and 7 of Table 2-3.

2.4. THERMODYNAMICS OF BLANKET OPTIONS

2.4.1. Introduction

This section presents the thermodynamic performance of candidate blankets for Cascade. To minimize the number of blanket designs investigated in detail, we performed a preliminary screening of the possible material combinations based on the following:

- LiO_2 is the only ceramic tritium-breeder which is capable of achieving an adequate tritium-breeding ratio (TBR) without a neutron multiplier. Thus, a blanket with SiC as the high-temperature surface layer material and LiO_2 as the tritium-breeder is attractive.

- If the surface layer is a neutron multiplier, then $LiAlO_2$ is more attractive than LiO_2 as the breeder because it has higher temperature capability and avoids LiOT compatibility concerns.

- Among the ceramic Be neutron-multipliers, BeO offers the highest temperature capability if uncoated. If a coating is required, Be_2C is the preferred kernel material.

The three prime material combinations selected are

- SiC surface layer, LiO_2 tritium-breeder,

- BeO surface layer, $LiAlO_2$ tritium-breeder, and

- SiC-coated Be_2C surface layer, $LiAlO_2$ tritium-breeder.

These are shown in Table 2-5 along with the applicable temperature limits from Table 2-4.

TABLE 2–5
MAXIMUM COMPATABILITY TEMPERATURE LIMITS OF PRIME CANDIDATE BLANKETS, K

	Materials Reaction Chamber/ Breeder/Front Zone	Reaction Chamber	Reaction Chamber/ Breeder/ Interface	Breeder	Breeder Front Zone/ Interface	Front Zone	Front Zone/ Coating Interface
1.	$SiC/Li_2O/SiC$	2100	1400	1400 *(peak)* 1200 *(avg)*	1200	2100	
2.	$SiC/LiAlO_2/BeO$	2100	1500	1500	1500	2300	
3.	$SiC/LiAlO_2/Be_2C–SiC$	2100	1500	1500	1500	2100	2100

In the next section, we present a preliminary comparison of the power-producing potential of these three blankets. Section 2.4.3 then presents the results of a first-order optimization performed on the $BeO/LiAlO_2$ blanket. It also presents the reference blanket design used in subsequent secondary system design and tritium analyses.

2.4.2. Preliminary Thermodynamic Performance Comparison

The Cascade blanket consists of a high-temperature front zone, followed by a tritium-breeding zone. From a thermodynamics perspective, the determination of the relative thicknesses of these zones is a neutronics optimization problem bounded by the need to achieve an acceptable TBR while maximizing the energy delivered by the blanket as well as the allowable delivery temperature. The power-producing potential of a Cascade blanket is highly dependent on the thermal conversion efficiency allowed by the outlet temperature distribution of the granules delivered from the reaction chamber to the primary heat exchanger. The allowable delivery temperature is a neutronics design problem because the chamber outlet temperature distribution is highly dependent on the nuclear heat deposition profile, in addition to the velocity flow distribution and degree of granule mixing within the blanket.

Figure 2-3 is a schematic representation of the blanket parameters entering the calculation of the outlet temperature distribution. Note that a surface layer of high-temperature material is explicitly shown in Fig. 2-3 moving at mass flow rate $\dot{m}_{SL}$. This surface layer accommodates the high surface heat flux and is independently controlled to move at a much higher velocity than the rest of the blanket. This rapid, highly turbulent surface layer has been experimentally observed (Ref. 2-23). The front zone and breeder zone move at rates of $\dot{m}_{FZ}$ and $\dot{m}_{BZ}$ with a parabolic velocity profile given by (Ref. 2-23)

$$v(r) = v_o[1 - 0.9(r - r_o)^2],$$

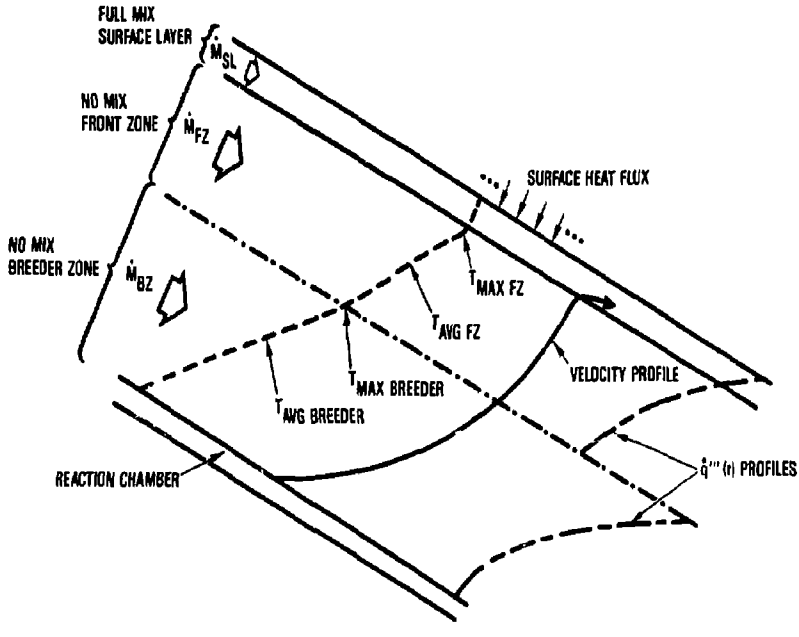

Figure 2-3. Schematic representation of parameters entering the calculation of blanket temperature distribution.

where r is the distance from the center of the chamber, r_o is the distance to the surface layer, and v_o is the velocity of the front zone just inside the surface layer. The volumetric neutron heat generation rate profile in the high-temperature front and breeder zones is given by $\dot{q}'''_{FZ}(r)$ and $\dot{q}'''_{BZ}(r)$.

The temperature distribution within the blanket can be obtained by examining a differential volume element for conservation of energy. Thus, the energy deposited via neutron absorption is equated to the energy transported to the heat exchanger by

$$v(r)c_p\Delta T(r)\cdot 2\pi r dr = \dot{q}'''(r)\cdot 4\pi r^2 dr,$$

where c_p is the specific heat of the material at radius r, and $\Delta T(r)$ is the temperature rise of the differential volume element in traversing the reaction chamber. Though the Cascade reaction chamber has a conical geometry, little error is introduced by this spherical approximation. This equation is solved for $\Delta T(r)$ so that for a uniform inlet temperature distribution, the outlet temperature distribution can be calculated. The optimum outlet temperature distribution is obtained by calculating v_o to satisfy the temperature limits given in Table 2-5. The temperature rise of the surface layer is treated similarly, except the velocity profile is constant through the cross-section due to full mixing, and in addition it handles the surface heat flux. The Cascade blanket can thus deliver energy to the heat exchanger at the three distinct temperatures of the surface layer, the front zone and the breeder zone.

The most useful figure-of-merit with which to evaluate blanket options at this stage in conceptual design is gross electrical output. With a single power conversion system working fluid, the gross electrical output, P_1, is given by

$$P_1 = P_{blanket}\times\eta_1(T_1),$$

where $P_{blanket}$ is the total thermal energy delivered by the blanket to the heat exchanger, and $\eta_1(T_1)$ is the power conversion system efficiency for a working fluid peak temperature of T_1. T_1 is given by

$$T_1 = T_{inlet,BZ} + \frac{\Delta T_{BZ}}{f_{BZ}} - \Delta T_{HX},$$

where $T_{inlet,BZ}$ is the uniform temperature of breeder material inlet to the reaction chamber, ΔT_{BZ} is the average temperature rise of the breeder zone, f_{BZ} is the fraction of energy deposited in the breeder zone, and ΔT_{HX}, the temperature drop across heat exchanger heat transfer areas is assumed to be 300 K. If three power conversion system working fluids are used, the gross electrical power output, P_3, is given by

$$P_3 = P_{blanket} \times \eta_3,$$

where η_3, the power-averaged efficiency is given by

$$\eta_3 = \sum_{i=SL,FZ,BZ} \eta(T_{outlet,i} - \Delta T_{HX}) \times f_i,$$

where $T_{outlet,i}$ is the average outlet temperature of zone i.

The thermodynamic performance was uniformly evaluated for three prime candidate blankets of comparable high-temperature zone neutronic thicknesses and total mass flow rates. The results are shown in Table 2-6. Neutronic performance data for the blankets were obtained from Ref. 2-24. Thermal conversion efficiencies at temperature are taken from Chapter 3. The results of this preliminary assessment show that the $BeO/LiAlO_2$ blanket has the highest temperature, efficiency and gross electrical power production capability, achieving a peak working fluid temperature of 860 K, a corresponding thermal efficiency of 47%, and 1540 MW of electrical output power for 3000 MW of fusion power. It was thus selected for the limited optimization presented in the next section. It is followed closely by the SiC/LiO_2 blanket. The results also show that the efficiency can be increased 3 to 6 points (70 to 100 MW) by using multiple power conversion system working fluids, each optimized to an individual zone. This increase probably does not offset the increased capital cost and complexity of the power conversion system.

TABLE 2-6
THERMODYNAMICS OF CANDIDATE BLANKETS
(3000 MW FUSION)

Blanket Option	SiC/Li_2O	$BeO/LiAlO_2$	Be_2C-$SiC/LiAlO_2$
Blanket power, MW(t)	3210	3280	3260
Total $\dot{m}$, m^3/s	5.2	5.2	5.2
Surface Layer			
Power fraction	0.29	0.29	0.29
$T_{avg\ outlet}$, K (η_1)[1]	2100 (0.65)	2300 (0.65)	2100 (0.65)
T_{inlet}, K	1600	2050	1700
$\dot{m}$, m^3/s	1.5	1.4	1.4
Front Zone			
Power fraction	0.08	0.12	0.11
$T_{avg\ outlet}$, K (η_1)[1]	1220 (0.48)	1500 (0.55)	1580 (0.57)
T_{inlet}, K	800	1200	1100
$\dot{m}$, m^3/s	0.5	0.5	0.5
Breeder Zone			
Power fraction	0.63	0.59	0.60
$T_{avg\ outlet}$, K (η_1)[1]	920 (0.40)	950 (0.40)	760 (0.35)
T_{inlet}, K	700	650	450
$\dot{m}$, m^3/s	3.2	3.3	3.3
T_1, K (ΔT, K)[2]	750 (350)	860 (510)	670 (520)
η_1	0.45	0.47	0.40
P_1, MW(e)	1440	1540	1300
η_3	0.48	0.49	0.46
P_3, MW(e)	1540	1610	1500

[1] Efficiency in parenthesis is evaluated at $T_{avg\ outlet} - \Delta T_{HX}$, assuming $\Delta T_{HX} = 300$ K.

[2] ΔT in parenthesis is total temperature rise of working fluid

2.4.3. Reference Blanket Design

The $BeO/LiAlO_2$ blanket is optimized by maximizing the energy delivered by the blanket as well as the delivery temperature. The constraints on this optimization are the need to achieve adequate TBR and the compatibility temperature limits. The controlling variables in this optimization are the neutronic thicknesses of the two material zones and the mass flow rates. The thermodynamic performance of three BeO-$LiAlO_2$ blankets of selected BeO zone thicknesses and mass flow rates are shown in Table 2-7. The gross electrical power output figures-of-merit P_1 and P_3 are displayed versus blanket volume flow rate in Figure 2-4. The neutronic data for these blankets were obtained from Ref. 2-25. All blankets achieve a TBR>1. For a given mass flow rate, the inlet temperature to each zone was adjusted to maintain the peak temperatures below the limits given in Table 2-5.

Thicker BeO zones maximize the energy delivered by the blanket by increasing blanket energy multiplication through increased neutron multiplication. Thicker BeO zones, however, also thermalize neutrons to a greater degree, limiting the penetration of the neutrons into the $LiAlO_2$ zone and resulting in highly peaked volumetric heat generation rates. The effect of thicker BeO zones is that the bulk of the energy in the breeder zone is deposited in a very narrow region near the BeO zone, resulting in more highly peaked temperature profiles of lower average temperature and requiring very high mass flow rates to meet the compatibility temperature limits. Thinner BeO zone blankets have flatter volumetric heat generation rates and temperature distributions, and thus have higher average outlet temperatures and lower mass flow rate requirements.

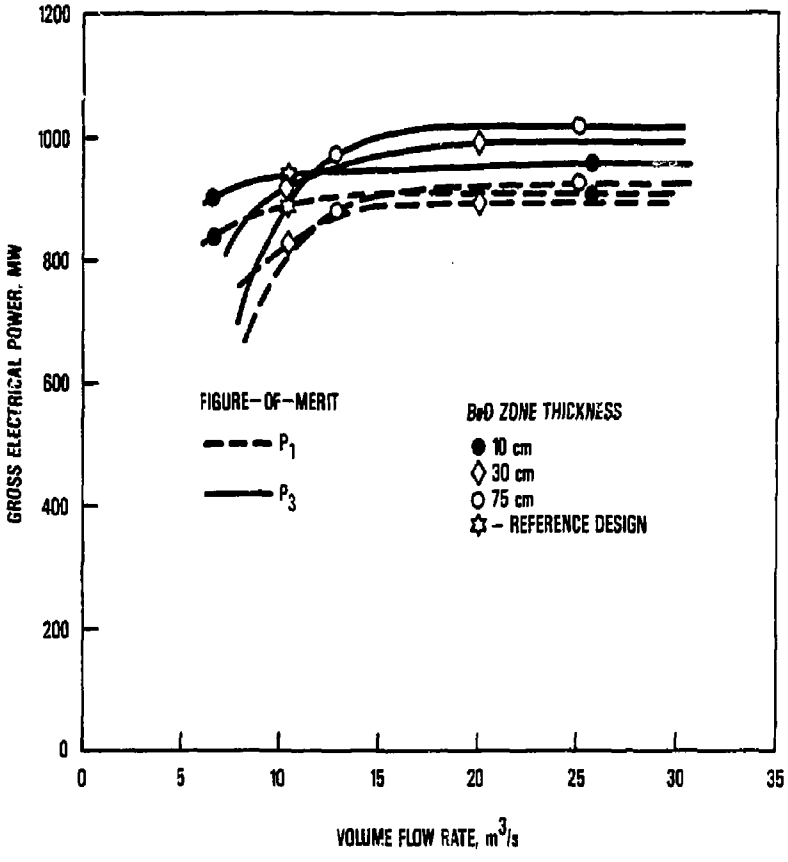

Figure 2-4. Gross electrical power output versus total blanket volume flow rate.

TABLE 2-7
THERMODYNAMICS OF CANDIDATE BLANKETS
(1500 MW FUSION)

BeO zone thickness, m	0.10	0.10	0.30	0.30	0.75	0.75
Blanket power, MW(t)	1670	1670	1790	1790	1840	1840
Total $\dot{m}$, m^3/s	5.3	26	10.4	20	13	25
Surface Layer						
Power fraction	0.29	0.29	0.27	0.27	0.26	0.26
$T_{avg\ outlet}$, K (η_1)	2300 (0.65)	2300 (0.65)	2300 (0.65)	2300 (0.65)	2300 (0.65)	2300 (0.65)
T_{inlet}, K	2100	2100	2100	2100	2100	2100
$\dot{m}$, m^3/s	1.0	1.0	1.0	1.0	1.0	1.0
Front Zone						
Power fraction	0.13	0.13	0.31	0.31	0.49	0.49
$T_{avg\ outlet}$, K (η_1)[1]	1510 (0.55)	1500 (0.55)	1510 (0.55)	1505 (0.55)	1540 (0.56)	1510 (0.55)
T_{inlet}, K	1350	1475	1450	1450	1475	1475
$\dot{m}$, m^3/s	0.6	3.3	3.7	7.4	10.6	21.2
Breeder Zone						
Power fraction	0.58	0.58	0.42	0.42	0.24	0.24
$T_{avg\ outlet}$, K (η_1)	1240 (0.48)	1450 (0.54)	1020 (0.40)	1260 (0.49)	820 (0.35)	1160 (0.47)
T_{inlet}, K	1100	1425	950	1225	700	1100
$\dot{m}$, m^3/s	3.7	21.8	5.8	11.5	1.5	3.0
T_1, K (ΔT, K)[2]	1040 (240)	1170 (45)	820 (170)	1030 (80)	900 (500)	1050 (250)
η_1	0.50	0.54	0.46	0.50	0.48	0.50
P_1, MW(e)	835	900	820	890	880	920
η_3	0.54	0.57	0.51	0.55	0.53	0.55
P_3, MW(e)	900	950	910	985	970	1010

[1] Efficiency in parenthesis is evaluated at $T_{avg\ outlet} - \Delta T_{HX}$, assuming $\Delta T_{HX} = 300$ K.

[2] ΔT in parenthesis is total temperature rise of working fluid

For consistency, it is necessary to compare blankets at comparable flow rates. Figure 2-4 shows that at comparable mass flow rates, the blankets have comparable gross electric power output. The gross electric output is a mild function of blanket flow rate above ~10 m^3/s for thinner BeO blankets, ~15 m^3/s for thicker BeO blankets. Since thinner BeO zone blankets have higher efficiencies, minimize Be inventory requirements and allow lower mass flow rates, a 10 cm BeO zone blanket is preferred for the reference design.

The thermodynamic performance of the BeO/$LiAlO_2$ Cascade blanket is presented in Table 2-8. The thermodynamic performance of the C/BeO/$LiAlO_2$ blanket, in which carbon is used for the surface layer as discussed below, is also included in the table. The resultant temperature and velocity profiles within the blankets are shown in Figs. 2-5 and 2-6. The first blanket delivers surface granules of BeO at 2300 K average temperature, the balance of the BeO front zone granules at 1505 K, and the $LiAlO_2$ at 1385 K. This allows a power conversion system efficiency of 55% with a single-fluid peak temperature of 1300 K using the optimized Brayton cycle power conversion system presented in Chapter 3. The total blanket volume flow rate is 11 m^3/s, delivering 1670 MW of thermal energy to the heat exchanger. The gross power conversion system output is 920 MW electrical.

If vaporization/recondensation of BeO presents a chamber evacuation problem, elemental pyrolytic carbon can be used for the surface layer granules. Following the same methodology of Section 2.3, Compatibility Temperature Limits, we determined a 1600 K temperature limit for the C/BeO interface for an overpressure limit of 1 Pa. A plot of overpressure versus interface temperature is shown in Fig. 2-7. The carbon is not expected to diffuse through the BeO zone into the $LiAlO_2$ zone. If it did, the temperature limit of the $LiAlO_2$ would be 1300 K at 1 Pa and 1400 K at 10 Pa, as shown in Fig. 2-8. Neutronically, this blanket is very similar to that presented above. This blanket would thus deliver surface granules of C at 1600 K average temperature, the BeO front zone granules

TABLE 2-8
THERMODYNAMICS OF $BeO/LiAlO_2$ AND
$C/BeO/LiAlO_2$ BLANKETS

	$BeO/LiAlO_2$	$C/BeO/LiAlO_2$
Fusion power, MW	1500	1500
Blanket power, MW(t)	1670	1670
Total $\dot{m}$, m^3/s	10.6	10.7
Surface Layer		
Power fraction	0.29	0.28
T_{inlet}, K	2100	1500
$T_{avg\ outlet}$, K	2300	1600
$\dot{m}$, m^3/s	1.0	2.2
Peak chamber exit velocity, m/s	1.9	4.4
Front Zone		
Power fraction	0.13	0.13
T_{inlet}, K	1435	1410
$T_{avg\ outlet}$, K	1505	1505
$\dot{m}$, m^3/s	1.3	1.0
Peak chamber exit velocity, m/s	0.25	0.22
Breeder Zone		
Power fraction	0.58	0.59
T_{inlet}, K	1325	1285
$T_{avg\ outlet}$, K	1385	1355
$\dot{m}$, m^3/s	8.4	7.5
Peak chamber exit velocity, m/s	0.25	0.22

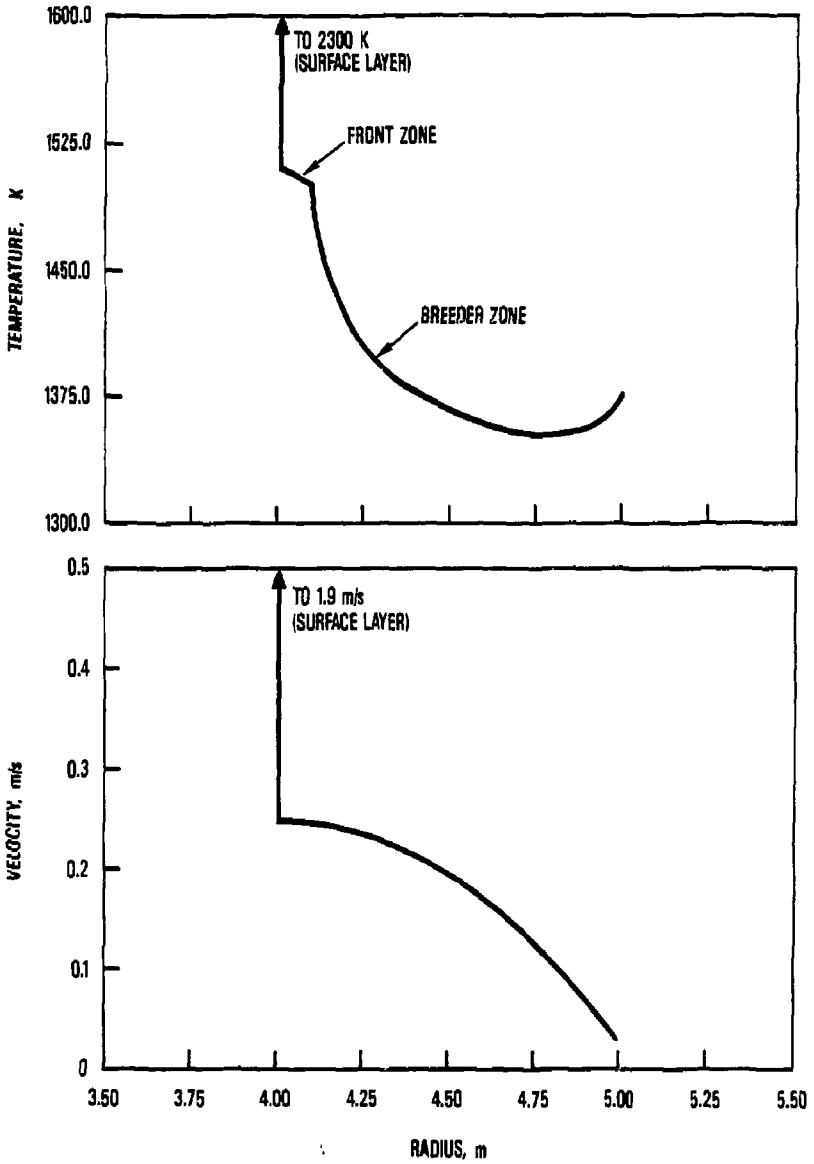

Fig. 2-5. Temperature and velocity profiles for the $BeO/LiAlO_2$ blanket.

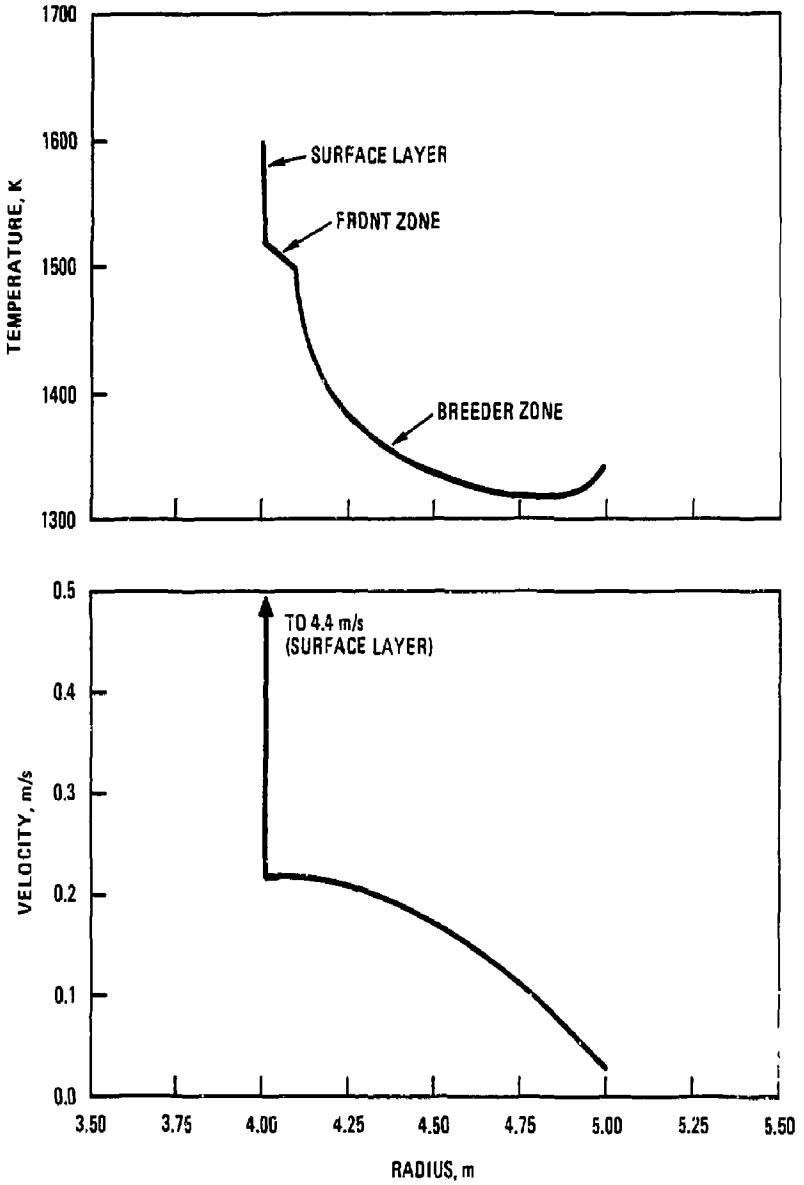

Fig. 2-6. Temperature and velocity profiles for the C/BeO/$LiAlO_2$ blanket.

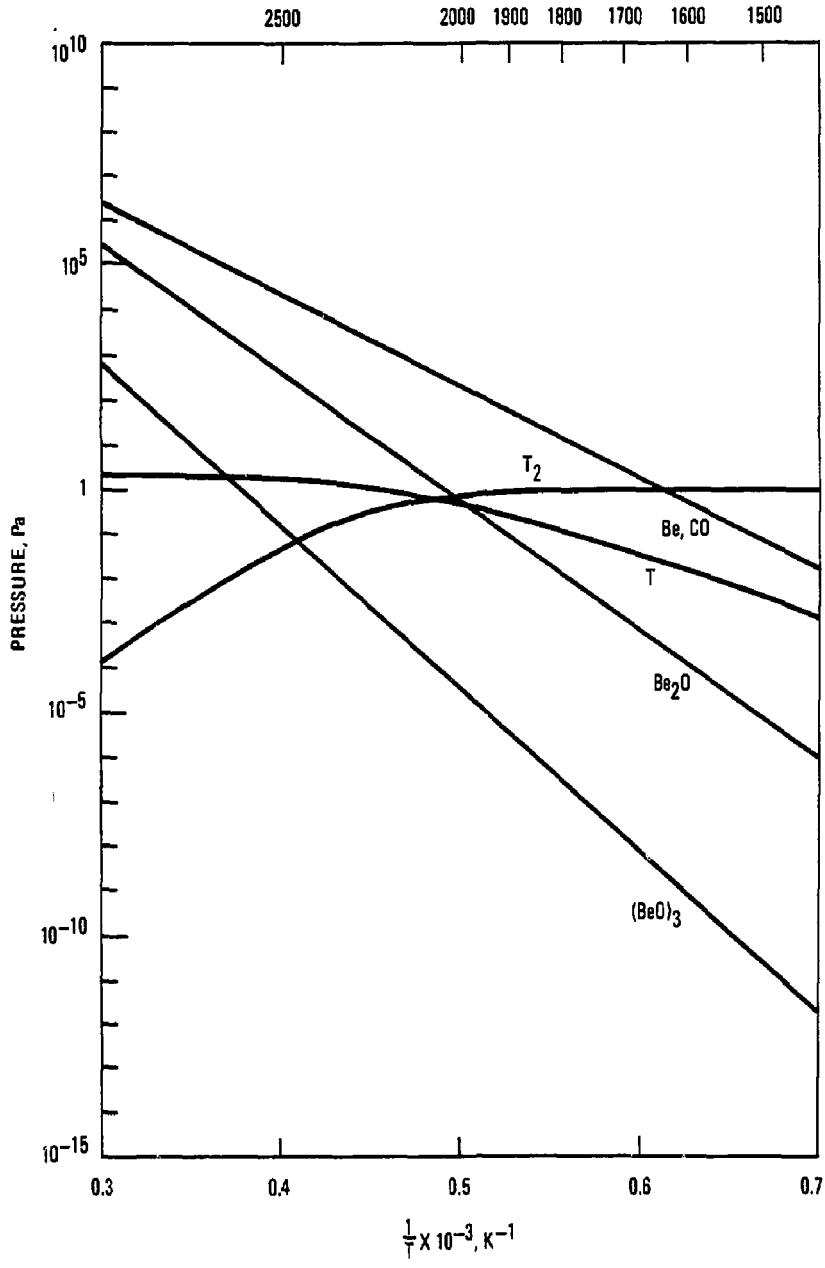

Fig. 2-7. Overpressure versus temperature at C/BeO interface.

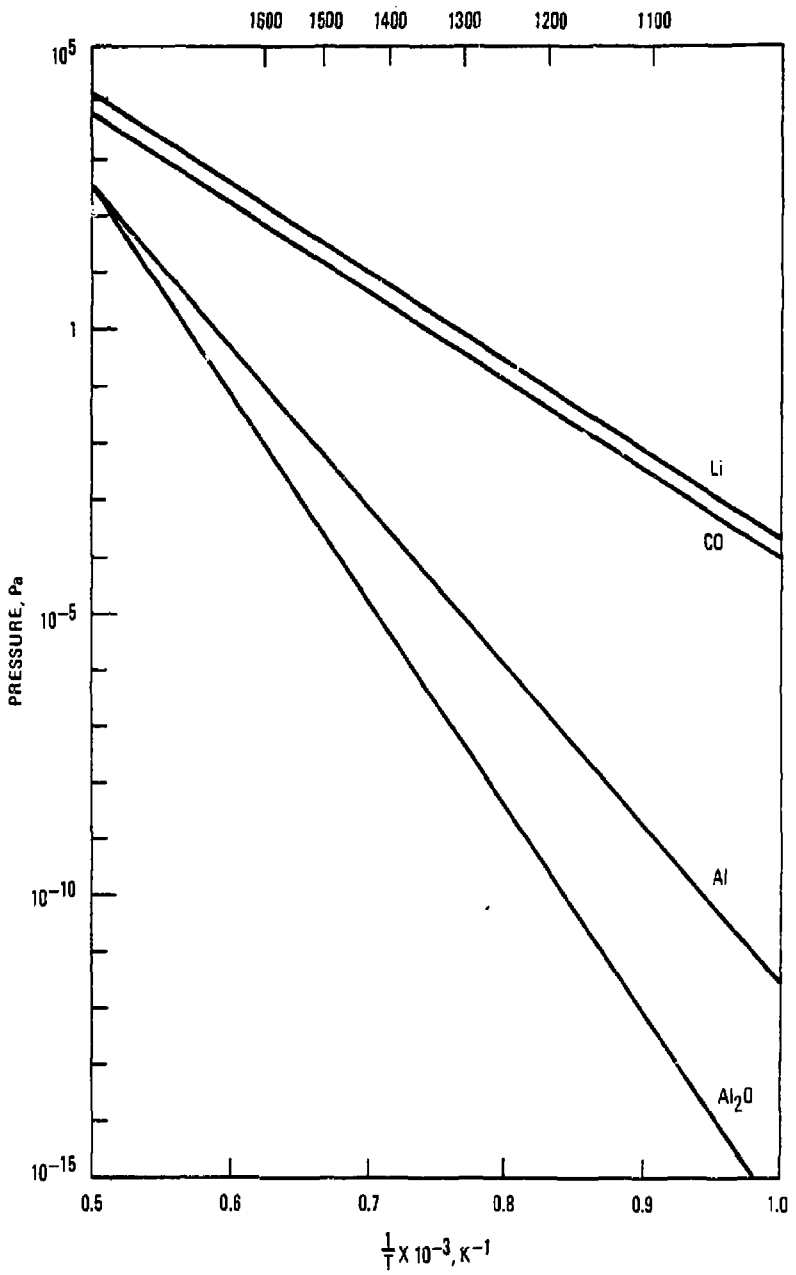

Fig. 2-8. Overpressure versus temperature at $C/LiAlO_2$ interface.

at 1505 K, and the $LiAlO_2$ granules at 1355 K. This also allows a power conversion system efficiency of 55% with a single-fluid peak temperature of 1300 K using the optimized Brayton cycle power conversion system presented in Chapter 3. The heat exchanger areas for this blanket would be greater than those of the blanket with BeO surface granules due to the smaller granule-working fluid temperature differentials. The total blanket flow rate, thermal power, and electrical power are the same for both blankets.

References for Chapter 2

2-1. J. H. Pitts, "Cascade: A Centrifugal-Action Solid-Breeder Reaction Chamber," *Nuclear Technology/Fusion*, Vol. 4, No. 2, part 3, September 1983, p. 967.

2-2. I. Maya, K. R. Schultz, *et al.*, "Inertial Confinement Fusion Reaction Chamber and Power Conversion System Study," GA Technologies Report, GA-A17267, September 1984; also Lawrence Livermore National Laboratory Report, UCRL-15642.

2-3. G. R. Hopkins and R. J. Price, "Fusion Reactor Design with Ceramics," *Nuclear Engineering Design/Fusion, 2* (1985).

2-4. GA Fusion Staff, "Fusion Reactor Design Studies," GA Technologies Report GA-A13430, April 1975.

2-5. "1984 Materials Selector," *Materials Engineering*, Special Issue, December 1983.

2-6. C. E. Johnson, *et al.*, "Solid Breeder Blankets", International Atomic Energy Agency Report ETR-INTOR/DIS/NUS/3, Chapter X (1984).

2-7. R. J. Price, "Properties of Silicon Carbide for Nuclear Fuel Particle Coatings," *Nuclear Technology*, Vol. 35, September 1977, p. 320. (1977).

2-8. M. T. Simnad, *et al.*, "BeO - A Review of Nuclear Applications," *Proc. Conf. on Nuclear Applications for Non-Fissionable Ceramics* (ed. A. Boltax and J.H. Handwerk), American Nuclear Society, 1966, p.169.

2-9. *Thermophysical Properties of Matter* (ed. Y. S. Toulokian, *et al.*), IFI/Plenum, New York, 1970.

3. POWER CONVERSION SYSTEM DESIGN

3.1. INTRODUCTION

The high blanket temperatures possible with Cascade offer the potential for high thermal conversion efficiencies. In the initial phase of this work, we evaluated a number of power conversion system options with respect to net thermal efficiency versus the peak working fluid temperature. These include three primary power cycle options: Rankine, with water working fluid; Brayton, with helium working fluid (an ideal gas); and a Rankine/Brayton hybrid called the Field cycle, [Ref. 3-1] also with water working fluid; and secondary options, including combinations of these in the form of topping and bottoming cycles, differing working fluids, nonideal gas Brayton cycles, such as the supercritical CO_2, and dissociating gas cycles. The results of this initial scoping study are presented in Section 3.2.

In the second phase of this work, selected power conversion systems were tailored to accommodate the power fraction outputs and inlet/outlet temperatures of the Cascade blanket. The results of this phase are presented in Sections 3.3 and 3.4. At the desired operating temperatures, the only functional materials are ceramics. In Section 3.5, we present the design of a ceramic heat exchanger which can accommodate the high temperatures.

3.2. SURVEY OF SECONDARY SYSTEM OPTIONS

3.2.1. Introduction and Power Cycle Options

An attractive power conversion system must have a high average heat addition temperature, a low average heat rejection temperature, minimum recirculating power, and some flexibility in operating pressures. From a thermodynamics perspective, it

is average temperatures that have the greatest impact on efficiency, whereas peak temperatures are important only with respect to their impact on these averages. As discussed below, this effect is most notable with steam cycle efficiencies, which tend to climb only slowly with peak superheat temperature. A useful figure of merit is the ratio of average heat addition/rejection temperature to their respective peak values. The closer to unity the better. Unity is approached on the hot end by high temperature boiling, if applicable, or by adding reheats. On the cold end, unity is approached by rejecting heat through condensation, if possible, or by a combination of regeneration and intercooling. The methods used in maximizing the average-to-peak ratio depend on the desired operating temperatures and whether or not the chosen working fluid has a useful two-phase region in that temperature range.

All heat cycles require recompression of the working fluid after heat rejection, and this recirculating power should be minimized. Compressing a liquid, if possible, is best because the work of compression is almost negligible. It is largely because of liquid compression that the Rankine cycle surpasses all others at low temperatures. Cycles having vapor compression require wide differences in fluid volume between expansion and compression in order to produce a reasonable net output, and this requires a wide difference between heat addition and rejection temperatures. Because the latter is constrained by available heat sinks, the former must be as high as materials and working fluids will allow. If a vapor must be compressed, the closer it is to the saturation line, usually the less the work required. This is a major feature of the Field cycle discussed below.

A power cycle is more appealing if the designer has some flexibility in choosing working fluid pressures so as to balance the hot-side coolant pressure, for example, or meet heat exchanger pressure drop requirements. The Rankine cycle is an example of one that is not flexible in this respect: Because so much heat addition occurs during the boiling phase, peak pressures must be very high so as to maximize the corresponding average heat addition temperature. The resulting thick walls in the steam generator tubes produce thermal gradients and thermal stresses that historically have

limited steam temperatures to under about 860 K. Also, to reject heat through condensation at minimum temperatures, cold end pressures must be very low, resulting in overall pressure ratios of up to 8000. The result is a broad range of equipment size, from very small turbomachinery at the hot end to very large turbine blades at the cold end. Low pressure ratios are desirable not only to facilitate turbomachinery design but heat exchanger design as well.

When the power cycle, working fluid, and operating temperatures are chosen such that the two-phase region is eliminated, or rendered less important, there is more flexibility in choosing system pressures. In the limit, we have the Brayton cycle, in which the working fluid is an ideal gas. With this cycle, pressures can be freely chosen to accommodate the heat exchangers and turbomachinery. But, because pressure drops go inversely as P^2 to P^3, depending on the parameters held constant, the incentive for high pressure remains.

For our application, the power conversion system must be tailored to accommodate the power outputs and inlet/outlet temperatures of the three reactor blanket zones. Temperature differentials between the granules and the working fluid(s) must be high enough to ensure reasonable heat exchanger dimensions. In our analysis, we have assumed that log mean temperature differences of 300 K are generally adequate.

The results of the initial phase of this work are displayed in Fig. 3-1, which shows net power conversion system efficiency versus peak working fluid temperature. This initial investigation showed that when the primary power cycle options are made reasonably sophisticated, such as by adding reheats, intercoolers, extractions, and the like, they become so efficient that the secondary options show no advantage. The latter were thus considered no further. In addition, with the temperatures achievable with a lithium aluminate blanket with a surface layer of BeO, net thermal conversion efficiencies in the range of 50% to over 60% were possible with the three primary cycles. These are further discussed below.

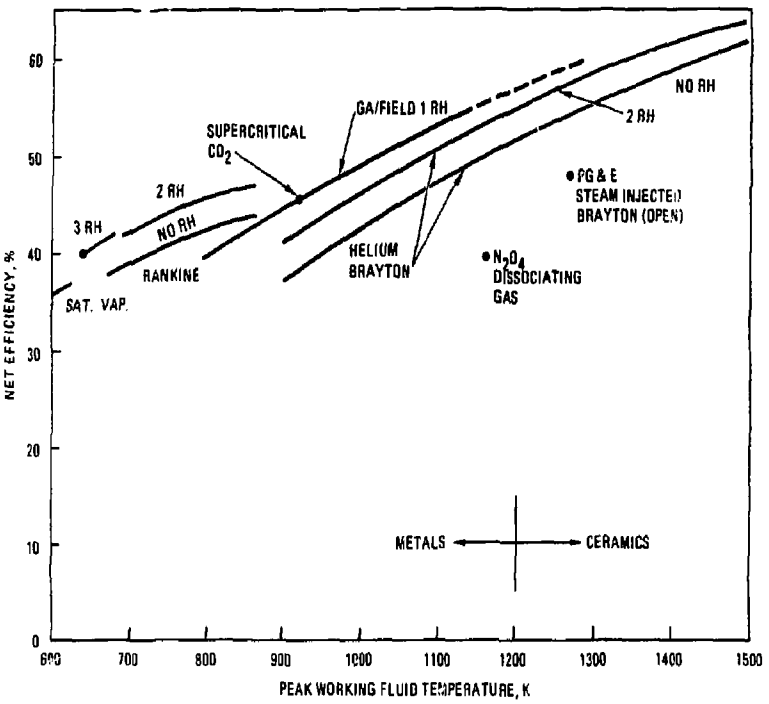

Fig. 3-1. Net efficiencies vs. peak temperature for several power cycles. The steam, Brayton, and GA/Field cycles are discussed in this chapter.

3.2.2. Steam Cycle

The steam cycle has shown remarkable longevity as witnessed by the fact that it still dominates in all large power plants and probably will for another century. Its success stems from good efficiency at temperatures acceptable to nonexotic metal alloys which can be readily joined leak-tight by simple welding. In addition, the working fluid is plentiful, stable, well-characterized, and nontoxic and has corrosion and other chemical properties that are controllable. Other possible working fluids, such as ammonia, mercury, sodium, potassium, and organics lack one of these features and consequently have made no inroads. Up to 47% net efficiency exists today (excluding stack loss) with steam cycles having two reheats and 7-8 feedwater extractions. These cycles operate supercritically with feedpump outlet pressures of 30 MPa (4400 psia) and temperatures of 839 K (1050°F). Attempts to go to higher pressures or temperatures have been made only in fossil-fueled plants, and have met with disappointment.

Figure 3-1 shows that steam cycle efficiency increases rather slowly with increasing peak superheat temperature. This is because increases in the peak temperature generally increase average heat addition temperature very slowly. Conversely, the slow variation with temperature can be exploited in fusion reactors where blanket chemistry limits coolant temperatures to low values. As shown in the figure, adding reheats does help. With three reheats, the steam cycle shown in Figure 3-2 achieves an efficiency of over 40% [Ref. 3-2] at peak temperatures of only 648 K (707°F). Because of the high efficiency at moderate temperatures, the Rankine cycle is a useful fallback option. However, Cascade blanket temperature are potentially higher and thus the steam cycle will be considered no further. The Brayton and GA-modified Field cycles are discussed below.

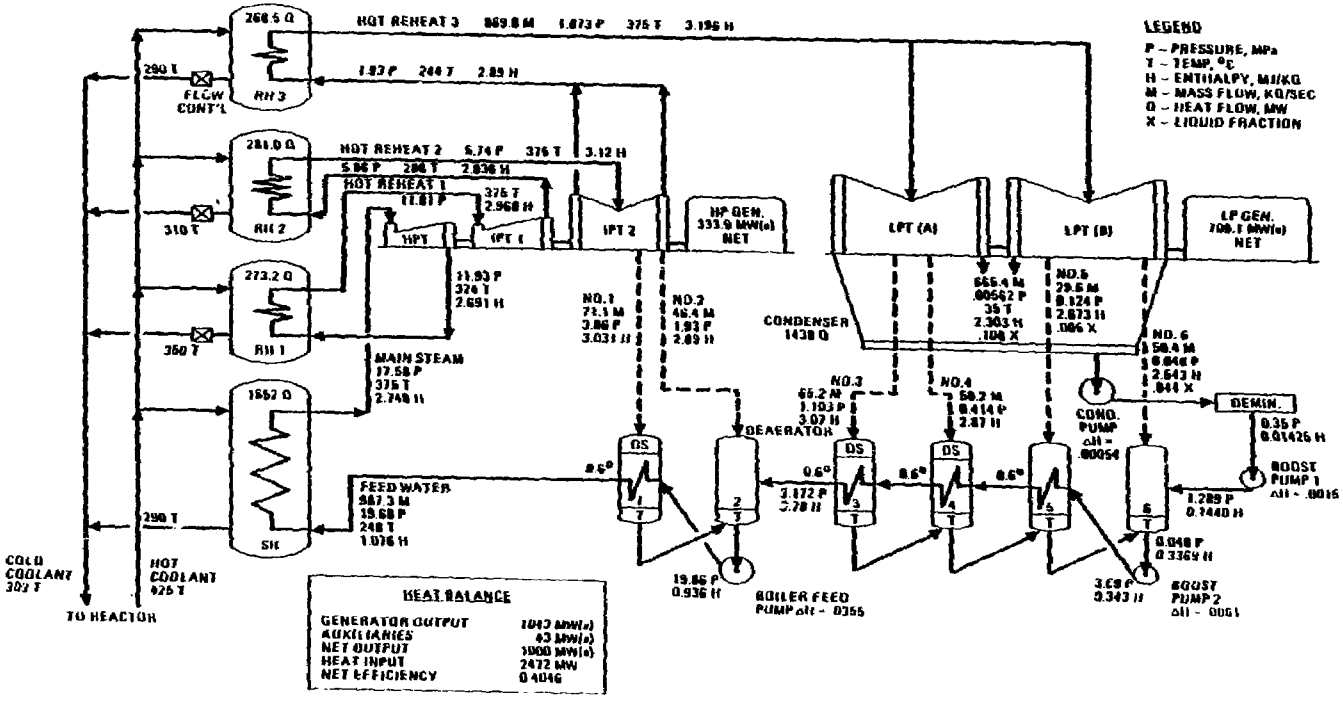

Fig. 3-2. A triple reheat steam cycle heat balance giving over 40% net efficiency at 648 K (375°C) peak steam temperature.

3.2.3. Brayton Cycle

For a given efficiency, the Brayton cycle with ideal gas compression requires the highest difference between average heat addition and average heat rejection temperatures. This difference can be increased, without increasing maximum or minimum temperatures, by dividing the compression and expansion into stages and adding intercoolers and reheats. As the number of expansion/compression processes increases, the cycle approaches an isothermal cycle, i.e., the Ericsson cycle. This is the most efficient limit for the Brayton cycle and the term Ericsson is often used for any Brayton cycle having more than one reheat and intercooler.

Figure 3-3 shows a pressure-temperature plot for a typical regenerative Brayton cycle with two reheats and two intercoolers. Although temperature-entropy (T-s) diagrams would present the same information, pressure-temperature (P-T) plots are more suitable for an ideal gas, and are simpler. Heating is represented by near-horizontal lines while compression (expansion) are shown by lines steeply sloping up (down) and to the right (left). The path around the cycle is clockwise. Note the narrow range of temperatures over which heat is added and rejected, which is indicative of high efficiency. Eliminating the reheats greatly simplifies the cycle but, as seen in Fig. 3-1, at some cost in efficiency. As seen in Fig. 3-3, an advantage in eliminating reheats is the wider spread in heat addition temperature. The two reheat cycle shown, which was not tailored to any heat source, has a net efficiency of 62.5%.

Brayton cycle efficiency is a function of pressure ratio as well as temperature. The pressure ratios around the cycle must be optimized for optimum net efficiency. (This is also true of the Field cycle discussed below.) The adiabatic efficiencies of the turbine and compressor are also a function of pressure ratio. The variations of compressor and turbine adiabatic efficiency with pressure ratio assumed in this analysis were taken from Ref. 3-3 and are shown in Fig. 3-4. Net efficiency is quite sensitive to these efficiencies, especially with the Brayton cycle. The assumed heat exchanger pressure drops were generally 1 to 2% depending on temperature rise. In general

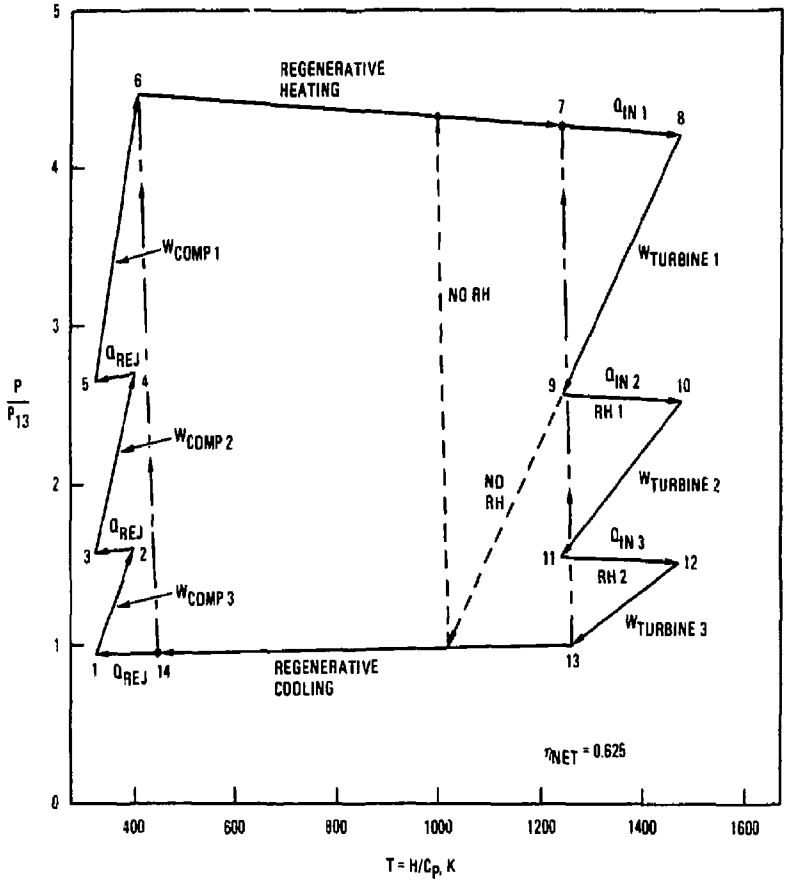

Fig. 3-3. Pressure-temperature diagram of a Brayton cycle with two reheats and two intercooling stages.

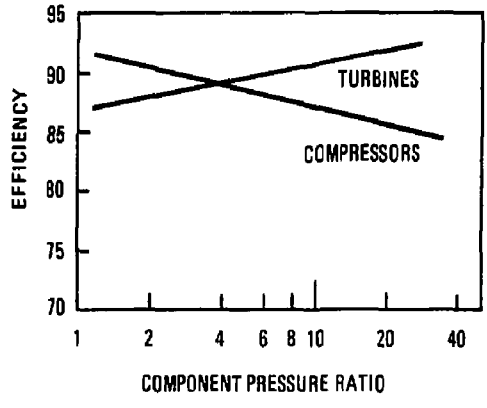

Fig. 3-4. Assumed variation of compressor and turbine adiabatic efficiency with pressure ratio (taken from Ref. 3-3).

pressure drop requirements set the lower limit on absolute pressure.

As seen in Fig. 3-1, the Brayton cycle is capable of very high efficiency provided one can achieve turbine inlet temperatures over 1200 to 1300 K. These temperatures are easier to achieve in an open-cycle gas turbine burning fossil fuel than in a closed cycle because heat addition does not have to pass through material walls, e.g., the primary heat exchanger. Nonetheless, even in the open-cycle case, consideration must be given to the highly stressed turbine blades. In both open and closed systems, ceramic blades must be considered for temperatures higher than 1200 K, although some Hastelloys retain strength to 1250 K. The high efficiency potential of the Brayton cycle makes it a prime candidate for Cascade application. It is tailored to the Cascade heat source in Section 3.3 below.

3.2.4. Field Cycle

In 1950, J.F. Field proposed a power cycle that was a blend of the Rankine and Brayton. [Ref. 3-1] Its appeal was based on the fact that (see Fig. 3-1) efficiency gains with temperature are greater for Brayton than Rankine cycles but, to achieve good absolute efficiencies in pure Brayton cycles required high temperatures. His hybrid cycle was intended to bridge the gap.

The essential elements of the original cycle proposed by Field are shown in Fig. 3-5. The T-s plane is used here rather than the P-T because it fully describes a nonideal fluid like steam. Wet steam (state 1) is compressed to saturated vapor (state 2), heated by regeneration (state 3), heated further by heat addition (state 4) and expanded through a high pressure turbine (state 5). After passing though the other side of the regenerator (state 6), the stream is split in two. Part is expanded through a low pressure turbine (state 7), then condensed to liquid (state 8) and recompressed (state 9). The other part, still superheated at state 6, is mixed with the compressed liquid to bring it back to the moist steam at the compressor inlet.

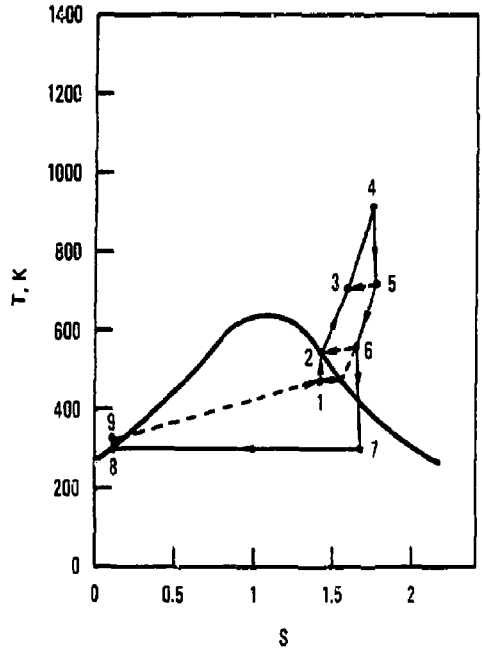

Fig. 3-5. Original Field cycle (see text).

By compressing moist steam and liquid, the work of recompressing the working fluid was substantially reduced and so the temperature spread between heat addition and rejection could be lowered. However, with wet compression in an axial compressor, the droplets would be centrifuged out. Radial blade or centrifugal compressors experienced other design or efficiency problems of their own. In addition, even if the droplets remained in the flow stream, the droplet evaporation time could be longer than the residence time in the compressor, thereby raising the work of compression because compression would essentially take place with dry steam.

Furthermore, the Field cycle did not show enough advantage over the Rankine cycle at temperatures compatible with then-contemporary materials, and thus did not gain in popularity. A subsequent paper [Ref. 3-4] explored some useful variations of the cycle, some of which have been adopted here. In Section 3.4 below, we propose additional modifications which overcome previous concerns, and explore the temperature regime of 1000 to 1200 K, where the cycle seems most attractive.

3.3. REFERENCE BRAYTON CYCLE DESIGN

The initial step in selecting a power cycle is to match the heat line of the power source. The Cascade heat line for the $BeO/LiAlO_2$ blanket is shown in Fig. 3-6. Because it is so discontinuous, we examined two Brayton cycle options to determine if the increased efficiency of a careful heat line match is worth the increased complexity. The first option, A, has three turbine expansion stages with reheats in between, similar to Fig. 3-3 except that reheat temperatures increase as the working fluid moves downstream, and turbine expansion ratios per stage are not identical. These adjustments are required to simultaneously match the power fractions in each zone of 58%, 13%, and 29% for the breeder zone, front zone, and surface layer, respectively, and achieve log-mean temperature differences in each of the heaters of about 300 K. The vertical dips shown in Fig. 3-6 indicate turbine expansion and subsequent regeneration. The second option, B, is a simple once-through system with no reheats. Criteria

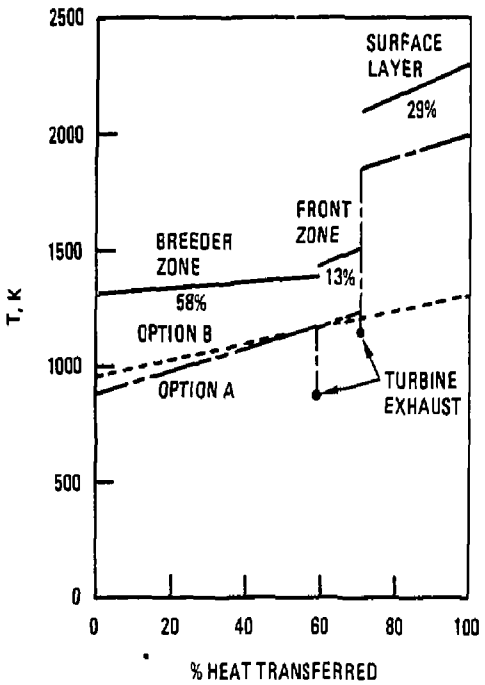

Fig. 3-6. Heat lines for Cascade blanket zones and two Brayton cycle options: A - two reheats, 300 K log-mean temperature difference everywhere, B - no reheats, 300 K minimum temperature difference.

here were relaxed in that log mean temperature difference had to be at least about 300 K, but could be much larger.

Pressure-temperature diagrams for the two options are shown in Figures 3-7 and 3-8. Both options give 54.8% net efficiency. The reason for this surprising result is that the difference in average heat addition temperatures $< T_{in} >$ is small compared to the difference in peak temperatures. As shown in the figures, it is about 1300 K for option A and 1140 K for option B. While one might expect option A to perform at least a little better based on these temperatures, such is not the case because so much of the high temperature expansions are at low pressure, and this feature reduces the available work that can be extracted. Using $< T_{in} >$ to calculate Carnot efficiencies, option A achieves 73% of Carnot while option B gets 76%. For comparison, Rankine cycles typically achieve 72 to 75% of Carnot.

Block diagrams showing flow paths and temperatures for the two options are shown in Figures 3-9 and 3-10. The increased complexity of option A is readily apparent; heater 3 and regenerator 3 both must be ceramic, as must the blades and nozzle for turbine 3. While ceramics may be required for heater 3 and the inlet turbine nozzle in option B, not only can the option B turbine blades be metal (much of the turbine expansion is in the nozzle), but the lower temperatures reduce the demands on those components that must be ceramic. Furthermore, the large log mean temperature difference of 949 K for heater 3 in option B substantially reduces the size and cost of this heat exchanger. The flexibility also exists in option B to lower the heater 3 granule temperatures.

Option B is therefore chosen as the reference design for Cascade because it achieves the same efficiency as option A with a simpler, lower temperature system. It also has a lower optimum overall pressure ratio, 2.3, compared with 3.5 for option A. For a given peak pressure, the downside regenerator pressure is therefore higher and pressure drop should be less.

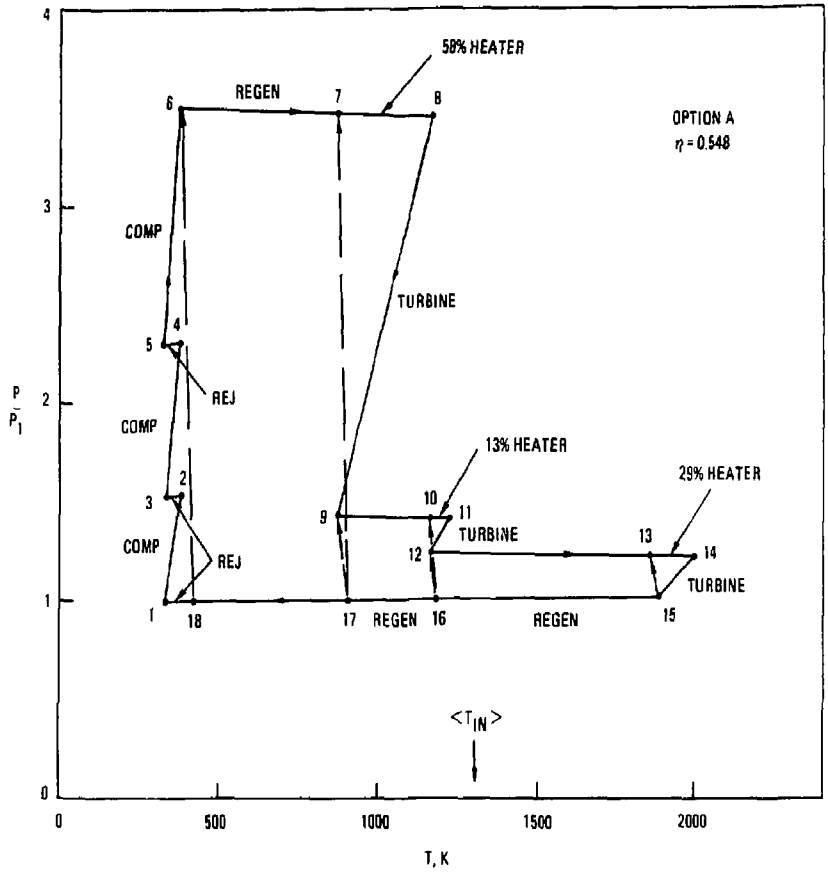

Fig. 3-7. Pressure-temperature diagram for option A.

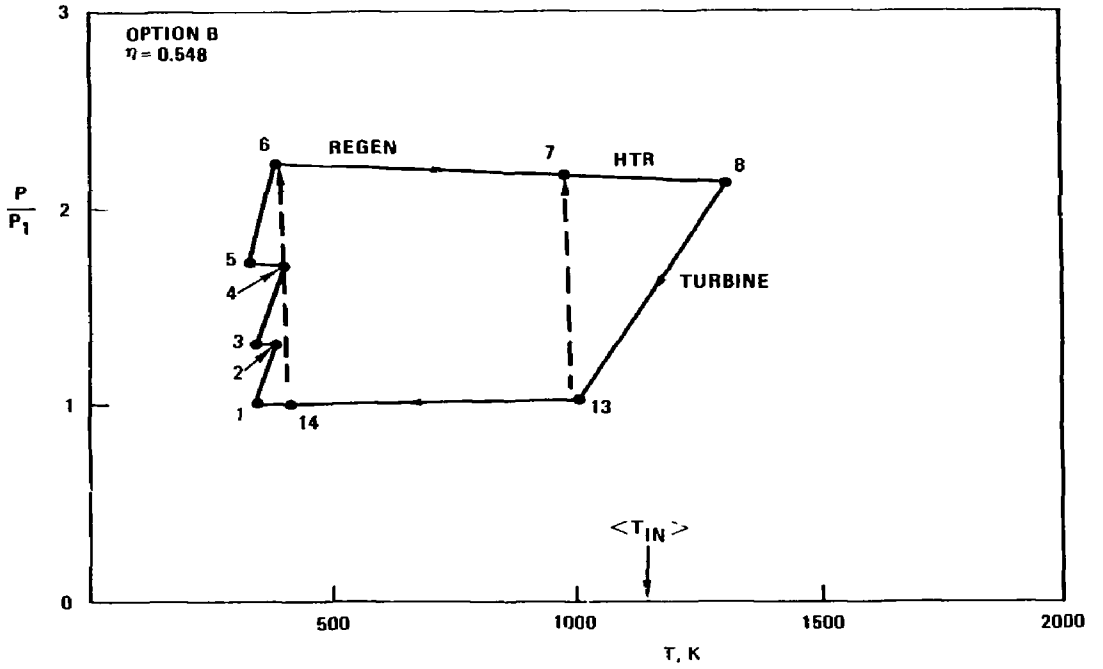

Fig. 3-8. Pressure-temperature diagram for option B.

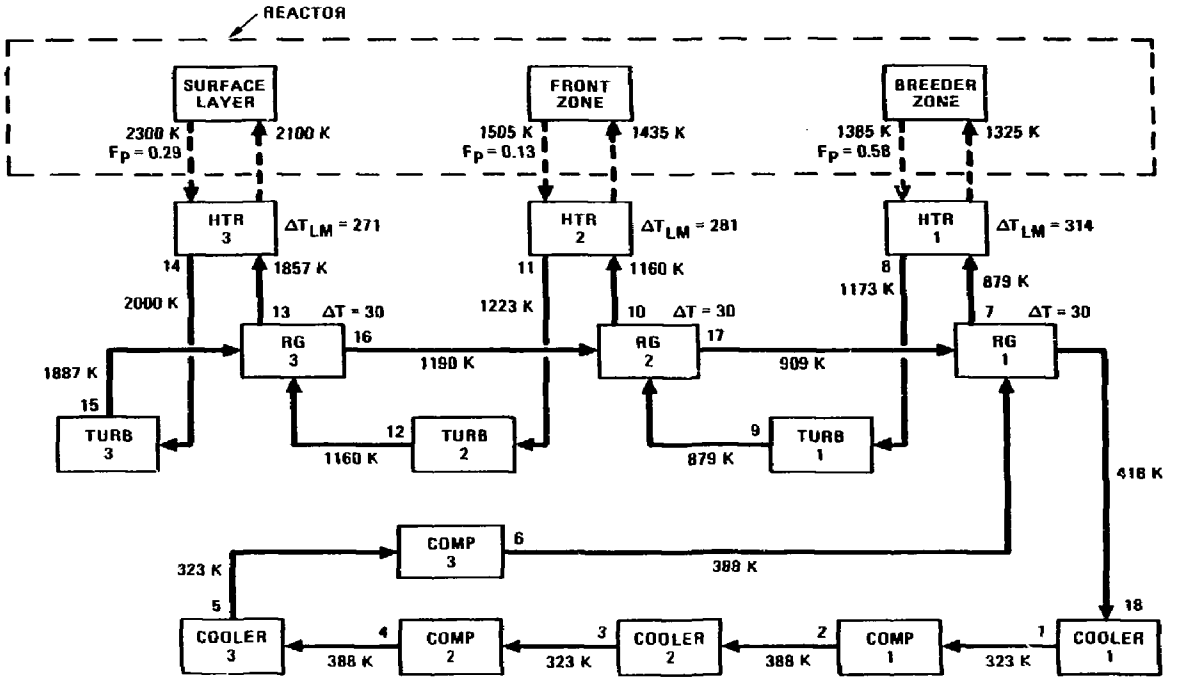

Fig. 3-9. Block diagram for Brayton cycle option A with 2 reheats, $BeO/LiAlO_2$ blanket.

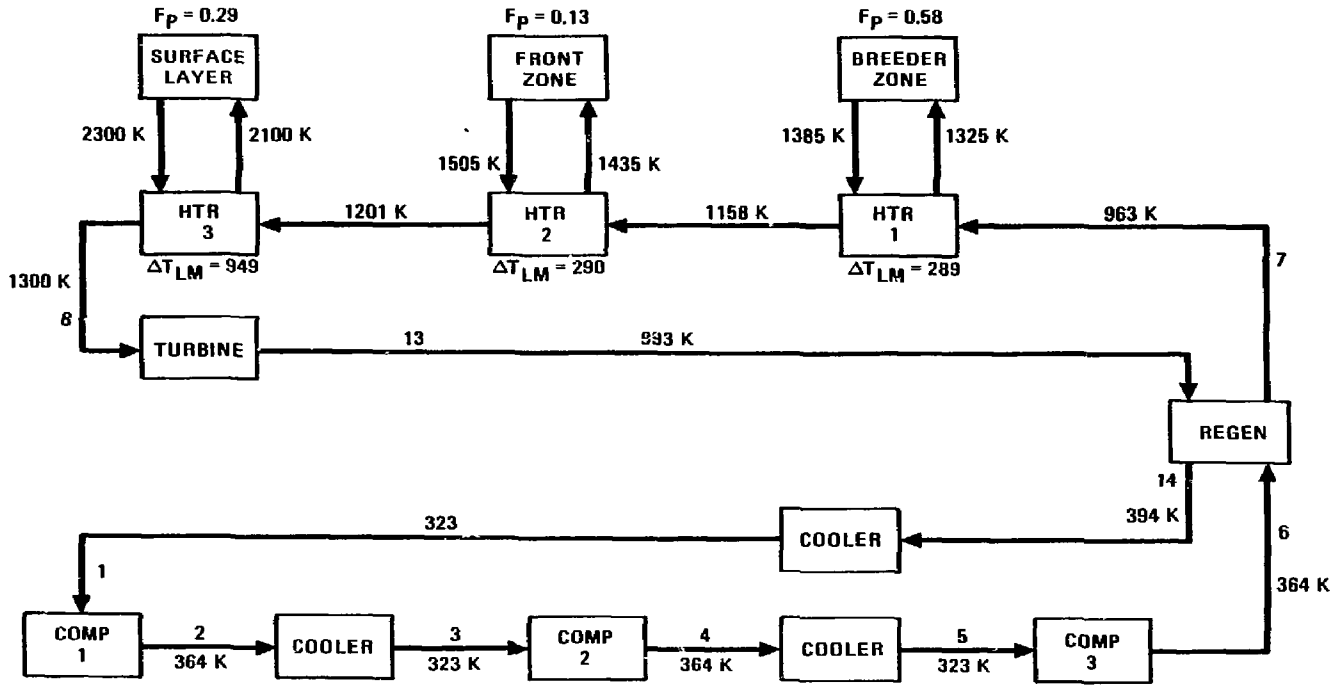

Fig. 3-10. Block diagram for Brayton cycle option B with no reheats, $BeO/LiAlO_2$ blanket.

In the double reheat option A, because the BeO surface layer contributes so little to performance, there is the question of lowering its temperature so that metal heat exchangers can be considered. To do so would require metal temperatures below about 1300 K. Figure 3-11 shows the effect of reducing the temperature of the surface layer granules. The other helium outlet temperatures were held constant and the required heat fractions from each heater were satisfied by adjusting relative turbine pressure ratios. Net efficiency falls below 52% at temperatures below 1300 K, which may still be acceptable. However, the Field cycle discussed below may be preferable at lower temperatures.

3.4. ALTERNATE FIELD CYCLE DESIGN

Figure 3-12 shows a temperature-entropy plot of the Field cycle as modified for present-day application. Parameters displayed in the figure are for the reference design discussed below. The controversial wet compression has been replaced by three stages of dry compression with liquid injection between stages to bring the steam back to saturation. Conventional axial compressors, well-developed by the aircraft industry, can now be employed. The feedwater is compressed to about 6 atm above the final compressor inlet pressure to ensure atomization in the mixing chambers. Even though the steam is dry, compression near saturation is still preferable. For example, the T-s diagram for water shown in Fig. 3-13 shows that the compression work over 100-200 psia near saturated vapor is half that needed in the ideal gas region for steam (above 800 K) for the same pressure range. Clearly, compressing the liquid portion is easiest of all.

Also shown in Fig. 3-12 is a reheat and one feedwater extraction. The reheat temperatures and high pressure turbine (HPT) expansion ratios have been tailored to match the heat line of our reactor. In this case, two regenerators are used. The reheat also decreases low-pressure turbine (LPT) exit moisture to tolerable levels (below 13%). Efficiency is fairly insensitive to extraction pressure. The latter is thus

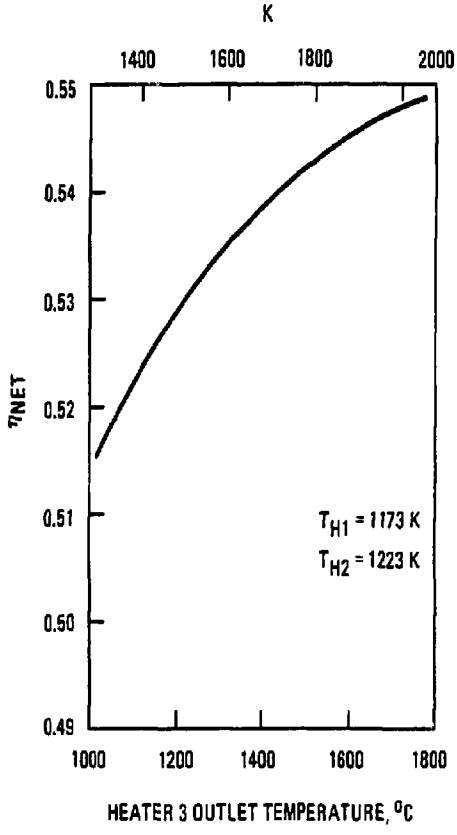

Fig. 3-11. Effect on efficiency of hot heater helium temperature. Heat fluxes from the three reactor blanket zones are constant, as are helium temperatures from the other heaters.

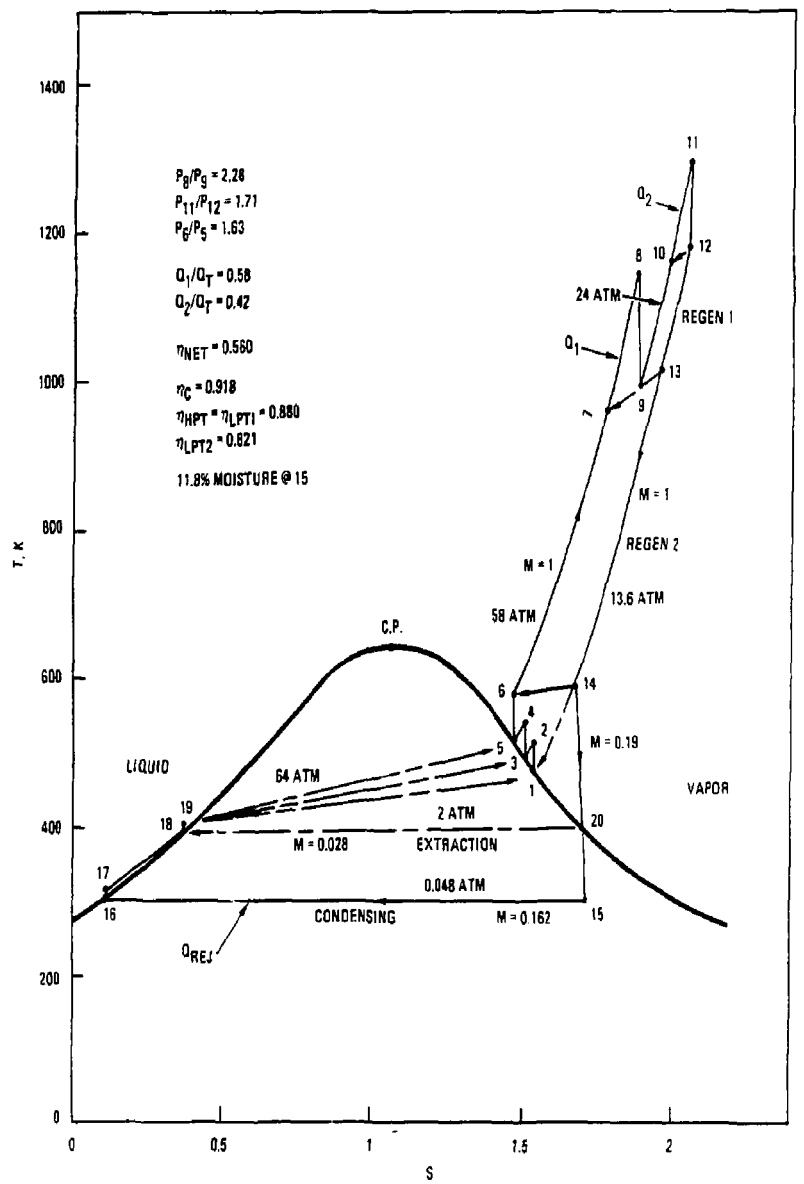

Fig. 3-12. The GA-modified Field cycle with dry compression, one reheat, and one feedwater heater.

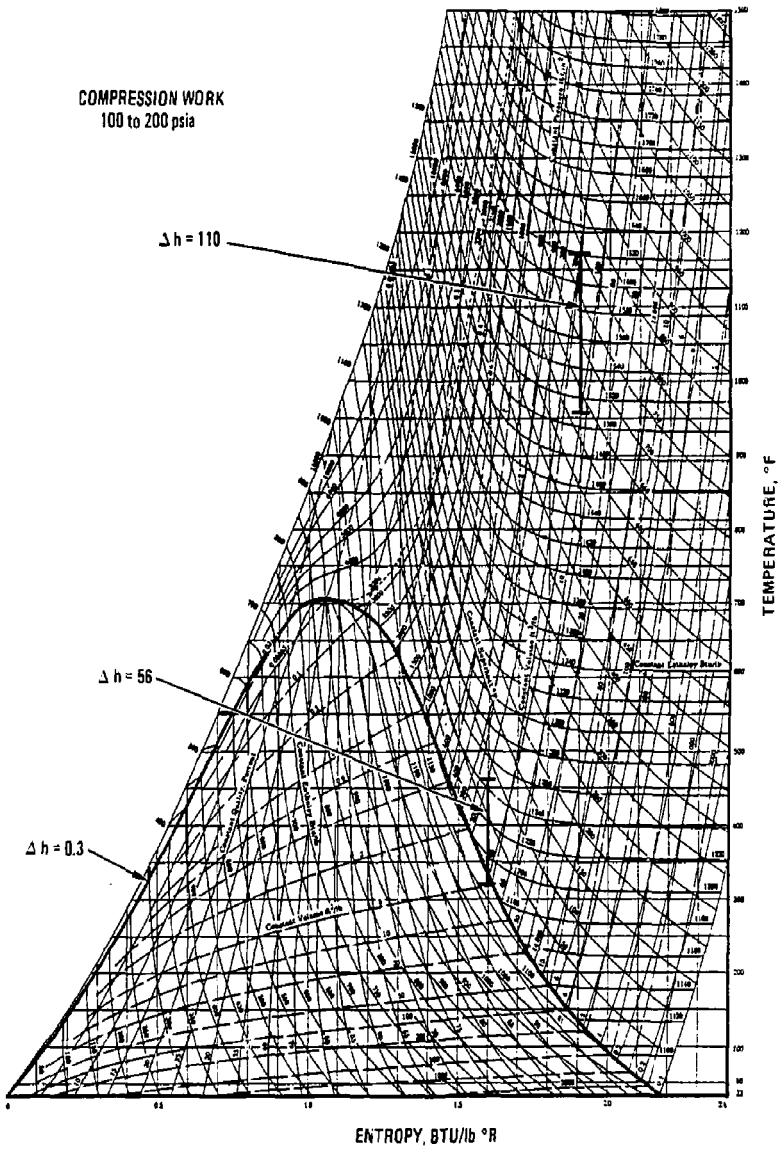

Fig. 3-13. T-s diagram for water showing reduction in compressor work near saturation and in liquid region, (from Steam Tables, by Keenan, Keyes, Hill, & Moore, John Wiley & Sons, Inc.).

chosen so as to minimize ducting size and in-leakage. A simple open extraction heater is all that is required.

The plot of efficiency versus peak steam temperature in Fig. 3-1 for the GA/Field cycle assumes equal main steam and reheat temperatures and equal pressure ratios for the two high pressure turbines. As with the Brayton cycle, these pressure ratios are optimized for maximum efficiency using the adiabatic efficiencies of Fig. 3-4. Only one regenerator is required in this case. From Fig. 3-1, it is seen that, at 1200 to 1300 K, the practical limit for metal heaters, over 58% efficiency is possible. Over 50% is possible at 1000 K, for which 300-series stainless steel is adequate at moderate steam pressures.

An advantage of this cycle is the flexibility in operating pressures even though it operates near the two-phase region. As with Brayton cycles, pressures must be high enough to keep heat exchanger pressure drops low. Here we assume 58 atm (850 psia) peak will suffice. Note that the hot side of the regenerator is not at the minimum pressure (0.048 atm), which would produce unacceptable pressure drops, but at a fairly high intermediate value of 13.6 atm. A simple liquid compression Brayton cycle with steam does not operate this way because the regenerator pressure drop on the low-pressure side would be prohibitive.

Another advantage to the cycle is that overall pressure ratio is reduced from 8000 or so in a Rankine cycle to about 1200. HPT blade heights are therefore adequate for good efficiency even at low power levels. And because less steam flows through the LPT compared to a conventional Rankine cycle, last stage blades are about 2/3 as high.

Figure 3-14 shows a block diagram of the reference GA/Field cycle of Fig. 3-12 as applied to the Cascade reactor blanket. Steam temperatures are chosen to match the reactor zone heat inputs, while maintaining 300 K minimum log-mean temperature differences. Because the steam pressure in the high temperature heater is only 28 atm, it can probably be made of a Hastelloy metal, an appealing result

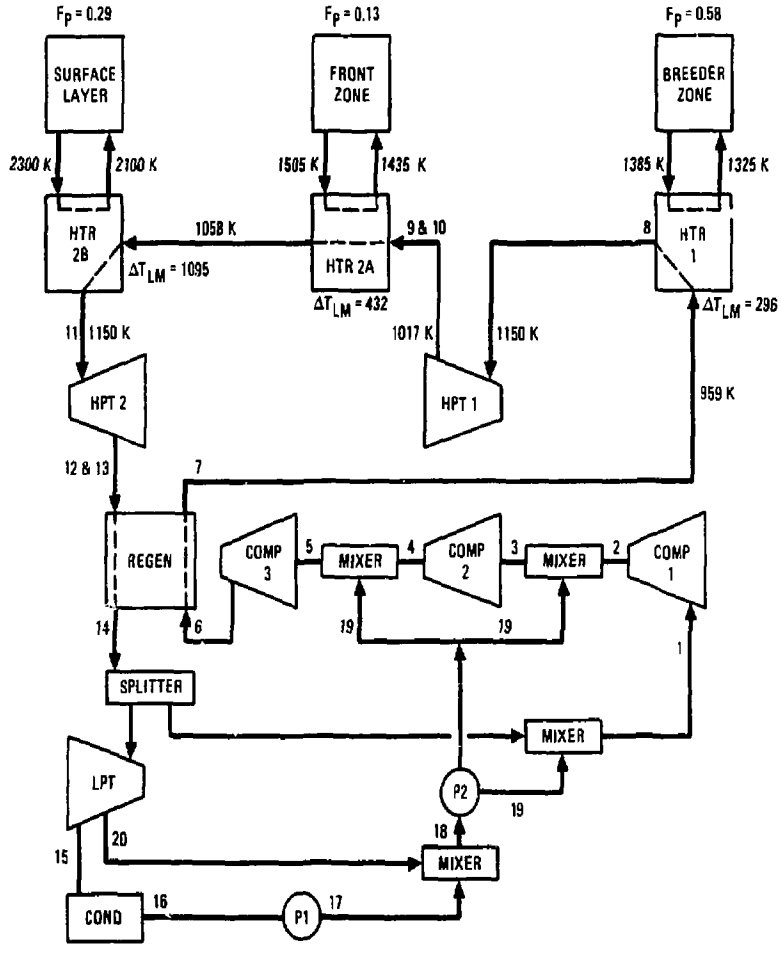

Fig. 3-14. Block diagram of 1300 K Field cycle. Net efficiency is 56.0%. Steam properties are given in Table 3-1.

particularly considering the achieved efficiency of 56%. The mixers shown in the figure are merely tanks for mixing the liquid and gas streams. The flow splitter is simply a regulated T-intersection. Note the modest pressure ratios shown in Fig. 3-12 for the HPT and compressor stages, which are conducive to good adiabatic efficiency and ease of design. Table 3-1 lists the steam properties at the state points shown in the figure.

At a cost of two points in efficiency, peak steam temperatures can be reduced to 1150 K, allowing some margin in material choice and a more near-term design. This cycle is shown in Fig. 3-15 and state point properties in Table 3-2. Note the further simplification of only one regenerator. The higher log-mean temperature differences for Heater 2 means a size reduction and cost savings. Whether these simplifications justify a two point efficiency loss can be determined only by a detailed examination of the entire system. If the laser recirculating power is modest, say, under 20%, the two point loss may not offset the potential cost savings.

Assuming that the requisite materials will be available at the proper time, if the main steam temperature is raised to 1175 K and the reheat temperature to 1500 K, a net efficiency of 58.4% is realized. These higher temperatures do reduce the log mean temperatures differences in the heaters. Steam side state points are given in Table 3-3. The block diagram in Fig. 3-14, except for the steam temperatures shown, serves here as well. Note that this last example is illustrative only and no attempt has been made to match it to the Cascade heat line. The heaters for both the BeO surface layer and front zone must be ceramic. The breeder zone heater can still be a high temperature metal alloy.

TABLE 3-1

STEAM PROPERTIES FOR FIELD CYCLE

SHOWN IN FIGURES 3-12 AND 3-14

State	P (atm)	T (K)	H (kJ/kg)
1	13.42	467	2784
2	21.83	524	2894
3	21.83	491	2796
4	35.51	550	2908
5	35.51	517	2799
6	57.76	579	2910
7	57.18	958	3855
8	54.43	1150	4313
9	23.87	996	3958
10	23.76	1162	4339
11	23.52	1300	4671
12	13.76	1184	4404
13	13.70	1018	4023
14	13.56	590	3078
15	.048	305	2274
16	.047	304	130
17	8.84	304	131
18	2.03	394	509
19	64.57	395	517
20	2.03	401	2721

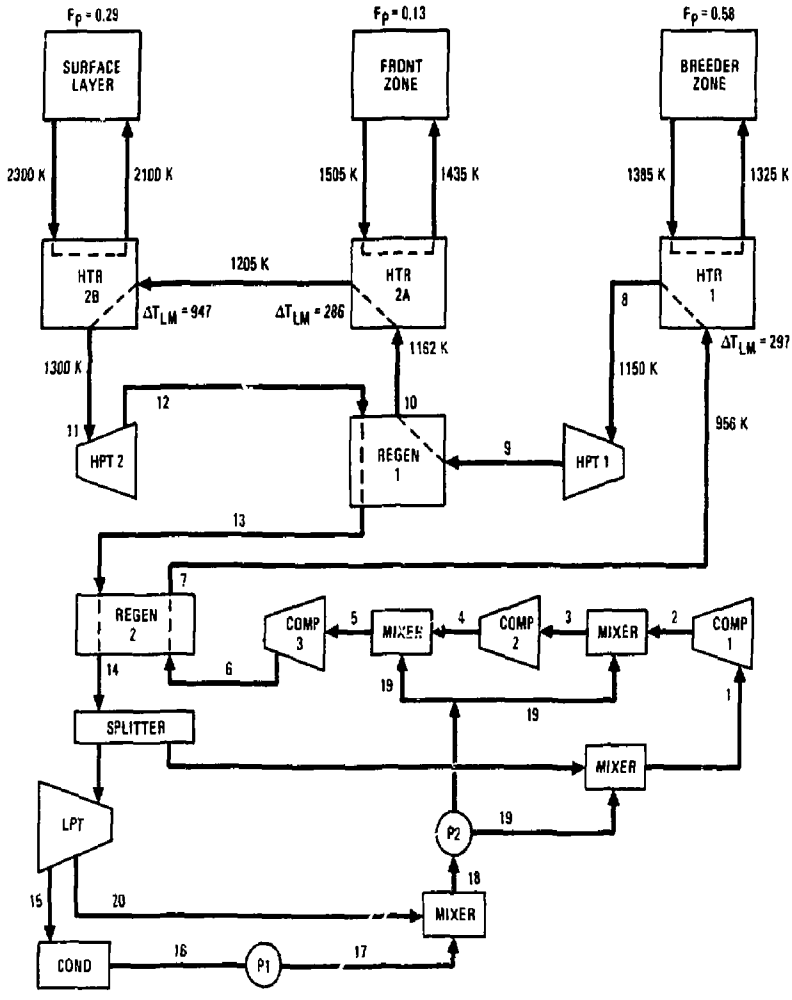

Fig. 3-15. More moderate temperature Field cycle with hot regenerator eliminated. Maximum steam temperature is 1150 K. Net efficiency is 53.9%. Steam properties are given in Table 3-2.

TABLE 3-2

STEAM PROPERTIES FOR LOW TEMPERATURE FIELD CYCLE

SHOWN IN FIGURE 3-15

State	P (atm)	T (K)	H (kJ/kg)
1	13.08	466	2783
2	21.61	525	2897
3	21.61	490	2796
4	35.67	551	2911
5	35.67	518	2799
6	58.89	581	2914
7	58.30	959	3857
8	54.43	1150	4312
9	26.95	1017	4007
10	26.81	1017	4007
11	26.55	1150	4324
12	13.42	1021	4027
13	13.35	1021	4027
14	13.22	592	3084
15	.048	305	2279
16	.047	304	130
17	8.79	304	131
18	1.98	394	505
19	65.69	395	514
20	1.98	403	2725

TABLE 3-3

STEAM PROPERTIES FOR HIGH TEMPERATURE VERSION OF FIELD CYCLE SHOWN IN FIGURE 3-15.

Net efficiency is 58.4% with a maximum temperature of 1500 K.

State	P (atm)	T (K)	H (kJ/kg)
1	12.89	465	2783
2	21.22	523	2895
3	21.22	489	2796
4	34.92	550	2910
5	34.92	516	2799
6	57.48	579	2913
7	56.91	968	3879
8	54.43	1175	4370
9	22.31	1006	3981
10	22.20	1350	4773
11	21.98	1500	5132
12	13.22	1372	4838
13	13.15	1028	4046
14	13.02	591	3081
15	.048	305	2279
16	.047	304	130
17	8.76	304	131
18	1.95	393	503
19	64.29	394	512
20	1.95	402	2723

3.5. CERAMIC HEAT EXCHANGER DESIGN

3.5.1. Introduction

In this section, we describe the design of the ceramic heat exchanger that transfers the fusion energy deposited in the high temperature granules to the helium working fluid of the closed-cycle gas turbine power conversion system. During the first year of the Cascade study, as reported in Ref. 3-5, we selected a heat exchanger concept based on vacuum heat transfer. The concept employs gravity-induced flow-mixing of the granules over the primary side of the heat exchange surfaces. We selected a horizontal array of staggered coolant tubes in a triangular pitch configuration to enhance granule mixing. The once-through coolant tubes containing the secondary-side working fluid pass back-and-forth, ascending countercurrent to the downward granule flow. That initial heat exchanger was designed to operate with <1200 K Li_2O primary-side granules and <800 K steam at 15 MPa on the secondary side. That design also incorporated double-walled tubes to prevent leakage of water into the Li_2O. The cost of that high temperature vacuum heat exchanger ranged between $360M and $560M, depending on the heat exchanger material, and was thus considered to be a high-leverage cost item.

In the present study, we investigated potential cost reductions by surveying the parameter space available for the heat exchanger design and configuration. The heat exchanger parameters surveyed include:

- Primary-side gas pressure and temperature
- Granule size and temperature
- Granule-tube contact time
- Tube pitch, diameter, and length
- Heat exchanger width, and
- Secondary-side Reynolds number.

Our design objectives were to minimize heat transfer area, pressure drop and pumping power, the number of heat exchanger tubes, and the active heat exchange height. The motivation for these objectives is as follows: heat transfer area, pressure drop, and pumping power translate directly into capital cost; the number of tubes serves as a relative measure of reliability; and the active heat exchange height dictates the minimum capability requirements of the granule throw system.

We developed an attractive heat exchanger mechanical design and adapted its design parameters to each of the three distinct blanket zones. Section 3.5.2 presents the mechanical design. Section 3.5.3 presents the primary-to-secondary heat transfer and thermal hydraulics design, and Section 3.5.4 presents the manifold coolant thermal hydraulics scoping calculations.

3.5.2. Mechanical Arrangement

At the operating temperatures of the present blanket materials (up to 1600 K), the only functional materials for the heat exchange surface are ceramics, such as SiC or Si_3N_4. To accommodate these high temperatures, the heat exchanger design of Ref. 3-5 was modified to incorporate SiC tubes. The major structural layout of the present mechanical design is shown in Fig. 3-16. An overview perspective showing the ducting arrangement is shown in Fig. 3-17. A single module is shown in Fig. 3-18. This design is used with each of the blanket materials. (An isometric perspective of all the heat exchangers in relation to the reaction chamber is presented in Fig. 4-3 of Chapter 4.) The heat exchanger design parameters for the three blanket zones are shown in Tables 3-4 to 3-6.

The solid granules comprising the blanket flow across the ceramic tube array in a vacuum (10 Pa), cross-countercurrent to the multipass helium working fluid contained within the tubes. Though developed independently, this configuration is similar to that developed for a ceramic recuperator in Ref. 3-6. With the present $LiAlO_2$ breeder, we eliminated the necessity for double-walled tubes, and in addition, the selection of a closed-cycle gas turbine for power conversion decreased the secondary-side working

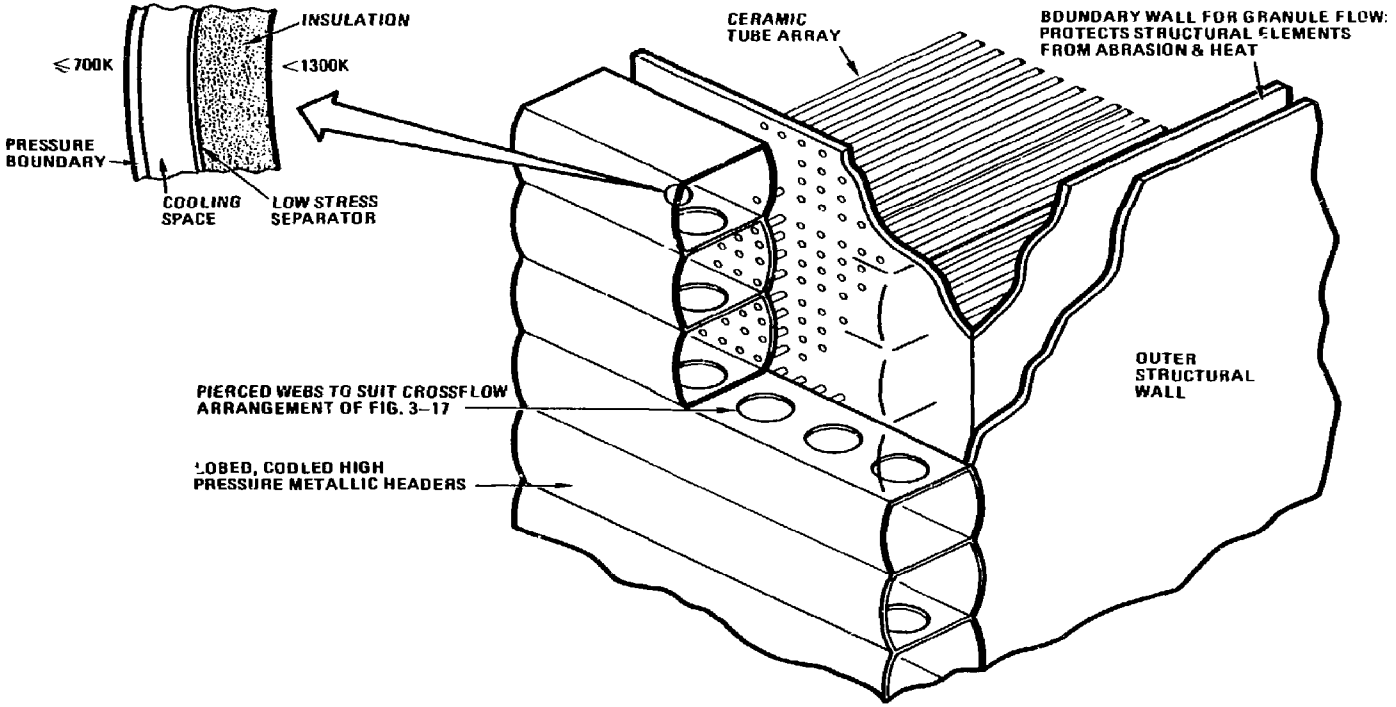

Fig. 3-16. Heat exchanger structure layout.

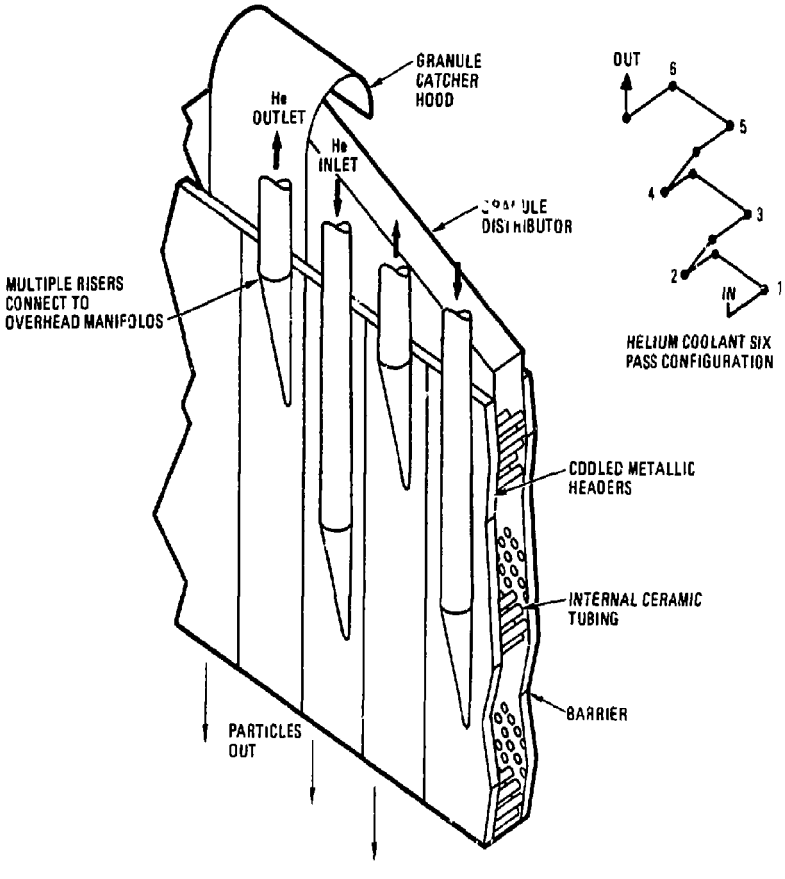

Fig. 3-17. Heat exchanger ducting arrangement.

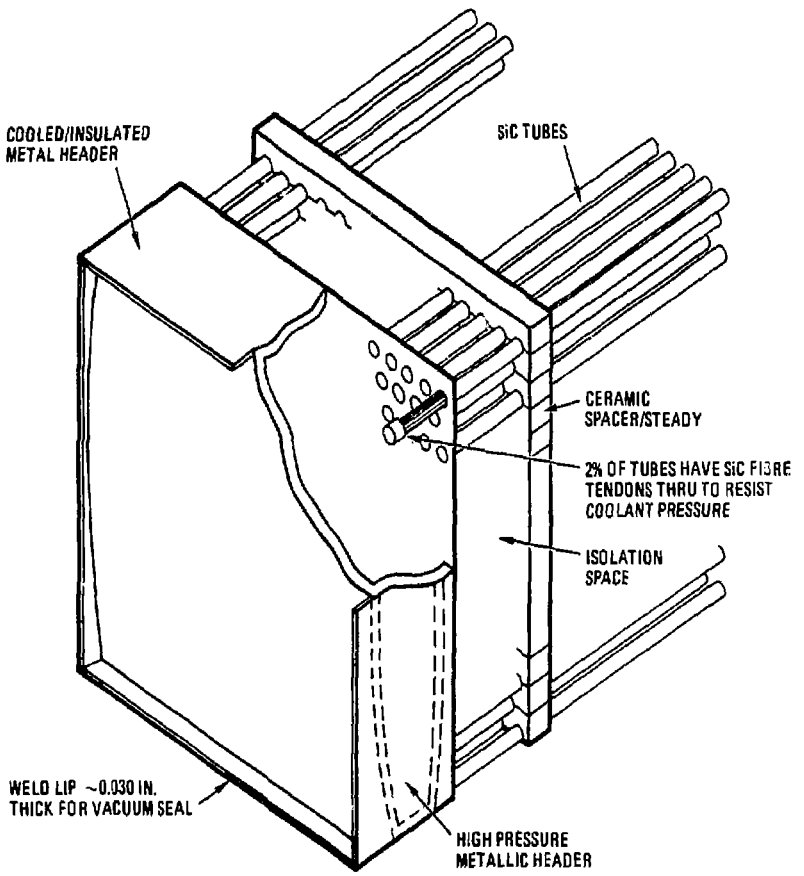

Fig. 3-18. Heat exchanger module detail.

TABLE 3-4

$LiAlO_2$ BREEDER ZONE HEAT EXCHANGER DESIGN

(990 MWt)

PRIMARY SIDE	
Gas pressure	10 Pa
Average gas temperature	1320 K
Granule diameter	1 mm
Granule inlet temperature	1355 K
Granule outlet temperature	1285 K
Bed porosity	0.5
Granule flow rate	7.5 m^3/s
Overall granule-to-tube heat transfer coefficient	490 W/m^2 K
Log-mean temperature difference	220 K
SECONDARY SIDE	
Helium pressure	5.0 MPa
Helium inlet temperature	945 K
Helium outlet temperature	1155 K
Helium velocity	69 m/s
Total helium mass flow rate	910 kg/s
Reynolds number	7.0×10^4
Fractional pressure drop	0.0088
Pumping power fraction	0.018
Heat transfer coefficient	3000 W/m^2 K
Log-mean temperature difference (film drop)	40 K
OVERALL HEAT EXCHANGER DIMENSIONS	
Heat exchange area	9000 m^2
Active height	5.7 m
Active width	20 m
Active tube length	1.5 m
Total number of tubes	8.2×10^4
Number of working fluid passes	5
Tube pitch	4.0 cm
Tube outside diameter	2.5 cm
Tube inside diameter	2.1 cm
Tube wall temperature difference	4 K
Granule flow area	11 m^2
Overall heat transfer coefficient	420 W/m^2 K
Overall log-mean temperature difference	260 K

TABLE 3-5
BeO FRONT ZONE HEAT EXCHANGER DESIGN
(220 MWt)

PRIMARY SIDE	
Gas pressure	10 Pa
Average gas temperature	1460 K
Granule diameter	1 mm
Granule inlet temperature	1510 K
Granule outlet temperature	1410 K
Bed porosity	0.4
Granule flow rate	1.0 m^3/s
Overall granule-to-tube heat transfer coefficient	660 W/m^2 K
Log-mean temperature difference	220 K
SECONDARY SIDE	
Helium pressure	5.0 MPa
Helium inlet temperature	1155 K
Helium outlet temperature	1200 K
Helium velocity	82 m/s
Total helium mass flow rate	920 kg/s
Reynolds number	1.5×10^5
Fractional pressure drop	0.0022
Pumping power fraction	0.022
Heat transfer coefficient	2500 W/m^2 K
Log-mean temperature difference (film drop)	60 K
OVERALL HEAT EXCHANGER DIMENSIONS	
Heat exchange area	1600 m^2
Active height	5.5 m
Active width	15 m
Active tube length	0.5 m
Total number of tubes	1.9×10^4
Number of working fluid passes	6
Tube pitch	7.0 cm
Tube outside diameter	5.0 cm
Tube inside diameter	4.6 cm
Tube wall temperature difference	6 K
Granule flow area	2.1 m^2
Overall heat transfer coefficient	510 W/m^2 K
Overall log-mean temperature difference	280 K

TABLE 3-6
SURFACE LAYER HEAT EXCHANGER DESIGN

Material	C	BeO
Power Level, MWt	460	480
PRIMARY SIDE		
Gas pressure, Pa	10	10
Average gas temperature, K	1550	2200
Granule diameter, mm	1	1
Granule inlet temperature, K	1600	2300
Granule outlet temperature, K	1500	2100
Bed porosity	0.5	0.5
Granule flow rate, m^3/s	2.2	1.0
Overall granule-to-tube heat transfer coefficient, W/m^2 K	790	2200
Log-mean temperature difference, K	220	580
SECONDARY SIDE		
Helium pressure, MPa	5.0	5.0
Helium inlet temperature, K	1200	1200
Helium outlet temperature, K	1300	1300
Helium velocity, m/s	90	150
Total helium mass flow rate, kg/s	910	940
Reynolds number	1.5×10^5	2.5×10^5
Fractional pressure drop	0.0045	0.0029
Pumping power fraction	0.023	0.015
Heat transfer coefficient, W/m^2 K	2600	2600
Log-mean temperature difference (film drop), K	70	320
OVERALL HEAT EXCHANGER DIMENSIONS		
Heat exchange area, m^2	2600	380
Active height, m	5.1	4.3
Active width, m	15	15
Active tube length, m	1.0	0.25
Total number of tubes	1.8×10^4	9100
Number of working fluid passes	6	6
Tube pitch, cm	7.0	9.0
Tube outside diameter, cm	5.0	5.0
Tube inside diameter, cm	4.6	4.6
Tube wall temperature difference, K	7	50
Granule flow area, m^2	4.3	1.7
Overall heat transfer coefficient, W/m^2 K	590	1300
Overall log-mean temperature difference, K	300	950

fluid pressure to 5 MPa. Thus, though the tubes are in hoop tension due to the internal helium pressure, the tensile stresses are modest (~50 MPa in 2 cm o.d. tubes with 1 mm wall thickness) and can be accommodated while allowing adequate reserve for thermal stresses. The state-of-the-art in proof-testing of ceramic components has advanced significantly in recent years (see e.g., Ref. 3-7, and references therein), and the small size and low stress levels in this design make this a suitable application for SiC tubes.

The design of the heat exchanger considers that the structure must eventually revert to metal. Thus, the high pressure headers shown in Fig. 3-16 are insulated and actively cooled metal (as shown in the detailed insert of Fig. 3-16), and incorporate a practical metal-to-ceramic joint, shown in Fig. 3-19. A low-stress ceramic boundary wall separates the granules from the metallic wall and protects the structural members from abrasion and heat. This configuration avoids extremely complex or highly stressed ceramic components, enhancing manufacturability. Heat exchanger reliability is also enhanced by the modular design, which allows the possibility of changing tubes, or more practically, a bank of tubes, as shown in Fig. 3-18.

The cooled, straightforward polymeric seal at the joint appears practical. The end of the tube is ground to accept the O-ring seal. The venturi serves to reduce the structural and seal cooling heat load by providing a region for insulating material. Minor tube leakage can also be stopped with the tube plugging arrangement shown in Fig. 3-20, in which the low pressure created by a failed tube drives the ball plug into the venturi. Since a joint of this form cannot take a tension, an exterior tie in the form of SiC fiber-reinforced tendons within selected tubes (shown in the detailed insert in Fig. 3-18) is required to keep the headers together. The headers resist bending by their substantial moment of inertia and internal shear webs.

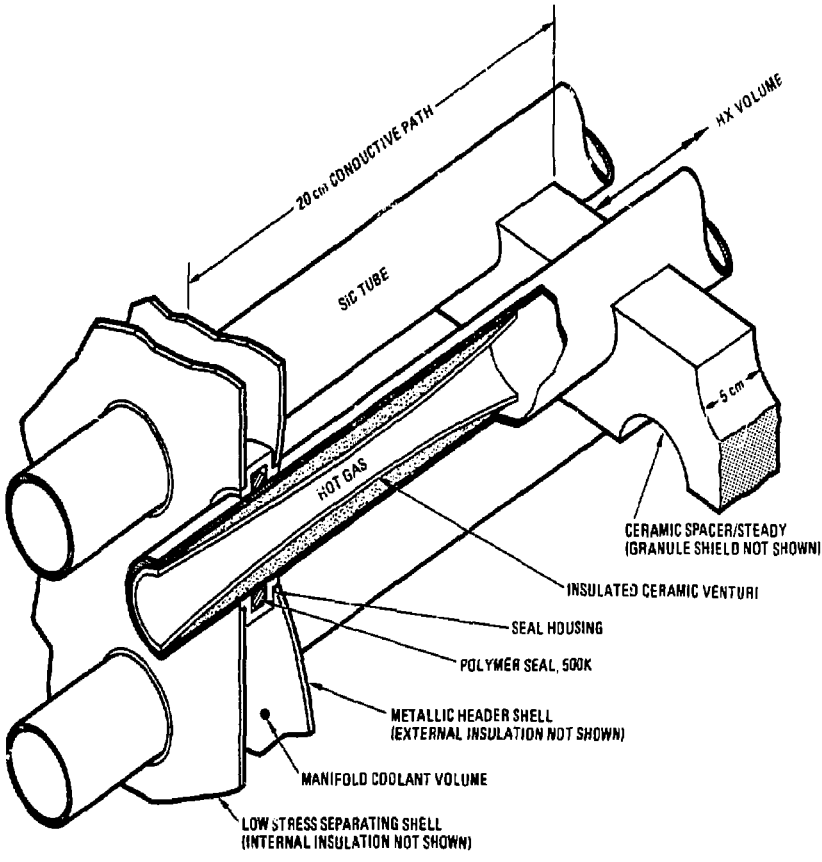

Fig. 3-19. Metal-to-ceramic joint and cold seal protection. The external and internal manifold structure insulation and granule shield are not shown for clarity.

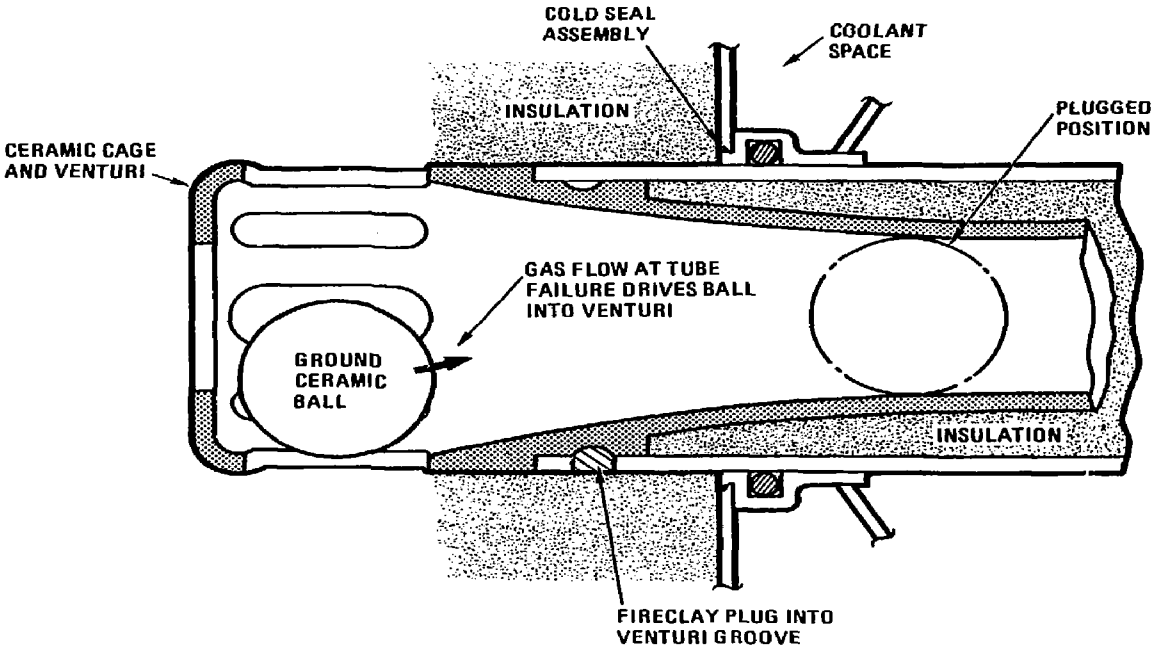

Fig. 3-20. Tube auto-plugging arrangement for minor leaks.

3.5.3. Primary-to-Secondary Heat Transfer and Thermal Hydraulics

The solid blanket granules, flowing across the SiC tubes in a vacuum, transfer their heat to the helium working fluid. As in Ref. 3-5, we calculated the primary-side heat exchanger performance by evaluating the heat transport characteristics of the granular flowing C, BeO and $LiAlO_2$ blanket. The methodology followed was the same as in Ref. 3-5 and the reader is referred to the original literature (Ref. 3-8) for a discussion of the stagnant and agitated granule bed heat transfer models of correlations. As shown in Tables 3-4 to 3-6, the primary-side granule-to-tube heat transfer coefficient presents the major resistance to heat flow. Secondary-side heat transfer was calculated using the Dittus-Boelter equation. The tube conductance offers negligible resistance to heat flow due to the high thermal conductivity of SiC.

The heat transfer area requirements of the Cascade gravity-flow heat exchangers are dominated by the granule-to-tube heat transfer coefficient. Parametric analysis of the primary-side variables of gas pressure, granule size, and temperature demonstrates that the controlling variable is the temperature. The effect of the latter is shown in Fig. 3-21, which presents heat transfer area versus average primary-side temperature, all other heat exchanger design parameters held constant at their reference values. The main effect of temperature is through the fourth-power dependence of the radiative heat transfer term in the granule-to-tube heat transfer coefficient. Increasing temperature decreases the required area, with attendant reductions in the total number of tubes, pressure drop, pumping power, and heat exchanger height. The secondary-side parameters of tube diameter and Reynolds number are of relatively minor importance in establishing the heat transfer area, as shown in Figures 3-22 and 3-23.

For a given heat transfer area, the heat exchanger configuration, i.e., height, width, and length, is determined by the constraints imposed by the granule transport system, tube manufacturing capability, and minimum number of working fluid passes. The width was constrained to a maximum of 20 m by the capability for lateral granule

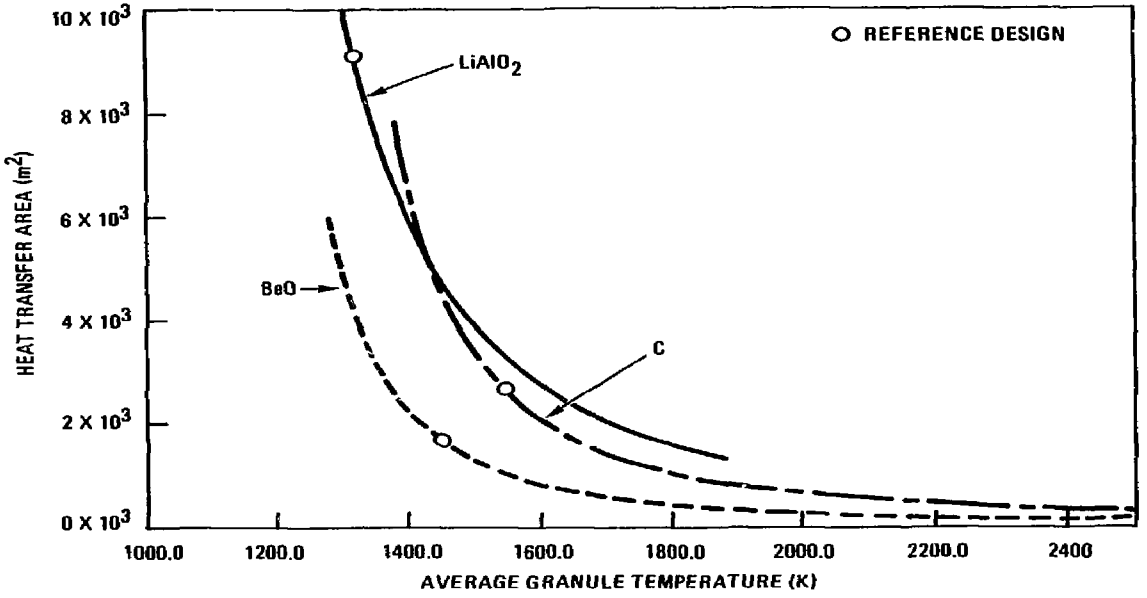

Fig. 3-21. The granule temperature has a strong effect on the required heat transfer area.

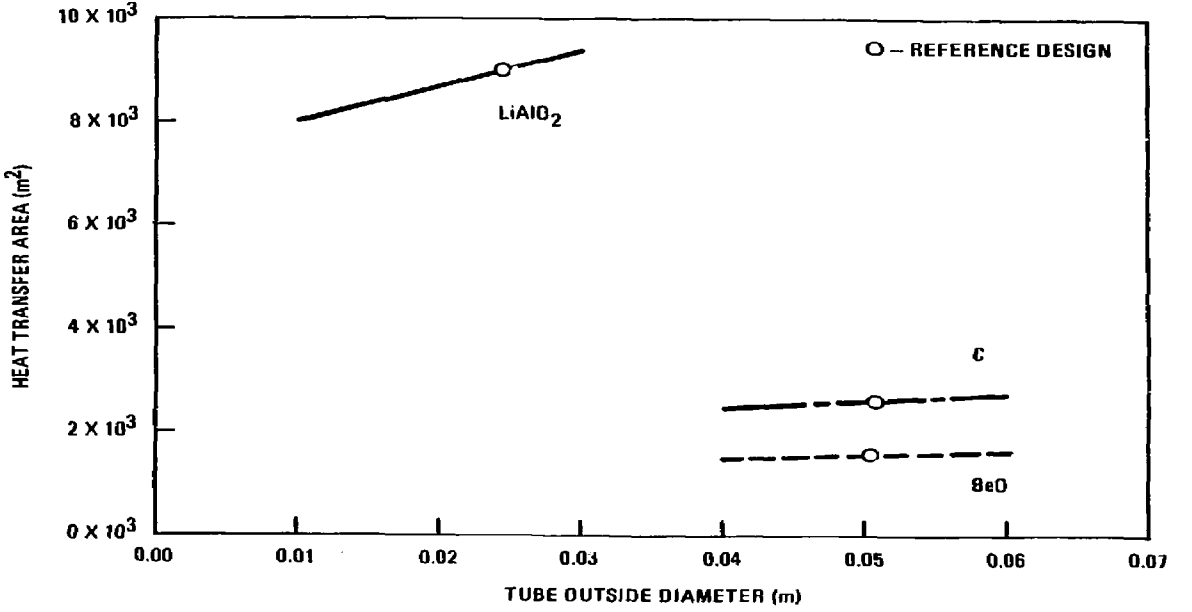

Fig. 3-22. The tube diameter has a minor effect on the required heat transfer area.

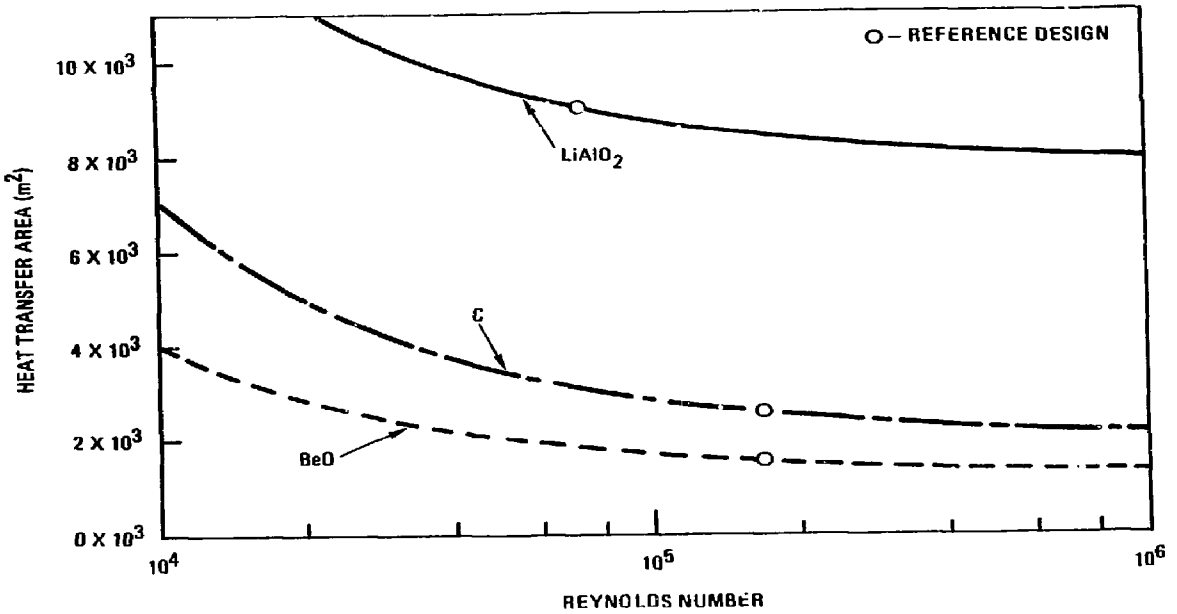

Fig. 3-23. The working fluid Reynolds number has a minor effect on the required heat transfer area.

throw by the scoop system, while the height was constrained to the 5 to 10 m range. The longest tube length used in current ceramic heat exchanger designs is 1 m. (Ref. 3-6) For our designs, a maximum length of 2 m was used based on projections of advancement in ceramic component manufacturing. A minimum of five passes of the working fluid are necessary to satisfy the cross-counterflow coolant configuration. These constraints are not severe and allow much flexibility for future design iterations.

Given the heat transfer area and heat exchanger configuration, the tube pitch and diameter are determined by the need to maintain adequate granule flow area, and minimize the heat exchanger height, number of tubes, and the pressure drop and pumping power. The tube pitch affects only the heat exchanger height and this was selected to result in heat exchangers approaching the minimum in the acceptable height range, i.e., 5 to 6 m. The tube gap spacing was determined from granule flow considerations, approximating our rectangular flow area condition with the Shirai equation for mass flow through a pipe, (Ref. 3-9)

$$\dot{V} = 1.055\ D^{2.5}$$

where $\dot{V}$ is the volume flow rate (m^3/s) and D is the pipe diameter (m). For the three heat exchanger volume flow rates, we calculated the necessary flow areas using the Shirai equation. We then calculated the equivalent hydraulic diameter (minimum tube spacing) for the selected tube lengths. The minimum gaps were thus calculated to be 1.5 cm for 1.5 m tubes in the $LiAlO_2$ heat exchanger, and 2 cm for 0.5 and 1.0 m tubes in the BeO and C heat exchangers. The minimum gap would be 4 cm for 0.25 m tubes in the BeO surface layer heat exchanger. For a given pitch, we achieve minimum heat exchanger height, number of tubes, pressure drop and pumping power by maximizing the tube diameter. Thus, having maximized the pitch from height considerations as described above, we obtained the maximum tube diameter by selecting the minimum acceptable gap.

At this point, the heat exchanger designs are completely specified except for the secondary-side Reynolds numbers. This design variable has the strongest effect on the pressure drop and pumping power. This effect is displayed in Figs. 3-24 and 3-25.

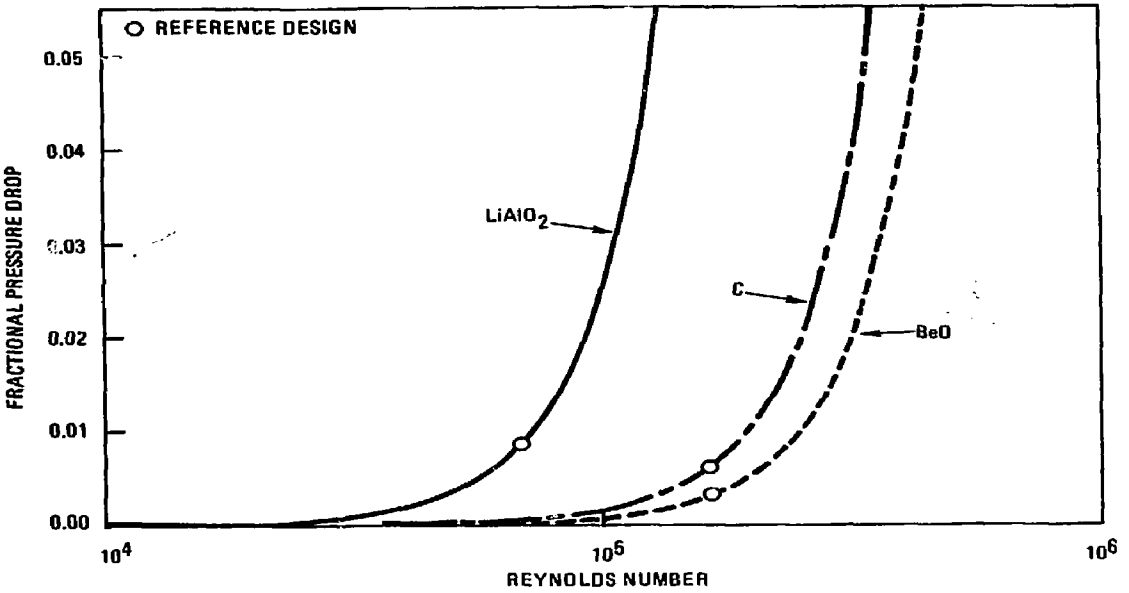

Fig. 3-24. The working fluid Reynolds number has a strong effect on the pressure drop.

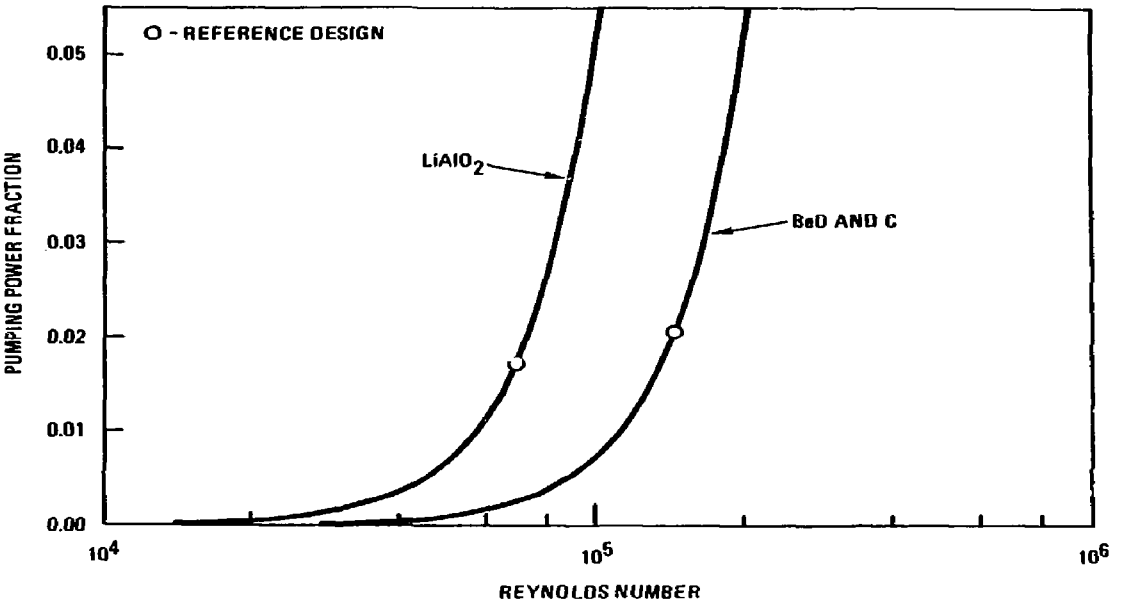

Fig. 3-25. The working fluid Reynolds number has a strong effect on the pumping power.

The Reynolds numbers shown in Tables 3-4 to 3-6 were obtained by restricting the fractional pressure drop and pumping power fractions to the 2 to 3% range. These levels are considered acceptable in current day thermal hydraulics design and were used in calculating the power conversion system efficiencies of the previous sections.

3.5.4. Manifold Coolant Thermal Hydraulics

The present heat exchanger concept employs actively cooled and insulated manifolds operating at metal temperatures (<1200 K). A polymer seal at each tube separates the 5 MPa working fluid from the 10 Pa vacuum of the primary side. In this section, we present the results of scoping calculations of the insulation and convection cooling requirements to maintain the metal manifold walls at 700 K, permitting the use of low cost carbon steels, and a seal temperature of 500 K, allowing a seal life of 30 years, while reducing power loss to an acceptable level. The one-dimensional square-duct calculational model shown in Fig. 3-26 was used for the manifold walls. The schematic of the calculational model used in the vacuum seal region is shown in Fig. 3-27.

The analysis for the manifold walls indicates that 5 cm of inner insulation and 20 cm of outer insulation will achieve the 700 K metal wall temperature while limiting the heat loss rate to 3 MW. The resistance to heat flow was calculated including the convective heat transfer at the inside surface of the insulator, and the thermal resistances of the thermal insulator and metal wall. Gap resistances were not included. The dominant resistance to heat flow was that of the thermal insulator. For the purposes of the calculation, the thermal conductivity of the thermal insulation was assumed to be that of Min-K, a rigid thermal insulator available from the Manville Building Materials Group. (Ref. 3-10) The thermal conductivity of Min-K in helium at 1200 K, 0.1 W/m K, was conservatively used in the calculations.

The seal assembly is maintained below 500 K by convective cooling within the coolant channel with 5 MPa helium. At the seal assembly, heat flow has two paths: one radially through the venturi and thermal insulation, and one axially through the

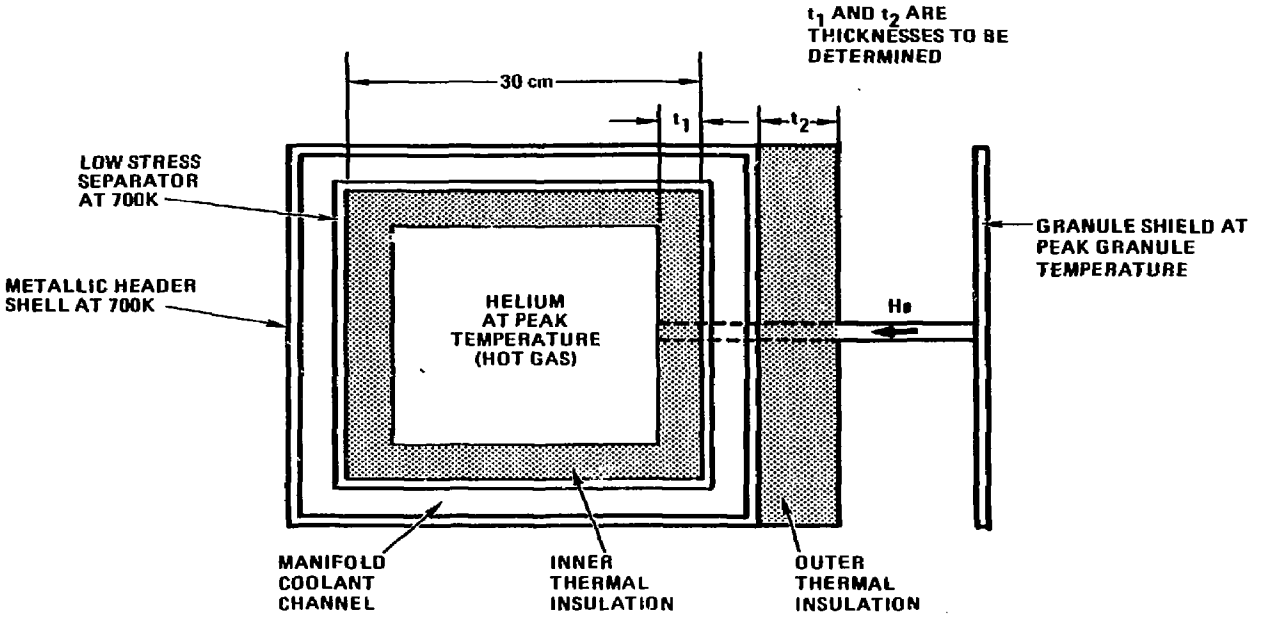

Fig. 3-26. Square-duct calculational model used to represent the manifold shown in Fig. 3-16 and Fig. 3-19.

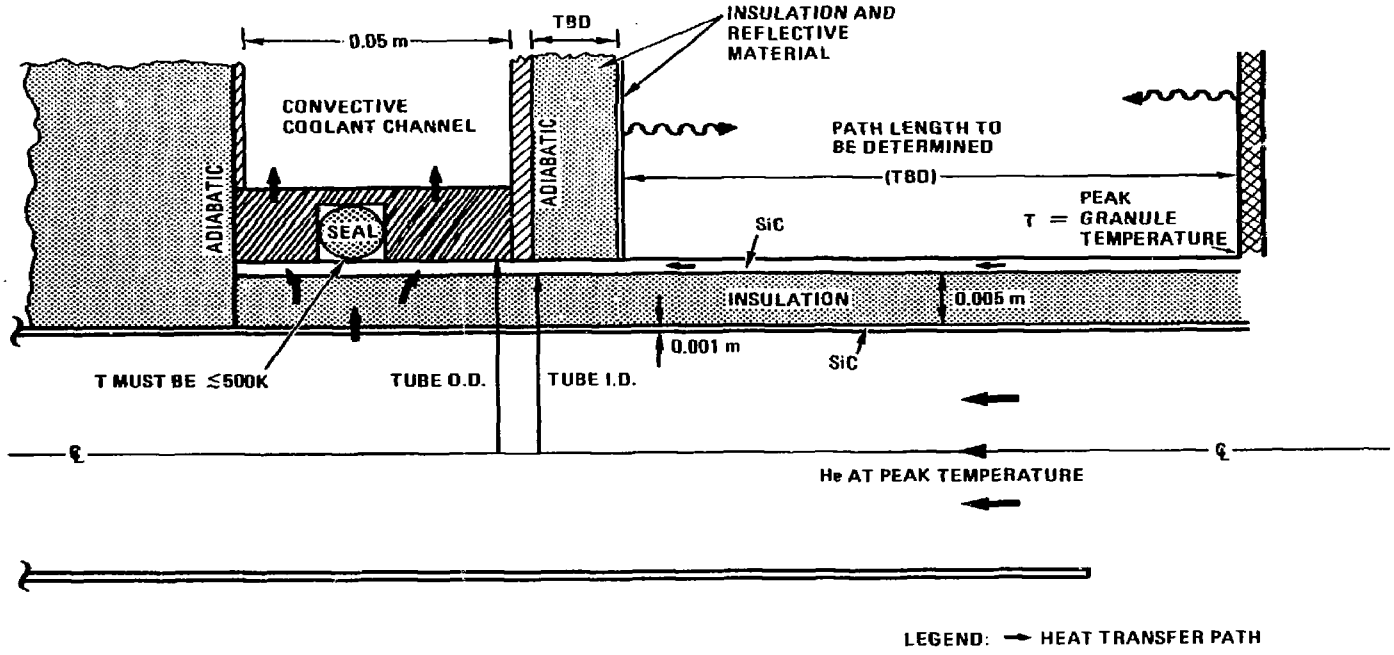

Fig. 3-27. Schematic of the calculational model used for the metal-to-ceramic vacuum seal region of Fig. 3-19.

SiC tube wall. The radial path is the dominant heat flow path, conducting a total of 13 MW to the manifold coolant with 5 mm of thermal insulation between the venturi and the SiC tube. Of this, 5 MW comes from the $LiAlO_2$ heat exchanger and 4 MW each from the BeO front zone and C surface zone heat exchangers. The resistance of the thermal insulation is much greater than that of the SiC components, seal housing, or inside and outside surfaces, and the heat loss could be decreased, particularly for the 5 cm tubes of the C and BeO heat exchangers, by increasing the insulation thickness. Heat loss through the axial path is controlled by adjusting the tube length between the hot granules and the cool seal assembly. A 20 cm path length results in a heat flow rate of 8 MW, 4 MW from the $LiAlO_2$ heat exchanger and 2 MW from each of the other two.

The total heat loss rate into the heat exchanger manifold coolants is 24 MW. For parallel cooling of all mainfolds, a coolant stream of 5 MPa helium flowing at 40 m/s would experience a temperature rise of 30 K. The pressure drops calculated for coolant flow across a triangular tube bundle (Ref. 3-11) are 0.6 MPa for the $LiAlO_2$ heat exchanger, and 0.3 MPa for the BeO and C heat exchangers. The pumping powers are only 5 MW for the former and 1 MW for each of the latter heat exchangers. Optimization of the manifold coolant circuit design should be performed to lower the pressure drop.

References for Chapter 3

3-1. J. F. Field, "The Application of Gas Turbine Technique to Steam Power", *Proc. I. Mech. Eng.*, **162**, 209 (1950).

3-2. R. F. Bourque, "An Efficient Low Temperature Steam Power Conversion System for Fusion Reactors", GA-A16783, GA Technologies (1982).

3-3. W. H. Krase, "Ericsson Cycle Gas Turbine Powerplants", R-2327-DOE, Rand Corp., Santa Monica, CA (1979).

3-4. J. H. Horlock, "The Thermodynamic Efficiency of the Field Cycle", ASME Paper No. 57-A-44, presented at ASME Annual Meeting (1957).

3-5. I. Maya, K. R. Schultz, *et al.*, "Inertial Confinement Fusion Reaction Chamber and Power Conversion System Study," GA Technologies Report, GA-A17267, September 1984; also Lawrence Livermore National Laboratory Report, UCRL-15642.

3-6. H. Strumpf *et al.*, "High-Temperature Ceramic Recuperator and Combustion Air Burner Programs - Final Report," AiResearch Manufacturing Co., Garrett Corp. Report for the Gas Research Institute, GRI-83/0039, February 1984.

3-7. G. R. Hopkins *et al.*, "Low Activation Materials Safety Studies," GA Technologies Reports GA-A16425, September 1981, and GA-A16005, December 1980.

3-8. *Heat Exchanger Design Handbook, Volume 2, Fluid Mechanics and Heat Transfer*, Hemisphere Publishing Corp.; Section 2.8.1, R. Bauer, "Stagnant Packed Beds;" Section 2.8.3, E. Muchowski, "Packed and Agitated Beds," 1983.

3-9. F. Zenz, "How to Predict Gravity Flow Rates," *Petroleum Refiner*, Vol. 36, No. 10, October 1957.

3-10. Product Literature, Manville Building Materials Group, POB 128, Manville, NJ 08835.

3-11. W. H. McAdams, *Heat Transmission*, McGraw-Hill Book Company, New York, 1954, p. 271.

4. BALANCE-OF-PLANT STUDIES

4.1. INTRODUCTION

In this chapter, we present an economic comparison of the Cascade ICF power plant to equivalent nuclear and coal power plants and a safety assessment of the Cascade concept. In Section 4.2, we develop an estimate of the capital cost of Cascade, assuming a mature plant design which has achieved equilibrium with the state of design of contemporary nuclear and coal plants. This capital cost development makes maximum use of existing GA estimates and historical data (Ref. 4-1 to 4-3) supplemented by estimates developed for unique Cascade components and systems. We also determine the plant operating costs of Cascade and the alternate reactors using a consistent economic methodology. (Ref. 4-4) The plant description which forms the basis for the estimates is presented in Section 4-3. We then present the safety and licensing issues of Cascade in Section 4.4. These are examined with the goal of minimizing safety-related costs by providing safety design guidance early in the design phase.

4.2. CAPITAL AND OPERATING COSTS

4.2.1. Cost Summary

Capital cost estimates for the Cascade ICF power plant are presented in the two digit summary format on Table 4-1. The capital cost estimates are presented for an "All Conventional" Cascade, constructed using well established, conventional fossil power plant construction methods, and requiring no nuclear-classified equipment or systems as described in Section 4.4; and a "Nuclear+Conventional" Cascade design

TABLE 4-1
Preliminary Capital Cost Summary
Equilibrium Cascade ICF Plant
($M, 1/85 Constant Dollars)

Acc. No.	Description	COST			
		Nuclear + Conventional			
		Nuclear	Conv.	Total	All Conv.
20	Land & Land Rights	(included in Owner's Cost)			
21	Structures & Improvements	65.3	19.0	84.3	37.3
22	Reactor Plant Equipment	282.8		282.8	254.0
23	Turbine Plant Equipment	183.7		183.7	156.1
24	Electric Plant Equipment	44.3	26.3	70.6	46.6
25	Reactor Maint. Plant Equip.	6.9	9.4	16.3	12.0
26	Heat Rejection System		21.5	21.5	21.5
27	Laser Plant Bldg. & Equip.		275.0	275.0	275.0
28	Fuel Pellet Fabrication Plant	100.0		100.0	100.0
	TOTAL DIRECT COST	683.0	351.2	1034.2	902.5
	Constr. Serv. & Field Engr.	170.8	52.7	223.4	135.4
	Home Office Engr. & Services	128.1	32.3	160.4	83.0
	Owner's Cost	98.2	43.6	141.8	112.1
	TOTAL PLANT INVESTMENT	1080.0	479.8	1559.8	1233.0
	Contingency	162.0	48.0	210.0	123.3
	AFUDC	119.1	50.6	169.7	130.1
	TOTAL CAPITAL REQUIREMENT	1361.1	578.4	1939.5	1486.4
	$/kWe net			2380.0	1824.0

constructed using a combination of fossil and fission reactor plant methods and standards, that which includes a combination of nuclear and non-nuclear systems similar to that found in modern fission reactor plants. (Ref. 4-1) The total capital requirements for the "All Conventional" construction plant were estimated to be $1,490M, or $1,820/kwe. The "Nuclear/Conventional" construction plant was estimated to be $1,940M, or $2,380/kwe. The resultant savings of $450M ($560/kwe) represents strictly the difference between Cascade ICF power plants designed and contructed to include equipment and systems that are nuclear safety-related versus all non-nuclear safety related. Cost estimate details at the three- and four-digit level are presented in Table 4-2.

An economic evaluation of the levelized busbar cost of electricity (COE) for the ICF power plant is presented in Table 4-3. Also presented in Table 4-3 is the levelized busbar cost of electricity for a High Temperature Gas-Cooled Reactor (HTGR), a Pressurized Water Reactor (PWR) and a Coal Plant, (Ref. 4-2) all estimated using the same economic ground rules and data base. The results of the economic evaluation provide an indication of the potential competitiveness of the Cascade ICF plant. The COE for the ICF was estimated to be 34 Mills/kwHr for the All Conventional and 41 for the Nuclear+Conventional plant. The estimated COE for the Coal Plant was 49 Mills/kwHr and the PWR and HTGR were 37 and 40 Mills/kwHr respectively. The economic ground rules of Ref. 4-4 were used for the economic comparison of COE. These results show that Cascade will be able to compete well with present day power plants. If full advantage can be taken of Cascade's safety features to eliminate the need for nuclear safety related equipment, Cascade has an economic advantage over present day alternatives.

4.2.2. Estimating Approach

The framework chosen for this ICF power plant estimate was the code of accounts developed for the U. S. Atomic Energy Commission (now the Department of Energy and Nuclear Regulatory Commission) by the NUS Corporation. This basic code of

TABLE 4 - 2
PRELIMINARY CAPITAL COST BREAKDOWN
EQUILIBRIUM CASCADE ICF PLANT
($M, 1/85 CONSTANT DOLLARS)

ACC. NO.	DESCRIPTION	COST NUCLEAR	COST CONV.	COST TOTAL	COST ALL CONV.
20	LAND & LAND RIGHTS (INCL. IN OWNERS COST)				
21	STRUCTURES & IMPROVEMENTS				
211	SITE IMPROVEMENTS & FACILITIES	5.4	1.6	7.0	.1
212	REACTOR BUILDING	26.4		26.4	6.9
213	TURBINE BUILDING		12.9	12.9	12.9
214	REACTOR MAINTENANCE BUILDING	14.9		14.9	3.6
215	TRITIUM RECOVERY BUILDING	14.9		14.9	3.6
216	ELECTRICAL EQUIPMENT BUILDING		0.4	0.4	0.4
217.1	ADMIN. & SECURITY BUILDING		2.7	2.7	2.7
217.2	CONTROL BUILDING	3.7		3.7	2.7
217.3	DIESEL GENERATOR BUILDING		0.4	0.4	0.4
217.4	HELIUM STORAGE AREA		0.0		0.0
217.5	MAINTENANCE BUILDING		0.3	0.3	0.3
217.6	WAREHOUSE		0.5	0.5	0.5
217.7	WATER TREATMENT BUILDING		0.2	0.2	0.2
22	REACTOR PLANT EQUIPMENT				
221	REACTION CHAMBER				
221.1	CHAMBER STRUCTURE	5.3		5.3	4.8
221.2	PRESTRESSING TENDONS	1.3		1.3	1.2
221.3	THERMAL INSULATION	0.1		0.1	0.1
221.4	SUPPORT & DRIVE GIRDER	0.5		0.5	0.5
221.5	OUTLET SHELVES	2.5		2.5	2.3
222	BLANKET				
222.1	SURFACE LAYER	6.8		6.8	6.1
222.2	MULTIPLIER	3.1		3.1	2.8
222.3	BREEDER	35.5		35.5	31.9
223	CHAMBER DRIVE				
223.1	ROLLERS	2.4		2.4	2.2
223.2	MOTORS	2.4		2.4	2.2
223.3	DRIVE SHAFTS	0.4		0.4	0.4
224	VACUUM SYSTEM				
224.1	VACUUM CHAMBER	110.0		110.0	99.0
224.2	VACUUM PUMPS	2.0		2.0	1.8
224.3	VACUUM CHAMBER COOLING SYSTEM	0.6		0.6	0.5
225	GRANULE TRANSPORT				
225.1	THROW SCOOPS	0.1		0.1	0.1
225.2	DUCTING & DISTRIBUTION PLENUMS	6.8		6.8	6.1
225.3	CHAMBER FEED PORTS	1.6		1.6	1.4

TABLE 4 - 2 (CONTD.)
PRELIMINARY CAPITAL COST BREAKDOWN
EQUILIBRIUM CASCADE ICF PLANT
($M, 1/85 CONSTANT DOLLARS)

ACC. NO.	DESCRIPTION	COST NUCLEAR	COST CONV.	COST TOTAL	ALL CONV.
226	PRIMARY HEAT EXCHANGERS				
226.1	TUBING & SHIELDS	18.6		18.6	16.7
226.2	MANIFOLDS & INSULATION	21.3		21.3	19.2
226.3	DUCTING	11.6		11.6	10.4
227	SHIELDING				
227.1	RADIATION SHIELD	17.1		17.1	15.4
227.2	BIOLOGICAL SHIELD	3.2		3.2	2.9
227.3	SHIELD COOLING SYSTEM	4.8		4.8	4.3
228	RADIOACTIVE MATERIAL HANDLING				
228.1	TRITIUM RECOVERY SYSTEM	12.9		12.9	12.9
228.2	RAD. WASTE PROCESSING SYSTEM	3.8		3.8	3.8
229	INSTRUMENTATION & CONTROL	8.1		8.1	5.1
23	TURBINE PLANT EQUIPMENT				
231	TURBINE GENERATOR	94.1		94.1	80.0
232	MAIN TURBINE BYPASS SYSTEM	0.8		0.8	0.7
233	HELIUM PIPING, PIPING SUPPORT & VALVES	4.7		4.7	4.0
234	HELIUM CIRCULATORS	16.7		16.7	14.2
235	HELIUM COOLERS	3.2		3.2	2.8
236	REGENERATIVE HEAT EXCHANGERS	54.5		54.5	46.2
237	HELIUM SERVICE EQUIPMENT	1.0		1.0	0.8
238	MAIN BEARING WATER SYSTEM	5.7		5.7	4.8
239	INSTRUMENTATION & CONTROL	3.0		3.0	2.6
24	ELECTRIC PLANT EQUIPMENT				
241	SWITCHGEAR	4.2	5.8	10.0	8.5
242	STATION SERVICE EQUIPMENT	4.5	3.5	8.0	8.0
243	SWITCHBOARDS	0.3	1.0	1.3	0.9
244	PROTECTIVE EQUIPMENT	1.9	1.5	3.4	2.5
245	ELECTRICAL STRUCTURE & WIRING CONTAINERS	12.4	5.2	17.6	9.8
246	POWER & CONTROL WIRING	18.7	9.3	28.0	15.8
247	DIESEL GENERATOR	2.3		2.3	1.1
25	REACTOR MAINTEN. PLANT EQUIPMENT				
251	TRANSPORTATION & LIFTING EQUIPT.		0.7	0.7	2.2
252	AIR & WATER SERVICE SYSTEM	4.8	6.9	11.7	7.8
253	COMMUNICATIONS EQUIPMENT	1.2	0.9	2.1	0.9
254	FURNISHINGS & FIXTURES	0.9	0.9	1.8	1.1
26	HEAT REJECTION SYSTEM				
261	STRUCTURES		0.8	0.8	0.8
262	MECHANICAL EQUIPMENT		20.7	20.7	20.7
27	LASER PLANT BUILDING & EQUIPMENT		275.0	275.0	275.0
28	FUEL PELLET FABRICATION PLANT	100.0		100.0	100.0

TABLE 4-3
ICF FUSION PLANT ECONOMIC COMPARISON
LEVELIZED BUSBAR COST OF PRODUCT
(Millions of 1-1-85 $, 2005 Operation Date)

	ICF PLANT				
	CONVENTIONAL CONSTRUCTION	NUC/CONVT. CONSTRUCTION	2240MWT HTGR-SC/E	2400MWT PWR	2300MWT P-COAL
PLANT CHARACTERISTICS					
THERMAL INPUT (MWT)	1670.0	1670.0	2240.0	2400.0	2285.0
NET ELECTRICAL RATING (MWE)	815.0	815.0	855.0	800.0	800.0
CAPACITY FACTOR	0.75	0.75	0.75	0.70	0.75
ANNUAL ELECTRICITY PROD. (KW-HRxE6)	5354.5	5354.5	5617.4	4906.8	5256.0
FIXED CHARGES					
TOTAL PLANT INVESTMENT ($xE6)	1368.3	1769.8	1411.0	1129.0	836.8
CONSTRUCTION PERIOD (MONTHS)	72.0	72.0	72.0	72.0	48.0
AFUDC ANNUAL RATE (%)	3.1	3.1	3.1	3.1	3.1
TOTAL CAPITAL REQUIRMENT ($xE6)	1488.4	1939.5	1546.3	1237.3	888.6
FIXED CHARGE RATE	8.7	8.7	8.7	8.7	9.0
ANNUAL FIXED CHARGES ($xE6)	129.3	168.7	134.5	107.6	80.0
O&M					
FIXED ($xE6)	50.0	50.0	35.0	38.0	20.0
VARIABLE: RATE (MILLS/KW-HR)	0.1	0.1	0.1	0.1	0.5
AMOUNT ($xE6)	1.5	1.5	2.0	1.8	7.5
TOTAL ANNUAL O&M ($xE6)	51.5	51.5	37.0	39.8	27.5
FUEL					
UNIT COST ($/MMBTU)	-	-	1.07	0.71	2.54
LEVELIZING FACTOR	-	-	1.00	1.00	1.14
ANNUAL FUEL COST ($xE6)	(small)	(small)	53.7	35.7	148.4
BUSBAR COST SUMMARY (MILLS/KW-HR)					
FIXED CHARGES	24.2	31.5	23.9	21.9	15.2
O&M	9.6	9.6	6.6	8.1	5.2
FUEL			9.6	7.3	26.2
TOTAL	33.8	41.1	40.1	37.3	48.7
RELATIVE COST					
(1200MWT P-COAL REF.)	0.69	0.84	0.82	0.77	1.00

accounts was expanded to accommodate the unique components required for a fusion power plant. This format was selected to allow for a uniformity in costing and comparison with reference PWR and coal power plants.

Capital costs for the overall plant were estimated on the basis of either "All Conventional" or "Nuclear+Conventional" construction methods. The "All Conventional" assumes that the ICF plant has all non-nuclear safety related systems and equipment. This is possible due to the high degree of inherent safety in the Cascade concept. The conventional construction method assumes that the systems and equipment perform the same function as in a conventional coal-fired plant. The "Nuclear+Conventional" assumes a combination of nuclear and non-nuclear related systems and equipment similar to that used in modern fission reactor plants. The basis for the selection of nuclear versus non-nuclear grade equipment is presented in Section 4.4.

The basic estimating approach used for this study was to evaluate the component, equipment or system on the basis of safety vs. non-safety requirement and apply the associated unit cost developed from the recent HTGR studies of the Modular HTGR (Steel Reactor Vessel) (Ref. 4-1) or the Monolithic HTGR (Prestressed Concrete Reactor Pressure Vessel) (Ref. 4-2) for nuclear-graded equipment, or the reference coal plant for conventional construction. (Ref. 4-2) Systems and equipment costs were adjusted for variations in size, capacity and function using scaling exponents (see Table 4-4) developed from the study of nuclear and coal plants of Ref. 4-2. The ground rules used as an estimating basis were developed by the Gas-Cooled Reactor Associates program for power plant comparative studies in Ref. 4-4. These ground rules were formulated and are continuously reviewed by program participants such as GA, BGI, SWEC, CE, ORNL, NUTEVCO, SDG&E, NE Utilities, EPRI/COMO, DOE, etc.

The economic comparison of the ICF plant concept with comparable sized fission and fossil plants is given in Table 4-3. This comparison is based on the revenue requirements method used by utilities to forecast rates. The method computes the

TABLE 4-4
Scaling Factors for Increased & Decreased Capacity
Cascade ICF Plant
Applicable Range = 400 to 1200 MW(e)

Account	Description	EXPONENT a[(a)]	
		Nuclear + Conv.	Conventional
20	Land & Land Rights	—	—
21	Structures & Improvements	.20	.76
22	Reactor Plant Equipment	.36	.91
23	Turbine Plant Equipment	.85	.79
24	Electric PlantEquipment	.38	.47
25	Misc. Plant Equipment	.18	.17
26	Heat Rejection System	.86	.80

(a) Application $Y_2 = Y_1 (X_2/X_1)^a$

where X_1 = Capacity of the First Unit

X_2 = Capacity of the Second Unit

Y_1 = Cost of the First Unit

Y_2 = Cost of the Second Unit

a = Scaling Exponent

annual revenue required to yield a return of and on capital investment and a return of all operating expenses (e.g. O&M, fuel, taxes, etc.). This is divided by the annual electricity production to obtain the levelized busbar cost of electricity which is used to compare alternatives. While the analysis is done in constant 1985 dollars, it is based on the real cost of money and the real escalation rates of fuel and other factors of production. Input assumptions used in this analysis are contained in Ref. 4-4. These ground rules maintain a consistency of financial and economic assumptions. Two assumptions were made for Cascade which are not contained in the ground rules. First, it was assumed that the capacity factor was the same as an HTGR plant, 0.75. Second, the O&M costs were assumed to be 30% higher than a PWR plant to account for on-site fuel processing facility expenses.

4.3. PLANT DESCRIPTION

4.3.1. Plant Parameters and Component Arrangement

The major Cascade ICF reactor design parameters are presented in Table 4-5. A flow schematic of the power balance is shown in Fig. 4-1. The baseline case is a reactor producing 1500 MW of fusion power, with a blanket energy multiplication factor of 1.11, resulting in 1670 MW of useful blanket power delivered to the heat exchangers. Of this, 25 MWt is lost to the heat exchanger manifold coolant at low temperature, and the 1645 MWt balance is converted into 905 MW of electrical power (55% efficiency) with a helium closed-cycle gas turbine. Neutron and gamma energy leakage through the blanket (not included in the 1670 MW) is deposited in the shield and vacuum chamber, which generate an additional 75 MW of non-useful (low grade) thermal power. The laser requires 75 MWe to operate and the reaction chamber requires 5 MWe to rotate at 50 rpm and elevate the blanket granules to the required height. An additional plant load of 10 MWe is included in the power balance for miscellaneous plant loads, e.g., running the manifold coolant pumps. The net plant electrical output is 815 MW.

TABLE 4-5
CASCADE ICF POWER PLANT DESIGN FARAMETERS

Power Balance	
Fusion Power	1500 MWf
Thermal Power	
Blanket Thermal Power	1670 MWt
Heat Exchanger Manifold Coolant Power Reject	25 MWt
Turbine Thermal Power Input	1645 MWt
Turbine Thermal Power Reject	740 MWt
Laser Thermal Power Reject	70 MWt
Shield System Power Reject	75 MWt
Plant Load Thermal Power Reject	10 MWt
Total Thermal Power Reject	920 MWt
Electrical Power	
Net Turbine Electrical Output	905 MWe
Laser Electrical Demand	75 MWe
Plant Load	15 MWe
Net Electrical Output	815 MWe
Net Plant Efficiency	49%
Primary Granule Loop	
Surface Layer	
Material	C
Thermal Power	460 MWt (28%)
Inlet Temperature	1500 K
Outlet Temperature	1600 K
Volume Flow Rate	2.2 m^3/s
Mass Flow Rate	2,300 kg/s
Front Zone	
Material	BeO
Thermal Power	220 MWt (13%)
Inlet Temperature	1410 K
Outlet Temperature	1505 K
Volume Flow Rate	1.0 m^3/s
Mass Flow Rate	1,200 kg/s
Breeder (Back) Zone	
Material	$LiAlO_2$
Thermal Power	990 MWt (59%)
Inlet Temperature	1285 K
Outlet Temperature	1355 K
Volume Flow Rate	7.5 m^3/s
Mass Flow Rate	9,600 kg/s
Power Conversion System	
Type	Closed Cycle Gas Turbine
Coolant	Helium
Number of Loops	1
Pressure	5.0 MPa
Inlet Temperature	960 K
Outlet Temperature	1300 K
Mass Flow Rate	960 kg/s
Net Thermal Conversion Efficiency	55%

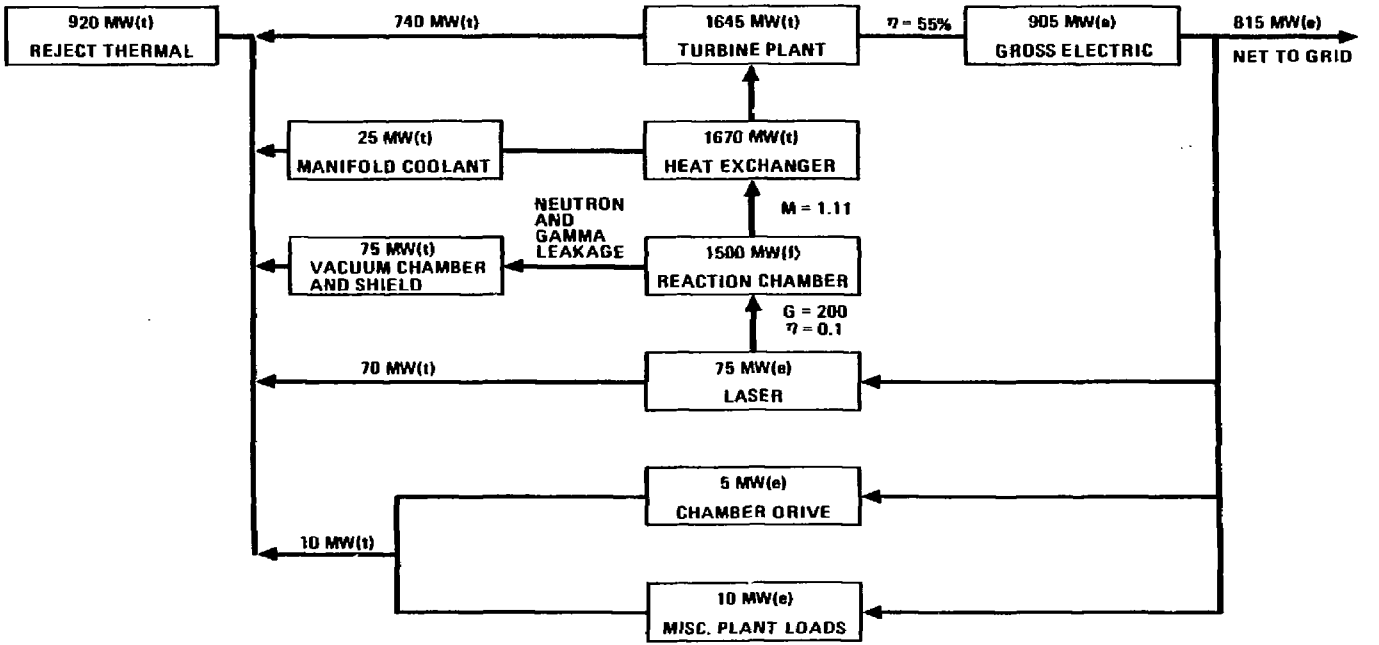

Fig. 4-1. Schematic of Cascade plant power balance.

The plant building arrangement is shown in Fig. 4-2. We determined the building dimensions by considering the form and function of comparable buildings in other reactor studies as detailed in the next section. Within the reactor building, the major components are the reaction chamber, heat exchangers, shielding and vacuum chamber. The arrangement of the former two is shown in the isometric perspective of Fig. 4-3. The integrated arrangement with the vacuum chamber is shown in Fig. 4-4. The individual components are described below. Other equipment within the reactor building includes only transportation, lift, and component-handling fixtures and equipment

4.3.2. Account Description and Cost Basis

This section describes the structures and systems comprising the Cascade ICF power plant. The description corresponds to the two and three digit level account structure of the cost estimate.

Account 20 - Land and Land Rights. This account includes the purchase and clearing of the land, and the relocation of buildings, utilities, highways, and other services necessary for plant construction. These costs are included within the indirect owner's cost account per the ground rules of Ref. 4-4.

Account 21 - Structures and Improvements. The structures for nuclear power plants are normally divided into two categories: Seismic Category I and non-Seismic Category I. Category I structures house all safety-related equipment and are designed to withstand the Design Basis Safe Shutdown Earthquake defined by having a peak ground acceleration of 0.25g. (The basis for the designation of safety-related equipment is presented in Section 4.4.) These structures generally consist of foundation mats, exterior walls, interior walls, floor slabs and roof slabs, all of reinforced concrete. The floor and roof slabs are normally supported on heavy structural steel framing.

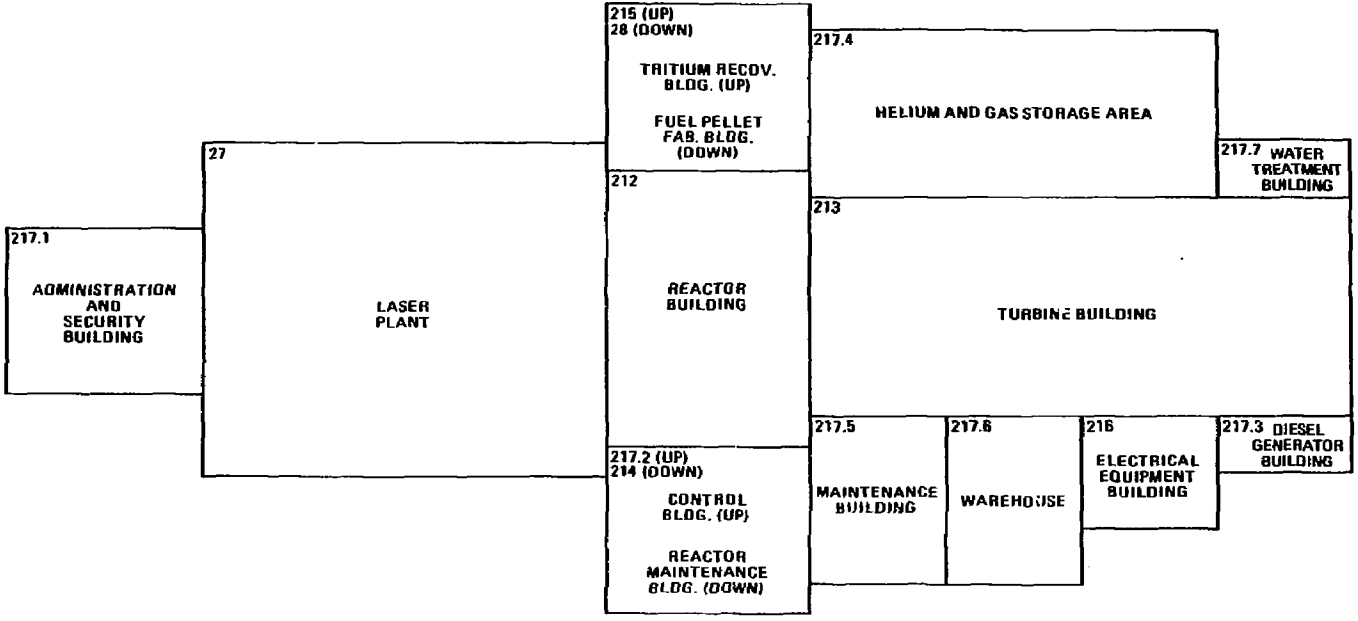

Fig. 4-2. Cascade power plant building arrangement.

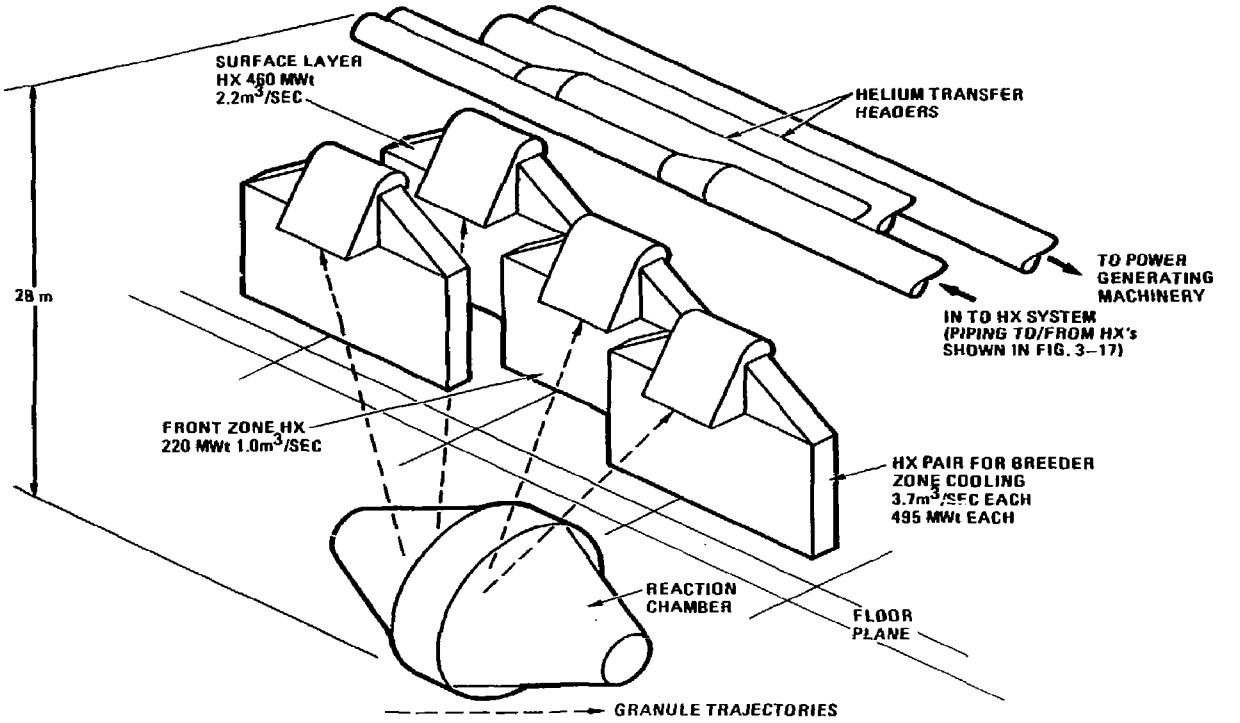

Fig. 4-3. Major component positions within vacuum chamber.

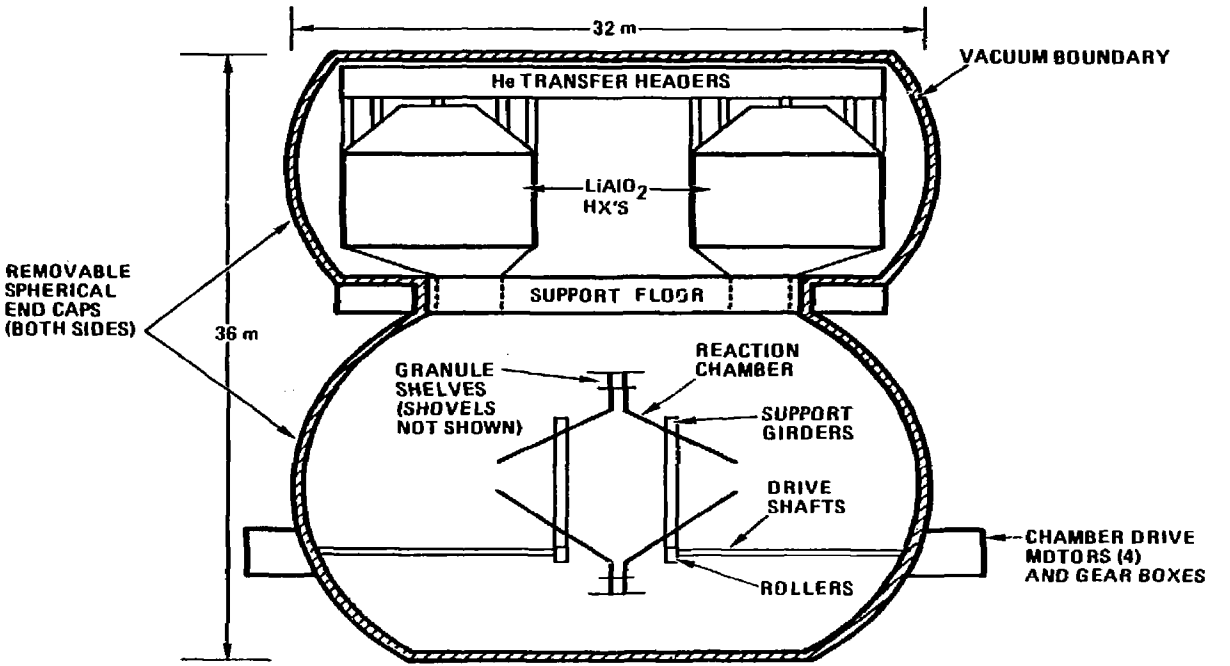

Fig. 4-4a. Vacuum chamber arrangement, side view, Sheet 1.

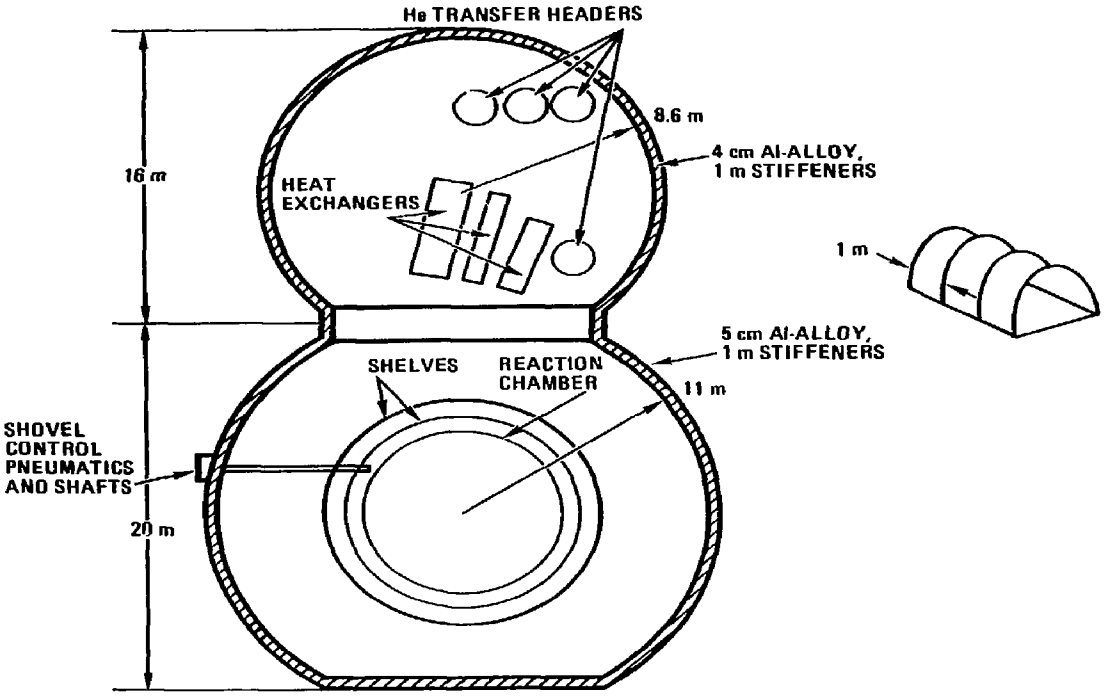

Fig. 4-4b. Vacuum chamber arrangement, end view, Sheet 2.

Non-Category I structures house equipment and components not required for plant safety. The majority of the structures at the Cascade site are of this category. These are generally steel frame structures with insulated metal sidings and built-up insulated roofs. The buildings are designed for normal dead and live loads, including expected loads from natural events and additional loads for seismic conditions as provided in the Uniform Building Code. Thus, they are similar to the buildings of coal-fired plants. When required by proximity, these buildings are designed so that their failure would not lead to loss of function of a Category I structure. The specifications for the Cascade plant buildings are consistent with the inherent safety resulting from the low levels of radioactivity within the Cascade site, as discussed in Section 4.4.

The buildings and structures for the Cascade plant included in Account 21 are the reactor building, turbine building, reactor maintenance, tritium recovery building, electrical equipment building, administration and security building, control building, diesel generator building, helium building, maintenance and warehouse buildings, and a water treatment building. The ultimate heat sink structures, the laser building, and target manufacturing building are included in Accounts 26, 27, and 28. Unit costs applied to the buildings are contained in Table 4-6. The resultant building costs are detailed in Table 4-7. The safety classification of the buildings is listed in Table 4-8.

Account 211 – Site Improvements and Facilities. This account includes earthwork, roadways, walkways and parking areas. It also includes installation of electrical and mechanical utilities, such as underground ductwork, lighting, emergency power generation, water systems, fire protection and a railroad spur. The cost of this account was scaled from Ref. 4-1.

Account 212 – Reactor Building. The reactor building houses the vacuum chamber, within which the reaction chamber and main heat exchangers are located, the vacuum system, the chamber drive system, the blanket granule scoop drive system, the shield system, the final turning and focusing mirrors, and the target injection

TABLE 4-8
STRUCTURES & IMPROVEMENTS UNIT COSTS COMPARISON
1/86 DOLLARS

CASCADE ACC NO.	DESCRIPTION	SBS (1) VOLUME CF x 1000	SBS (1) COST $/CF	HTGR (2) VOLUME CF x 1000	HTGR (2) COST $/CF	PWR (3) VOLUME CF x 1000	PWR (3) COST $/CF	CASCADE NUCL COST $/CF	CASCADE CONV. COST $/CF
21	STRUCTURES & IMPROVEMENTS								
212	REACTOR BUILDING	1,777.8	12.46	2,960.0	19.50	3,000.0	33.41	12.46(1)	3.25(4)
213	TURBINE BUILDING	1,824.0	2.85	4,862.0	2.33	7,500.0	4.78		2.85(1)
214	REACTOR MAINTENANCE BLDG.	315.8	31.20	1,132.0	11.94	1,140.0	22.95	31.20(1)	7.60(5)
215	TRITIUM RECOVERY BUILDING							31.20(1,8)	7.60(5)
216	ELECTRICAL EQUIPT. BLDG.								2.85(6)
217.1	ADMIN. & SECURITY BLDG.	290.0	9.66	998.00	6.80	1,500.0	6.36		9.66(1)
217.2	CONTROL & INSTR. BLDG.	180.0	13.33	1,500.0	15.37	900.0	32.78	13.33(1)	9.66(7)
217.3	DIESEL GENERATOR BLDG.			994.0	10.03	630.0	18.28		2.85(6)
217.4	HELIUM STORAGE AREA	20,000 SF	20.00(9)	41,900 SF	33.54(9)				20.00(1)
217.5	MAINTENANCE BLDG.	2,262.0	1.19						1.19(1)
217.6	WAREHOUSE	138.6	2.16	70.0	3.70				2.16(1)
217.7	WATER TREATMENT BUILDING								7.41(5)

(1) 4 x 250 MW(t) HTGR PLANT SIDE-BY-SIDE STEEL VESSEL CONCEPT (3/86)
(2) 2240 MW(t) HTGR-SC ELECTRICAL GENERATING PLANT (1/80 $'s ESC. TO 1/86 at 47%)
(3) 1139 MW(e) PWR (1/83 $'s ESC. TO 1/86 at 12%)
(4) RICHARDSON CONSTRUCTION ESTIMATING STANDARDS (1/86)
(5) 800 MW(e) COAL FIRED FOSSILE PLANT (1/80 $'s ESC. TO 1/86 at 47%)
(6) *BASED ON TURBINE BUILDING COST*
(7) BASED ON NON-CATEGORY I ADMINISTRATION & SECURITY BUILDING
(8) BASED ON REACTOR MAINTENANCE BUILDING
(9) $/SQUARE FOOT

TABLE 4-7
PRELIMINARY CAPITAL COST DETAILS
OF CASCADE ICF PLANT BUILDINGS
1/86 $ x 000

ACC. NO.	DESCRIPTION	QTY.	UNIT	UNIT COST NUCL.	UNIT COST CONV.	TOTAL COST NUCL.	TOTAL COST CONV.	TOTAL	ALL CONV. UNIT COST	ALL CONV. TOTAL
21	STRUCTURES & IMPROVEMENTS									
211	YARDWORK					5.4	1.6	7.0		3.1
212	REACTOR BUILDING	2,118,780	CUB.FT.	12.46		26.4		26.4	3.25	6.9
213	TURBINE BUILDING	4,620,260	CUB.FT.		2.86		12.9	12.9	2.86	12.9
214	REACTOR MAINTENANCE BUILDING	476,750	CUB.FT.	31.20		14.9		14.9	7.60	3.6
215	TRITIUM RECOVERY BUILDING	476,750	CUB.FT.	31.20		14.9		14.9	7.60	3.6
216	ELECTRICAL EQUIPMENT BUILDING	141,260	CUB.FT.	0.00	2.86		0.4	0.4	2.86	0.4
217.1	ADMIN. & SECURITY BUILDING	276,000	CUB.FT.		9.66		2.7	2.7	9.66	2.7
217.2	CONTROL & INSTR. BUILDING	277,000	CUB.FT.	13.33		3.7		3.7	9.66	2.7
217.3	DIESEL GENERATOR BUILDING	141,260	CUB.FT.		2.86		0.4	0.4	2.86	0.4
217.4	HELIUM STORAGE AREA	1,800	SQ.FT.		20.00		0.0	0.0	20.00	0.0
217.5	MAINTENANCE BUILDING	423,800	CUB.FT.		1.19		0.3	0.3	1.19	0.3
217.6	WAREHOUSE	423,800	CUB.FT.		2.16		0.5	0.5	2.16	0.5
217.7	WATER TREATMENT BUILDING	28,250	CUB.FT.		7.41		0.2	0.2	7.41	0.2
	TOTAL STRUCTURES & IMPROVEMENT					65.3	19.0	84.3		37.3

UNIT COSTS REF. TABLE 4-6

TABLE 4-8
BUILDINGS AND STRUCTURES

Potentially Category I
Reactor Building
Reactor Maintenance Building
Tritium Recovery Building
Control Building
Target Fabrication Plant Building

Non-Category I
Turbine Building
Electrical Equipment Building
Administration and Security
Diesel Generator Building
Helium Storage Area
Maintenance Building
Warehouse
Water Treatment Building
Heat Rejection Structures
Laser Plant Building

system. Also included are portions of the secondary helium loop, shield cooling and recirculating gas cooling systems. The building is a rectangular metal structure, 40 m by 30 m by 50 m high, supported on concrete footings and framed with structural steel. The ground floor is a concrete slab and the upper floors are grating. Costs are scaled from Ref. 4-1.

Account 213 – Turbine Building. The turbine building contains the turbine generator, helium compressors, regenerative heat exchanger, intercoolers and the support equipment necessary to generate electricity. This three-level, non-Category I building is estimated to be 40 m by 80 m by 40 m high based on the 913 MWe turbine building designed and costed in Ref. 4-2.

Account 214 – Reactor Maintenance Building. This building provides working areas for radiation containment during maintenance, assembly, disassembly, and repair functions outside the reactor building. Specifically included in this account are a warm cell for hands-on maintenance of radioactive components, an area for decontamination of activated components and target activation removal, and a waste processing area. The building is estimated to be 30 m by 30 m by 15 m high and costed based on Ref. 4-2.

Account 215 – Tritium Recovery Building. This building contains the tritium recovery system, including the Fuel Cleanup System, Atmosphere Detritiation system, and the Water Detritiation System. It is estimated to be 30 m by 30 m by 15 m high based on the similar design of Ref. 4-5, and costed using the unit costs of Ref. 4-2.

Account 216 – Electrical Equipment Building. This building houses the power conditioning and electrical distribution equipment and is estimated to be 20 m by 20 m by 10 m high based on the design and cost of the system of Ref. 4-1.

Account 217.1 – Administration and Security Building. This is a 3-story steel-framed structure, with dimensions 30 m × 30 m. The walls are insulated siding, and the roof is metal deck with insulation and built-up roofing as in Ref. 4-1.

Account 217.2 – Control Building. This three-story building has estimated dimensions of 30 m × 30 m. The Category I option has reinforced cast-in-place concrete walls, floors and roof which are supported on a continuous concrete mat foundation at grade. The non-Category I building is structural steel framed with insulated metal siding. The design and cost basis is Ref. 4-1.

Account 217.3 – Diesel Generator Building. This building houses the backup diesel generator used to generate emergency power in the event of failure of the off-site source of auxiliary power. Dimensions are estimated as 20 m by 20 m by 10 m high based on Ref. 4-1.

Account 217.4 – Helium Storage Area. This is a non-Category I concrete paved area estimated to be 60 m × 30 m suitable for storage tanks as in Ref. 4-1.

Account 217.5 – Maintenance Building. This is a non-Category I steel-framed structure with metal siding and roof. Dimensions are estimated to be 30 m by 15 m by 10 m. Costs are based on Ref. 4-1.

Account 217.6 – Warehouse. This is a non-Category I steel-framed structure with metal siding and roof, suitable for storing construction and maintenance supplies and equipment. Dimensions are estimated to be 30 m by 20 m by 10 m. Unit costs are based on Ref. 4-1.

Account 217.7 – Water Treatment Building. This is a non-Category I building with steel framing, uninsulated metal siding and roof with dimensions of 20 m by 10 m by 4 m high. Design and cost is based on Ref. 4-1. This building treats less water than the building of Ref. 4-1 because Cascade uses water only for ultimate heat rejection and not for the secondary, power producing loop.

Account 22 – Reactor Plant Equipment. The Reactor Plant Equipment account includes the fusion device and all of its directly supporting services. Thus, the major elements of this account are the reaction chamber, blanket, chamber drive, vacuum

system, granule transport system, primary heat exchangers, shielding, tritium recovery system, and instrumentation and control. The costs listed below assume nuclear qualification of all reactor plant equipment. Conventional costs are obtained by applying a cost reduction factor of 0.9 to reactor plant equipment. This factor is based on GA and architect/engineer experience and reflects the reduced quality assurance documentation requirements of conventional facilities not requiring the three-tier quality assurance levels of nuclear equipment. The cost reduction factor for instrumentation and control equipment is 0.63 based on comparative analysis of nuclear versus coal plant instrumentation and control system costs.

Account 221 – Reaction Chamber. The reaction chamber is configured as two attached conical frustrums of 5 m maximum radius with 35° half-angle sloping walls. The reaction chamber is constructed of 2 cm thick silicon carbide box-shaped tiles, 50 cm on a side, and held in together in compression by 3 cm longitudinal and circumferential prestressing tendons of Al/SiC composite. Installed costs are \$5.3M for the 3.2×10^4 kg SiC structure and \$1.3M for the 4.5×10^3 kg tendons, based on vendor unit prices and in-house fabrication labor estimates. (Table 4-9 and Ref. 4-6) The 270 m^2 surface outside surface area of the chamber is lined with 15 cm of thermal insulation and covered with an Al/SiC composite shroud. The total cost of this item is \$0.1M. Cost of the 2000 kg Al/SiC composite support and drive girders is \$0.5M, and that of the 1.1×10^4 kg SiC outlet shelves is \$2.5M. Total direct capital cost of the reaction chamber is thus \$9.7M.

Account 222 – Blanket. The blanket mass of C in the Cascade chamber is 1.6×10^3 kg. An additional 5.1×10^4 kg is located in the heat exchangers and in transit through the primary loop.

Cost of the 5.3×10^4 kg total mass of C in the system is \$6.8M. The blanket mass of BeO in the Cascade chamber is 1.6×10^4 kg with an additional 3.8×10^4 kg in the heat exchangers and in transit through the primary loop. Cost of the 5.4×10^4 kg is \$3.1M. The blanket mass of $LiAlO_2$ is 2.2×10^5 kg with an additional 1.7×10^5 kg in the heat exchangers and in transit through the primary loop. Cost of the 3.9×10^5 kg

TABLE 4-9
COST ESTIMATE
SiC MATERIALS AND FABRICATION

Size/Configuration	Fabricated Cost (1985, $/kg)
Small/simple	90
Small/complex	140
Large/simple	180
Large/complex	280
Fiber	600

Notes:

Add $20/kg for high purity.

Add 10% for installation.

Reduce by factors of 2 to 3 for volume demand.

of breeder is estimated at $35.5M. These costs are based on recent GA purchases of these materials, adjusted for large commercial volume. Total cost of the blanket materials is $45.4M.

Account 223 – Chamber Drive. The reaction chamber rotates on 24 Al/SiC composite 0.75 m diameter rollers. The total cost of these 300 kg (each) rollers is $2.4M. Chamber drive is accomplished via 4 axle shafts of 8 cm diameter also made of Al/SiC composite. The installed cost of these shafts is $0.4M. The four 1.3 MW chamber drive motors are sized to elevate 1.3×10^4 kg/s of blanket material to a height of 20 m, assuming 50% scoop efficiency. The cost of these constant speed motors is $2.4M based on similar units in Ref. 4-2. The total cost of the Chamber Drive account is thus $5.2M.

Account 224 – Vacuum System. The Vacuum System consists of those components which provide the low pressure environment required for laser propagation. This includes the vacuum chamber, pumps, ducts, valves, and instrumentation and control. This account also includes the vacuum chamber cooling system.

The vacuum chamber provides a barrier between the reactor building atmosphere and the evacuated space within the reaction chamber, granule transport and heat exchangers. This account includes the chamber structure, support structure, coolant hardware, seals, insulation, and local instrumentation. The vacuum chamber is configured as two cylindrical aluminum alloy vessels attached along their length, with spherical endcaps. It is shown in Fig. 4-4. The upper 8.6 m diameter cylinder is self-supporting against buckling forces, having a structural thickness of 4 cm and stiffeners at 1 m intervals. It surrounds the heat exchangers. The lower cylinder has a diameter of 11.2 m and thickness of 5 cm and is also stabilized by stiffeners at 1 m intervals. It surrounds the reaction chamber and most of the granule transport system. Total aluminum alloy weight is 5.8×10^5 kg. Total installed cost is $99M based on the conventional vacuum vessel construction cost of Ref. 4-7. The vacuum pumping requirements for Cascade are given in Ref. 4-8. These scale to a vacuum pumping speed of 40,000 l/s at a pressure of 0.01 Torr for 1500 MW of fusion power. The cost

of this pumping system is estimated at $1.8M based on the vacuum pumping system of Ref. 4-7. Cost of the 2 kW shield cooling system is $0.6M based on a similar system in Ref. 4-2. Total cost of the vacuum system is $101.3M for conventional grade and $112.6M for nuclear grade.

Account 225 – Granule Transport. This account consists of the SiC components and mechanisms to transport and distribute the blanket granules from the reaction chamber to the primary heat exchangers. This includes the throw scoops, ducting and distribution plenums and chamber feed ports. The throw scoop system consists of the four shovel blades, the rotational shafts and the operational hydraulics. Total SiC mass of these large, complex components is 200 kg. Total system installed cost is $0.1M. The mass of the ducting and distribution plenums is 3.1×10^4 kg. These large, simple SiC components are estimated to cost $6.8M. Mass of the chamber feed ports is 7.1×10^3 kg and their cost is $1.6M. Total cost of the granule transport system is $8.5M.

Account 226 – Primary Heat Exchangers. Included within this account are the primary heat exchangers used to extract the heat from the circulating hot granules. These are described in detail in Section 3.5. Components included within this account are the SiC tubing and shields, steel manifolds and insulation, and interconnecting ducting. The tubing mass is 1.1×10^5 kg, costing $11.4M, and the shield mass is 3.7×10^4 kg, costing $7.3M. The coaxial steel manifolds have a mass of 1.7×10^5 kg and 2600 m^2 of thermal insulation. Cost of the manifolds is $2.0M and that of the insulation is $19.3M based on a similar insulated, coaxial manifold design costed in Ref. 4-3. The 3.5×10^5 kg of insulated steel ducting is estimated to cost $11.6M also based on Ref. 4-3. Total heat exchanger cost is $51.5M.

Account 227 – Shielding. Shielding consists of those components which provide neutron and gamma attenuation with the intent of minimizing activation of reactor components. This account includes both radiation and biological shielding, and the associated shield heat removal systems. The radiation shield is an aluminum alloy tank containing borated water which fits around the reaction chamber. (See

Chapter 6.) The shield tank consists of two concentric double cones of aluminum alloy, with inner and outer wall thickness of 3.25 and 4.2 cm. The water-filled shield is 2 m thick, and is spaced 2 m from the reaction chamber. The shield requires 9.0×10^4 kg of high purity aluminum alloy. Costs are based on unit costs developed in Refs. 4-2 and 4-7. The biological shield is 3 m thick concrete, external to the vacuum chamber to an elevation above the reaction chamber but below the heat exchangers, and internal to the vacuum chamber, i.e., as the floor to the heat exchangers, above the reaction chamber. Biological shielding requirements are met with 1.1×10^4 m^3 of concrete. This concrete is normally poured into horizontal, interlocking blocks, moved to the shielding area and stacked. Cost of this rebar-reinforced concrete is $3.2M. The design basis for the shield cooling system assumes a heat load of 75 MWt using a water-to-air heat exchanger. The cost is $4.8M based on Ref. 4-3. Total cost of the shielding system is $25.1M.

Account 228 – Radioactive Material Handling. This account includes the tritium recovery system and the systems required to collect, store, and process radioactive materials for disposal. The tritium recovery system includes all the equipment required to recover tritium from the vacuum chamber exhaust stream, secondary coolant, shield coolant, vacuum chamber coolant, and the atmospheric recovery system used externally to the vacuum chamber within the reactor and tritium recovery buildings. It is described in Chapter 5 and costs were obtained for all components by scaling the cost of similar components in Ref. 4-9. The cost of the Fuel Cleanup System processing the vacuum chamber exhaust is $4.1M. The cost of the Atmosphere Detritiation System handling the secondary coolant flow and building atmospheres is $4.6M. The cost of the Water Detritiation System handling the shield and vacuum chamber coolants is $4.2M. The total tritium recovery system cost is thus $12.9M. The radioactive waste processing system design/cost basis is assumed to be that of Ref. 4-3. A 50% reduction in the liquid waste handling cost is included as an allowance for the smaller size of Cascade's water loops, which are only used for vacuum chamber wall and shield cooling. The resultant cost is $3.8M.

Account 229 – Instrumentation and Control. This account includes all of the centralized processing, monitoring, controlling, and diagnostic systems for the reactor plant equipment. This includes the data acquisition systems, man-machine interfaces, diagnostics, and central data processing and operations software. Costs for a nuclear-grade system is estimated to be $8.1M based on Ref. 4-3, and $5.1M for a conventional system based on Ref. 4-2.

Account 23 – Turbine Plant Equipment. This account includes the equipment and systems required to utilize the helium Brayton Cycle for power conversion. The design of the the power conversion system is described in Chapter 3. The basic cost reference used for the helium Brayton Cycle is Ref. 4-3, which was performed by United Engineers and Constructors for GA. The Turbine Plant Equipment cost is $183.7M for nuclear grade equipment and $156.1 for conventional equipment. The major sub-accounts are discussed below.

Turbine Generator, Pedestal and Accessories. The total cost for this sub-account is $80.0M for conventional construction and $94.1M for nuclear grade construction. The helium-driven turbine was costed on the basis of $70/kWe. To provide perspective on the dimensions of the turbine, the design of the 400 MWe turbine of Ref. 4-3 employed a machine casing of 4.0 m diameter and a machine length of 11.3 m. An extrapolation of the design to 600 MWe projected the same casing diameter and a length of 15.8 m. The 905 MWe of Cascade would require a comparable extrapolation and is not expected to have a significant impact on the unit cost. These turbines are projected to last the full life of the plant (280,000 h). The pedestal for the Cascade turbine requires 10^4 m^3 of concrete.

Main Compressors. The cost of the main helium circulators was estimated to be $14.2M for conventional equipment and $16.7M for nuclear safety grade equipment based on the auxiliary circulators of Ref. 4-3. The circulators are located on the shaft driven by the turbine. These components are approximately 10 m long and have a maximum diameter of 4 m.

Helium Coolers. The cost of the helium coolers was estimate at $2.8M for conventional equipment and $3.2M for nuclear grade based on the auxiliary heat exchanger design of Ref. 4-3. That 1170 MWt helium-to-water heat exchanger design has 700 tubes with an active tube height of 7 m, and heat exchange area of 430 m^4. The heat exchanger has an outside diameter of 1.2 m.

Regenerative Heat Exchanger. The cost of the intermediate heat exchanger design of Ref. 4-3 was scaled to the power rating of Cascade. We obtained a cost of $46.2 for a conventional component and $54.5 for nuclear rated heat exchanger. For reference, the 1170 MWt helium-to-helium design of Ref. 4-3 has an outside diameter of 2.4 m and employees 1.6×10^4 tubes of 14 m length and 9.0×10^3 m^2 surface area.

Account 24 - Electric Plant Equipment. This account includes the equipment which distributes the power generated in the plant to the utility system and plant loads. In the absense of power generation, the electric plant equipment distributes power from the utility system to the plant loads. It is also the source of power for plant control and minor loads in the absence of off-site power. Equipment in this account includes switchgear, station service equipment, switchboards, protective equipment, electrical structure and wiring containers, power and control wiring, and a diesel generator. The plant load during operation is 15 MWe, plus an additional 75 MWe for the laser. Costs for both nuclear and conventional electrical plant equipment are scaled from Ref. 4-2. Costs include an allowance for two diesel generators in the nuclear design and one in the conventional Cascade to operate the turbine plant equipment, the chamber drive, to handle reactor building cooling loads and essential services during reactor startup and other times when the reactor is not generating electricity. The nuclear versus conventional split of equipment was derived from the similar approach adopted in Ref. 4-1. Total cost of this account is $70.6M for the "Nuclear+Conventional" reactor, and $46.6M for the conventional Cascade.

Account 25 – Reactor Maintenance Plant. The reactor maintenance plant account includes all general purpose and special purpose equipment needed to perform maintenance operations on reactor components and support services systems. This includes transportation and lifting equipment, air, helium and water services systems, helium storage and transfer system, diesel cooling water system, communications equipment, furnishings and fixtures, water treatment equipment, fire detection system, security system, monitoring equipment, and the equipment for decontamination and radioactive waste treatment, processing, packaging, and shipping. Costs scaled from Ref. 4-2, using the nuclear/conventional split of Ref. 4-1 yield a total account cost of $16.3M. The cost for an all-conventional reactor is $12.0M.

Account 26 – Heat Rejection System. The heat rejection system consists of the structures and mechanical equipment necessary to reject heat from the turbine, shield, vacuum chamber, etc. to the atmosphere. For Cascade, a natural draft cooling tower with water makeup was selected to provide flexibility in site selection. This account includes the cooling tower structures, makeup water intake structure, discharge structure, circulating water pump house, makeup water treatment building, chlorination building, and cooling tower switchgear building. The mechanical equipment includes the piping instrumentation and controls for water intake system, circulating water system, cooling tower and main makeup system, blowdown system, and makeup water pre-treatment system. This non-Category I structure rejects a total of 920 MW thermal. The design/cost basis is the shell-and-tube heat exchanger design of Ref. 4-2. The site is assumed to have adequate makeup water capability. The design includes a small mechanical draft tower for ultimate heat rejection in emergency situations. The cost of this account is $21.5M.

Account 27 – Laser Plant Building and Equipment. This account includes all elements of the laser, laser power, optics, etc. It was estimated to cost $275M by LLNL. (Ref. 4-10)

Account 28 – Fuel Pellet Fabrication Plant Building and Equipment. This account includes all elements of the Fuel Pellet Fabrication Plant, from processing of the D-T gas stream processed by the Tritium Recovery System to delivery into the reaction chamber. This account was estimated to cost $100M by LLNL. (Ref. 4-10)

Accounts 91 to 94 – Indirect Costs. In addition to the direct costs related to the construction of the ICF plant, the capital cost estimates include undistributed costs (indirect costs) related to the support of construction. These costs include expenditures for material, equipment, and labor needed to support fabrication and construction, engineering design and construction management of the plant as well as tools, equipment, temporary structures, and services used in building and start-up of the plant.

Indirect rates were determined by extrapolations from best estimates for a single 2240 MW(t) HTGR plant (Ref. 4-2) plus actuals from recent fossil and successful LWR plants. These extrapolated rates were presented in tabular form as percentages of the direct Capital Cost within the GCRA Groundrules, Ref. 4-4. The HTGR and PWR rates were used for the nuclear construction and the fossil rates were used for the conventional construction of the ICF power plant.

Owner's costs are included in the indirect accounts. These include costs for: the purchase and licensing of the site; relocation of existing facilities on the site; engineering and quality assurance; project integration and licensing activities performed by the utility staff; preparation of training materials and training and licensing of operators and maintenance personnel prior to start of plant operations; insurance premiums; state and local property taxes on the site and improvements during construction; transportation and sales tax on purchased materials and equipment; Owner's G&A; initial stock of supplies, consumables and spare parts needed at start of plant operations, and permits, licenses, and hearings and fees. These costs were calculated for the Cascade ICF Power Plant based on percents of direct capital costs as outlined in the Ref. 4-4.

Contingency includes an allowance for the cost estimate uncertainty due to the lack of definition in the plant design and cost estimate basis. Contingency factors of 15% and 10% were used for nuclear and conventional costs, respectively.

4.4. SAFETY

4.4.1. Introduction

The Cascade approach to fusion power offers some very attractive safety features. First, tritium inventory and routine permeation release are very low. Second, the use of low activation materials brings the benefits of minimum radioactive inventory and decay heat production. Third, the use of a solid breeder avoids the potential for a large uncontrolled chemical energy release. Cascade minimizes both the radioactive source term as well as the mechanism for its release and thus approaches the inherent safety and environmental potential of fusion. These inherent advantages can be translated into an economic advantage by exploiting the cost savings of conventional versus nuclear classification of plant components and equipment and by avoiding unnecessary safety systems. By providing safety design guidance early in the design stage, we can minimize safety-related costs. In this section, we review the fission-industry's licensing criteria on accidental and routine releases of radioactivity and waste disposal and discuss their applicability to Cascade. We then determine the appropriate licensing boundary classifications and develop the system design requirements which will maximize Cascade's advantages and minimize the need for dedicated safety systems.

4.4.2. Licensing Criteria

The basic goal of licensing criteria is to ensure the safety of the general public by providing for safe shutdown of reactor operations from any credible event relying only on safety-related equipment. In the context of nuclear power plant design practice and standards, safety is the quality of averting or not causing undue radiological effect on the health of the public. (Ref. 4-1 and 4-2) Thus, from a regulatory perspective,

safety is measured strictly with respect to public dose criteria. The prevention of economic damage to the reactor is the purview of the plant owner, but economics are a secondary issue in the consideration of safety-related equipment. Safety-related equipment includes all systems and components with functions necessary to ensure the capability to prevent events or mitigate the consequences of events that could result in offsite exposures which approach or exceed regulatory dose limits. (Ref. 4-1 and 4-2)

The general approach to evaluating safety and establishing safety requirements is to analyze postulated accidents to determine consequences in terms of the release of radioactivity and doses to operators and the public, including such factors as the length of time for accident progression and the time available for corrective action. Damage to equipment is considered only in so far as it leads to a radioactive release. The data generated in these analyses, together with regulatory guidelines, are used to determine the equipment classification, design criteria, and quality assurance criteria of the systems which are called upon to respond to the events. These include:

- system specifications and component requirements, e.g., containment building requirements (leaktightness) and cooling system performance
- auxiliary system and redundancy requirements, e.g., extent of instrumentation
- automation of responses and related instrumentation
- quality assurance requirements
- in-service environmental qualifications of equipment.

At present, classification systems for safety (structural/mechanical/electrical), seismic, and quality assurance level have been developed. (Ref. 4-11 and 4-12) The safety classifications were motivated by the need to maintain the integrity of the reactor coolant pressure boundary and adequate core cooling and geometry, and to provide radioactivity holdup or isolation. The seismic and quality classifications also assign levels to equipment and systems which are indicative of their importance to

safety. These classification systems were developed for the fission-nuclear industry, and their applicability to fusion in general has not been determined. However, for Cascade in particular, much of the safety classification system would appear to be inappropriate due to the absence of a pressure retaining primary coolant boundary. Nonetheless, we can satisfy the intent of a safety classification system by identifying the equipment necessary to satisfy the radiological safety requirements.

Although the accident scenarios and classification systems developed by the fission industry may not apply, the dose guidelines used by the fission industry will probably either be directly applicable or serve as as useful references in defining the radiological safety requirements. The current Nuclear Regulatory Commission (NRC) regulations covering fission reactors are described in the code of Federal Regulations in Sections:

- 10CFR20 – Standards for Protection Against Radiation (Ref. 4-13)
- 10CFR50 – Domestic Licensing of Production and Utilization Facilities (Ref. 4-14)
- 10CFR100 – Reactor Site Criteria (Ref. 4-15)

The present industry guidelines for satisfying the regulations are shown in Table 4-10. The numerical dose limits are shown in Table 4-11. These NRC regulations define the maximum dose limits and releases of radioactivity during routine and anticipated operations (10CFR20 and 10CFR50) and during severe hypothetical accidents (10CFR100). In general, these guidelines were established based on the biological effect of a radioactive release and are thus independent of the source of the release. Therefore, even though the regulations frequently reference nuclides of importance to nuclear fission which will have no significance in fusion, e.g., thyroid dose from iodine-131, the intent of the guidelines remains valid.

To assist licensees in complying with the regulations, the NRC issues Regulatory Guides which describe acceptable methods of evaluating specific problems and postulated accidents. The Regulatory Guides are not regulations and compliance with them is not required. Methods different from those described therein are acceptable if they provide the basis for the findings requisite to demonstrating compliance with the regulations. Again, though the specific accident scenarios and radionuclide release assumptions considered in the Regulatory Guides may not apply to fusion, many of the analysis techniques, such as the nuclide transport mechanisms and meteorological assumptions, remain valid. USNRC Regulatory Guides of greatest interest to Cascade include but are not limited to:

- Regulatory Guide 1.3 – Assumptions Used for Evaluating the Potential Radiological Consequences of a Loss of Coolant Accident for Boiling Water Reactors (contains assumptions for atmospheric diffusion and dose conversion during severe accidents)
- Regulatory Guide 1.109 – Calculation of Annual Doses to Man from Routine Releases of Reactor Effluents for the Purpose of Evaluating Compliance with 10CFR50, Appendix I (contains calculational models for the estimation of radiation doses from routine effluent releases)
- Regulatory Guide 1.111 – Methods for Estimating Atmospheric Transport and Dispersion of Gaseous Effluents in Routine Releases from Light-Water-Cooled Reactors (complements Regulatory Guide 1.109)

4.4.3. Safety Design Guidance

In this section, we present the design guidance obtained by applying the established and applicable safety analysis and licensing methodology to Cascade. We have then designed Cascade such that the numerical dose limits are inherently satisfied to the greatest extent possible, nuclear classification of equipment is avoided wherever possible, and the number of additional systems required for compliance is minimized. Below, we present design guidance on the maximum decay heat level which

TABLE 4-10
PRESENT INDUSTRY GUIDELINES ON DOSE EXPOSURE (Ref. 4-11)

Frequency of Occurrence (F) per Reactor Year[1]	Plant Condition (PC)	Offsite Dose Criterion
Planned Operations	1	10CFR50, App. I[2]
$F > 10^{-1}$	2	10CFR50, App. I[2]
$10^{-1} > F > 10^{-2}$	3	10% of 10CFR100[3]
$10^{-2} > F > 10^{-4}$	4	25% of 10CFR100[3]
$10^{-4} > F > 10^{-6}$	5	100% of 10CFR100[3]

[1] Data compiled from fission reactor license applications reviewed by the Nuclear Regulatory Commission.

[2] Dose objectives of 10CFR50, Appendix I must be met for the summation of radioactive releases due to PC-1 events and the annual average of PC-2 events. Individual radionuclide concentration limits are given by 10CFR20, Appendix B.

[3] Dose limits during preliminary design and review are 80% of the maximum allowable whole body limit, and 50% of the maximum allowable limits for all other doses.

TABLE 4-11
NUMERICAL DOSE LIMITS

10CFR20 – Routine Release	
• Maximum permissible concentrations of radionuclides in air and water	
– specified by individual isotopes for occupational and public areas in Appendix B	
• Occupational exposure of	
– whole body or individual organs	5 rems/y
– extremities	75 rems/y
– skin	30 rems/y
10CFR50, Appendix I (Public)[1] – Routine Release	
• Gases	
– total body	5 mrem/y
– skin	15 mrem/y
• Liquids	
– total body or any organ	5 mrem/y
– total release per reactor (except tritium and dissolved gases)	5 Ci/y
• Particulates	
– any or	15 mrem/y
• As Low As is Reasonably Achievable (ALARA)	
– cost/benefit guideline expenditure to reduce exposure	$1000/man-rem
10CFR100 – Accidental Release	
• Two-hour dose at site boundary, or dose during entire event at low population zone	
– whole body	25 rem
– thyroid	300 rem
– bone, lung, and other organs [2]	150 rem

[1] The DOE recently proposed a limit of 100 mrem/y annual dose from all routine operations to members of the public nearby DOE facilities. (Ref. 4-16)

[2] Inferred from 10CFR100 intent. (Ref. 4-17)

will preclude melting of the blanket. By designing the Cascade blanket accordingly, we eliminate the major energy source which could lead to the release of radioactivity. Cascade's ability to meet this guideline is a significant achievement, approaching the fusion goal of inherent passive safety. We also present design guidance on the maximum tritium inventory and leakage allowable to avoid nuclear qualification, i.e., seismic leak-tightness of the reactor building, and dedicated safety and tritium control systems. As shown below, the Cascade design meets these criteria as well, leading to significant safety, engineering, and cost advantages.

In the activation analysis of Chapter 6, we determined that the major contributor to decay heat is the ^{24}Na produced from (n,α) captures in ^{27}Al. This is a threshold-type reaction, and the level of ^{24}Na in the $LiAlO_2$ can be controlled by moderating the neutron flux entering the $LiAlO_2$ zone below the (n,α) threshold energy. This can be accomplished by adjusting the thickness of the BeO front zone. Figure 4-5 plots the total power generated at shutdown from the decay of ^{24}Na, as a function of the BeO zone thickness. Given the 15.02 h half-life of ^{24}Na, we can calculate the total energy produced as a result of the radioactive decay of this isotope. The result is given analytically by

$$E = \frac{Q_o}{\lambda},$$

where E is the total energy produced, Q_o is the decay power at shutdown, and λ is the radioactive decay constant for ^{24}Na, 1.28×10^{-5} s^{-1}.

We now compare the heat capacity of the materials in the Cascade blanket with the total decay heat generated from ^{24}Na. The data presented in Table 4-12 shows the energy required to heat blanket materials from their average operating temperature to their melting points. The power capacities shown in Table 4-12 are to be compared with the results shown in Fig. 4-5. We see that, conservatively considering only the heat capacity of the blanket materials, a BeO zone thickness of 5 cm will keep the

TABLE 4-12
Heat Capacity of Cascade Materials

Material	Quantity (kg)	Specific heat (v/kg K)	Melting Temp. (K)	Avg. Operating Temp. (K)	Heat Capacity (GJ)	Power Capacity[a] (MW)
BLANKET						
C	5.26×10^{4}	2000	3800	1500	240	3.1
BeO	5.37×10^{4}	2000	2800	1460	140	1.8
$LiAlO_2$	3.94×10^{5}	1500	1880	1320	330	4.2
SUBTOTAL					710	9.1
CHAMBER (SiC)	3.2×10^{4}	1300	3000	1160	80	1.0
INSULATION (C)	1.0×10^{4}	2000	3800	780	60	0.8
SUBTOTAL					850	10.9
SHIELD (c)	2.4×10^{6}	2000	3800	300	1.7×10^{4}	220

[a] Heat capacity $\times$ λ, where λ = radioactive decay constant for $^{24}Na = 1.28\times10^{-5}$ s^{-1}

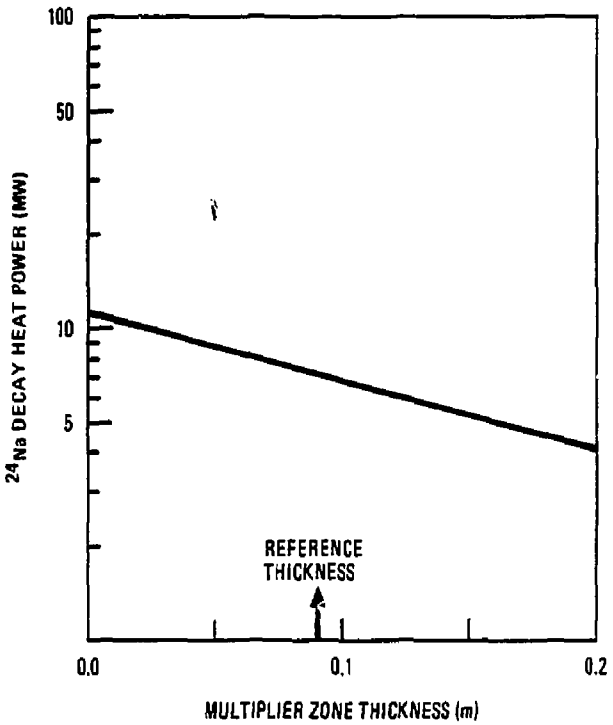

Fig. 4-5. ^{24}Na decay heat power at shutdown versus front zone thickness.

total decay energy below the 710 GJ heat capacity of the blanket, and will preclude melting of the blanket. Thus, the reference blanket, with a 9 cm BeO front zone thickness will not melt. Furthermore, for the reference blanket, the radiation shield provides a massive ultimate heat sink which can passively absorb the total amount of decay energy produced with a temperature rise of only 100 K. An active ultimate heat sink is not necessary.

This analysis assumes that heat generated within the $LiAlO_2$ will be uniformly distributed to the other materials. In an accident situation, the chamber will slow to a stop and the chamber contents will be mixed as it does. This may not be the case in the heat exchangers and granule transport system. Though we did not conduct any detailed transient thermal analyses, we can calculate the thermal diffusivity of the $LiAlO_2$ using the property data of Chapter 2 and thus a thermal time constant for heat conduction. This is to be compared with the $LiAlO_2$ adiabatic heatup time to melt of 13 h. For 1 mm granules the thermal time constant is 0.43 s. The thermal time constant of a slab of $LiAlO_2$ granules will be less than 13 hours for a slab thicknesses less than 25 cm. This means that if the heat exchangers and granule transport system can have a maximum $LiAlO_2$ thickness of no more than 25 cm, melting will not occur. For passive heat transfer to the radiation shield via thermal radiation, the controlling resistance is the insulation. The thermal time constant for a 15-cm thickness of insulation with 0.1 W/m K conductivity and 250 kg/m^3 density is 30 h. In the longer time scale, this heat transfer mechanism would further limit the heat rise in the blanket.

The above analysis indicates that the Cascade blanket is inherently safe from meltdown and thus from accidental radioactivity release. Detailed thermal analysis is recommended to confirm these results, and include additional radioactive nuclides as identified in Chapter 6. In addition, the vapor pressures of the activation products at elevated temperatures must be included in safety analysis of radioactivity release.

Nonetheless, these results form the foundation for eliminating dedicated active safety cooling systems from the baseline reactor design, reducing the containment requirements imposed on the reactor building, and also reducing the costs of system components by specifying conventional construction and qualification rather than "nuclear safety" grade.

Considering tritium events, we can determine the maximum routine tritium leakage rate which will satisfy 10CFR50 and the maximum accidental tritium release which will satisfy the requirements of 10CFR100. The former calculation was performed recently in Ref. 4-18. The results of that calculation indicate that a tritium leakage rate from all sources of 100 Ci/d from a 100 m stack, neglecting nontritium contribution to dose, will meet the 5 mrem/y limit. The allowed leakages from a 10 m stack and ground level would be 10 and 1 Ci/d. The design limits would be lower than these values to account for nontritium contributions to dose and uncertainties.

We then calculated the maximum tritium release which will meet current accident guidelines. The results of that calculation are presented in Table 4-13. The table shows that the maximum inventory is a function of the building containment characteristics and release height. Of greatest interest to Cascade is the result that a tritium inventory of 210 g releasable over 12 h will meet the 25 rem regulatory guideline of 10CFR100 (170 g to satisfy 80% guideline during design stage) without requiring containment leak-rate or seismic qualification of the reactor building, or an effluent release stack.

Based on the findings presented in Chapter 5, Cascade's tritium inventory and leakage rate will meet current regulatory guidelines without requiring safety classification of equipment or dedicated safety systems. Thus, with respect to tritium events, Cascade is inherently safe.

TABLE 4-13

MAXIMUM PERMISSIBLE ACCIDENTAL TRITIUM RELEASE RATES
200 g IN 12 h RELEASE, ACCIDENT METEOROLOGY,
425 m SITE BOUNDARY, 2500 m LOW POPULATION ZONE

Case	Dose (rem)		Maximum Permissible Release Rate (g/12 h)	
	2 h EAB[1]	30 d LPZ[2]	2 h EAB	30 d LPZ
1. No holdup	23	6.6	210	750
2. Confinement at 5.0% vol/d	0.050	0.35	1.0×10^{5}	1.4×10^{4}
3. Confinement at 1.5% vol/d	0.015	0.14	3.4×10^{5}	3.6×10^{4}
4. Containment at 0.1% vol/d	0.001	0.01	5.0×10^{6}	5.0×10^{5}
5. Containment and 100 m stack	1.1×10^{-5}	1.7×10^{-3}	4.5×10^{8}	3.0×10^{6}

[1] EAB – exclusion area boundary.

[2] LPZ – low population zone.

References for Chapter 4

4-1. Bechtel Group Inc., "Preliminary Concept Evaluation Report, 4 x 250 MWt HTGR Plant, Side by Side Steel Vessel Concept," GA Document No. 907974, March 1985.

4-2. United Engineers and Constructors, "The HTGR for Electric Power Generation – Design and Cost Evaluation," GCRA/AE/78-1, Revision 1, August 1981.

4-3. United Engineers and Constructors, "The 1170 MWt HTGR – Reformer Equilibrium Plant," Cost Report - CONCICE Version 5, September 22, 1980.

4-4. J.E. Russ III, "Economic Ground Rules for the HTGR Program," Gas-Cooled Reactor Associates (GCRA) Document HP-20702, Revision 5, January 7, 1985.

4-5. C.C. Baker et al., "STARFIRE – A Commercial Tokamak Fusion Power Plant Study," Argonne National Lab Report ANL/FPP-80-1, September 1980.

4-6. I. Maya, K. R. Schultz et al., "Inertial Confinement Fusion Reaction Chamber and Power Conversion System Study," GA Technologies Report, GA-A17267, September 1984; also Lawrence Livermore National Laboratory Report, UCRL-15642.

4-7. W.C. Finch and K.A. Young, "Doublet III Vacuum Vessel Program – Probabilistic Cost Estimate, Initial Evaluation," GA Project 4804 Internal Memorandum, February 1981.

4-8. Lawrence Livermore National Laboratory, "Laser Program Annual Report 82," UCRL-50021-82, August 1983.

4-9. B.G. Logan et al., "Mirror Advanced Reactor Study, Final Report," Lawrence Livermore National Laboratory Report UCRL-53480, July 1984.

4-10. W. Meier, Lawrence Livermore National Laboratory, Telephone Communication to I. Maya, April 26, 1985.

4-11. American Nuclear Society, "Nuclear Safety Criteria for the Design of Stationary Boiling Water Reactor Plants," ANSI/ANS - 52.1, 1983.

4-12. GA Technologies, "Nuclear Safety Plant Specifications for the HTGR SC/C, 2240 MWt," Report 905842, June 1983.

4-13. USNRC, Code of Federal Regulations, Title 10, Chapter 1, Part 20, June 1979.

4-14. USNRC, Code of Federal Regulations, Title 10, Chapter 1, Part 50, June 1984.

4-15. USNRC, Code of Federal Regulations, Title 10, Chapter 1, Part 100, April 1975.

4-16. R.E. Tiller, "Proposed Revision of DOE Order 5480.1A, Radiation Standards for Protection of the Public," U.S. DOE Memorandum PE-243 to W.H. Hoover, A.W. Trivelpiece and J.W. Vaughan, September 17, 1984.

4-17. K.R. Schultz, F.S. Dombek et al., "Part IV, Section 1, Safety Considerations – Field-Reversed Mirror Pilot Reactor," Electric Power Research Institute Report EPRI AP-1544, September 1980.

4-18. D.L. Smith et al., "Blanket Comparison and Selection Study – Final Report," ANL/FPP-84-1, September 1984.

2-10. M. L. Stehsel, *et al.*, "Modulus of Rupture Measurements on BeO at Elevated Temperatures," *Mechanical Properties of Engineering Ceramics* (ed. W. W. Kreigel and H. Palmour III), Interscience Publishers, New York, 1961, p. 225.

2-11. S. C. Carniglia, *et al.*, "Hot Pressing for Nuclear Applications of BeO: Process, Product and Properties," *J. Nucl. Mater.*, Vol. 14, 1964, p. 378.

2-12. R. E. Fryxell and B. A. Chandler, "Creep, Strength, Expansion, and Elastic Moduli of Sintered BeO as a Function of Grain Size, Porosity, and Grain Orientation," *J. Am. Ceram. Soc.*, Vol. 47, 1964, p. 283.

2-13. C. G. Collins, "Radiation Effects in BeO," *J. Nucl. Mater.*, Vol. 14, 1964, p. 69.

2-14. G. W. Keilholtz, *et al.*, "Properties of MgO, Al_2O_3, and BeO Compacts Irradiated at 150, 800, and 1100°C," *op. cit.*, American Nuclear Society, 1966.

2-15. R. S. Wilks, "Neutron Induced Damage in BeO, Al_2O_3, and MgO: A Review," *J. Nucl. Mater.*, Vol. 26, 1968, p. 137.

2-16. C. A. Brandon, *et al.*, "BeO-Graphite In-Reactor Compatibility at 1500 K and Resulting ^{6}Li Distribution," *Nucl. Appl.*, Vol. 4, 1968, p. 23.

2-17. R. H. Marion and W. A. Muenzer, "Development of Be_2C-Graphite-UC_2 Fuel for Pulsed Reactors," *Trans. Am. Nuclear Soc.*, Vol. 28, 1978, p. 204.

2-18. J. H. Coobs and W. J. Koshuba, "The Synthesis, Fabrication, and Properties of Beryllium Carbide," *J. Electrochemical Soc.*, Vol. 99, No. 3, March 1952, p. 115.

2-19. C. Baker, D. Smith, *et al.*, "Blanket Comparison and Selection Study," Argonne National Laboratory Report ANL/FPP-84-1, 1985.

2-20. JANAF Thermochemical Tables, NSRDS-NBS 37, 1978.

2-21. F. L. Horn, *et al.*, "Performance of Ceramic Materials in High Temperature Steam and Hydrogen," *J. Nucl. Mat.*, Vols. 85 and 86, 1979, p. 439.

2-22. G. H. Rinehart and R. G. Behrens, "Vapor Pressure and Thermodynamics of Beryllium Carbide," *J. Chem. Thermodynamics*, Vol. 12, 1980, p. 835.

2-23. J. H. Pitts, personal communication, September 12, 1984.

2-24. W. Meier, personal communication, July 9, 1984.

2-25. W. Meier, personal communication, November 5 and 21, 1984.

5. TRITIUM ISSUES

5.1. INTRODUCTION

In this chapter we present the tritium inventory, permeation, and recovery systems associated with Cascade. We calculate the tritium inventory in the $BeO/LiAlO_2$ blanket materials, SiC chamber and granule distribution and transport components, heat exchangers and helium manifolds, shielding, vacuum chamber atmosphere, aluminum vacuum chamber, and the tritium recovery systems. We also examine tritium permeation and transport into the vacuum system, vacuum chamber cooling system, shield cooling system, helium working fluid, and the reactor building atmosphere. Finally, we design a tritium recovery system which incorporates the flow from all tritium-bearing streams and maintains tritium concentrations below public exposure guidelines. A flow schematic of the tritium system is shown in Fig. 5-1. The D-T pellet injection system, pellet manufacturing and fuel storage system are assumed to be part of the Fuel Pellet Fabrication Plant and are thus not considered here.

Inventory and permeation calculations were performed assuming classical Arrhenius behavior for solubility and diffusivity, (see e.g., Ref. 5-1) i.e.,

Solubility, g T_2/g solid: $S = S_o e^{(-Q_s/RT)} \times p^{\frac{1}{2}}$

and

Diffusivity, cm^2/s: $D = D_o e^{(-Q_d/RT)}$,

where the pre-exponential S_o is the solubility coefficient in g T_2/g of solid/$atm^{\frac{1}{2}}$, Q_s is the heat of solution in kcal/mole, R is the universal gas constant, 1.9872×10^{-3} kcal/mole/K, T is the temperature of the solid in K, the pre-exponential D_o is the diffusivity coefficient in cm^2/s, and Q_d is the activation energy for diffusion in kcal/mole. Characteristic release times, τ, were conservatively calculated using

$$\tau = \frac{L^2}{15D},$$

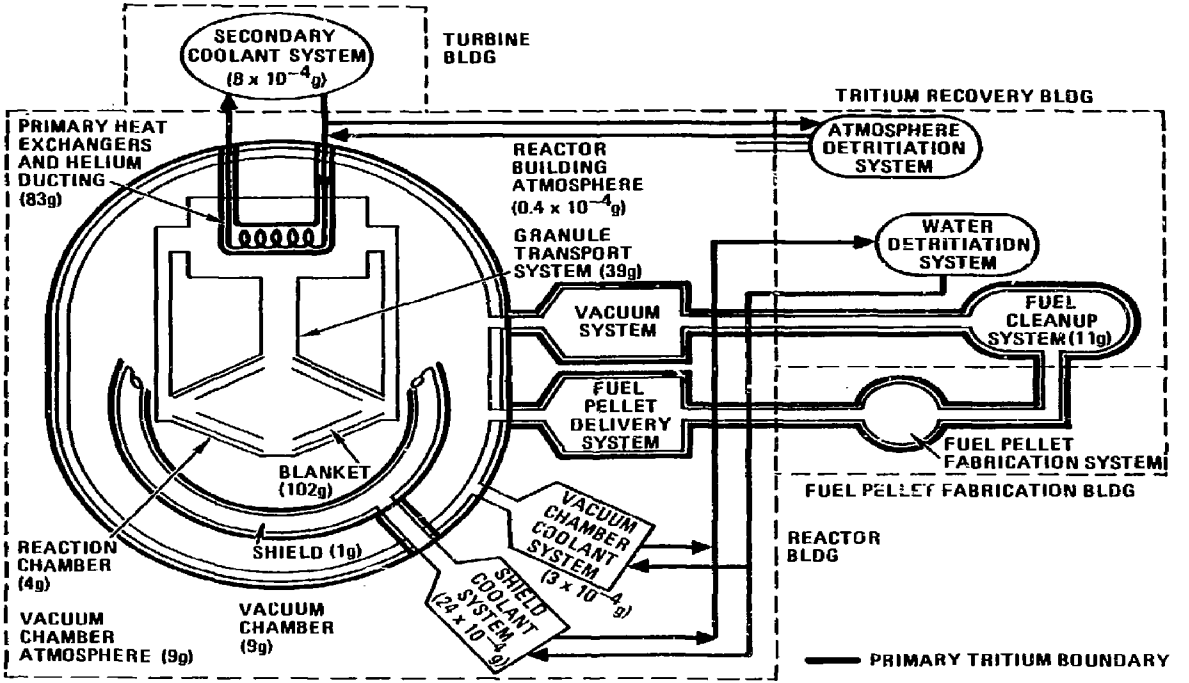

Fig. 5-1. Tritium recovery system and flow schem tic.

where L is a characteristic dimension for escape of the tritium contained in each component. The characteristic release time is the time required for $1/e$ of the inventory to permeate out of the component when the surface concentration is suddenly reduced to zero. This gives a measure of the vulnerability of the tritium inventory to accidental release. An excellent discussion of tritium migration and solubility mechanisms in metallics and ceramics is contained in Chapter 7, Vol. 2 of the LLNL Mirror Advanced Reactor Study Final Report (Ref. 5-2). The tritium recovery system is based on the Tritium System Test Assembly design (Ref. 5-3) and extrapolations to a power reactor as in Chapter 16, Vol. 1-B of Ref. 5-2.

5.2. INVENTORY

The tritium inventories in Cascade were calculated by determining the tritium solubility as described above as a function of temperature and tritium overpressure for each of the materials and components exposed to tritium in the Cascade reactor design. The solubilities were multiplied by the masses of the corresponding materials and components and summed to obtain the total inventory. The tritium overpressure is set by the injection rate of DT pellets into the reaction chamber, the tritium breeding rate, and the vacuum pumping system specifications. We sized the vacuum system to maintain a 0.01 Torr total pressure throughout the reaction chamber and granule transport system. The fraction of tritium is slightly below 40%, giving a tritium overpressure of 0.004 Torr. The tritium inventories and characteristic release in Cascade materials and components are shown in Fig. 5-2 and Table 5-1. Details of the calculations are given below. Table 5-2 summarizes the reference reactor operation parameters used in the calculations. Table 5-3 summarizes the component design data used in the calculations. The solubility and diffusion data used are summarized in Table 5-4.

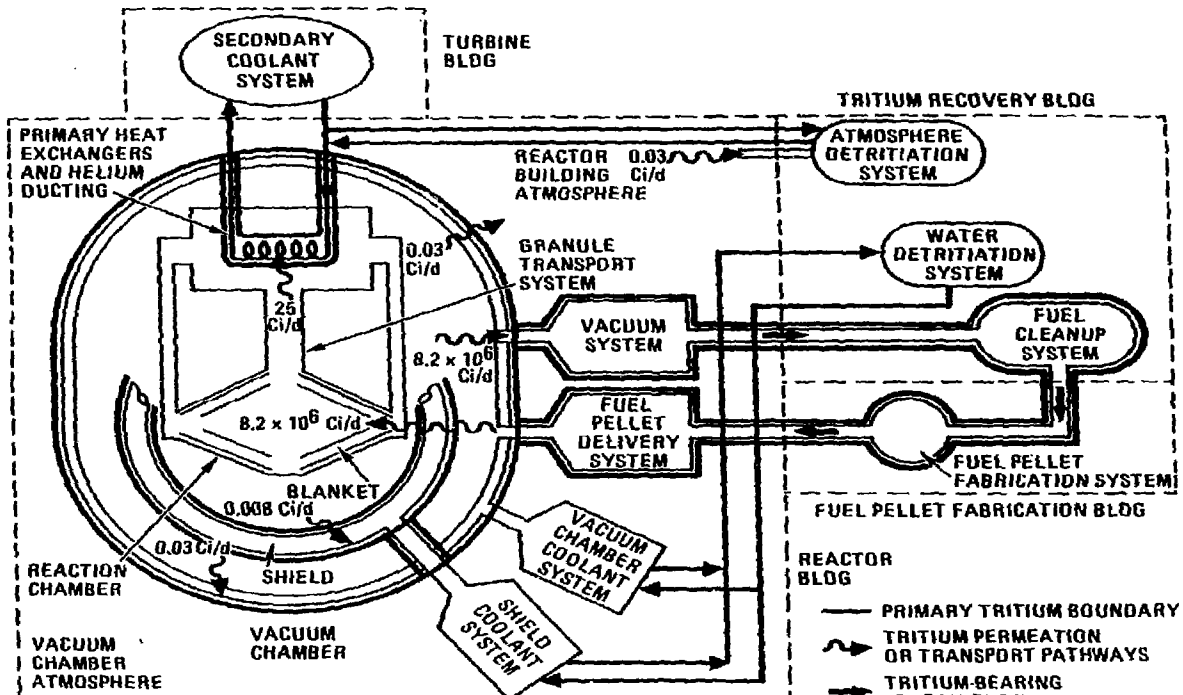

Fig. 5-2. Tritium inventory in Cascade components.

TABLE 5-1
TRITIUM INVENTORIES AND CHARACTERISTIC RELEASE TIMES IN CASCADE COMPONENTS

Component	Tritium Inventory, g	Characteristic Release Time
BeO (based on Al_2O_3)	2	0.4 h
$LiAlO_2$	100	10 h
SiC chamber	4	130 y
SiC granule distribution and transport components	39	100 y
SiC in primary heat exchangers	75	120 y
Steel manifolds in primary heat exchangers	2	74 h
Steel helium ducting	6	12 d
$Al/H_2O/C/B_4C$ shielding (based on steel)	1	28 d
Vacuum chamber atmosphere	9	0
Aluminum vacuum chamber (based on steel)	9	19 d
Fuel Cleanup System	11	0
Total, releasable in less than 30 d	140	
Total, secure	118	
Total	258	

TABLE 5-2
REFERENCE REACTOR OPERATION PARAMETERS USED IN TRITIUM ANALYSIS

Fusion power	1500 MW
Vacuum chamber total pressure	0.01 torr
Tritium partial pressure	0.004 torr
Deuterium flow rate	3.8×10^{-6} kg/s (3.4 moles/h)
Tritium flow rate	8.3×10^{-6} kg/s (5.0 moles/h) (7.2×10^{5} Ci/d)
Helium flow rate	7.1×10^{-6} kg/s (6.4 moles/h)

TABLE 5-3
REFERENCE COMPONENT DESIGN PARAMETERS USED IN TRITIUM ANALYSIS[a,b]

Blanket (within chamber and granule transport system)	
Total BeO mass in surface layer, 2200 K	1.0×10^4 kg
Total BeO mass in front zone, 1470 K	3.3×10^4 kg
BeO grain size	10 μm
Total $LiAl_2O$ mass (temperature as in Fig. 2-5)	3.2×10^5 kg
$LiAlO_2$ grain size	10 μm
Chamber, 2.5 cm thick SiC at 1200 K	
Area (inside + outside)	540 m^2
Mass	3.2×10^4 kg
Granule Distribution System, 2.5 cm thick SiC (shelves, ducting, and ports)	
Area (inside + outside), <1300 K	900 m^2
>1300 K	320 m^2
Mass, <1300 K	3.6×10^4 kg
>1300 K	1.3×10^4 kg
Heat Exchangers	
Tubing, 0.2 cm thick SiC	
Area, <1300 K	1.0×10^4 m^2
1600 K	360 m^2
Mass, <1300 K	6.4×10^4 kg
1600 K	2.3×10^3 kg
Shrouds, 2.5 cm thick SiC	
Area (both sides), <1300 K	640 m^2
>1300 K	160 m^2
Mass, <1300 K	2.6×10^4 kg
>1300 K	6.4×10^3 kg
Manifolds, 1.0 cm thick stainless steel at 700 K	
Area	920 m^2
Total Mass	1.2×10^5 kg
Helium Ducting (within vacuum chamber), stainless steel at 700 K	
Area with 4 cm wall thickness	570 m^2
Area with 2 cm wall thickness	1060 m^2
Total Mass	3.5×10^5 kg
Shield	
Area, 0.5 cm wall thickness Al cooling tubes at <500 K	2.8×10^4 m^2
Mass, aluminum	1.1×10^5 kg
$C + B_4C$ at <500 K	3.8×10^6 kg
Vacuum Chamber, 2.5 cm thick aluminum at 700 K	
Volume contained	2.8×10^4 m^3
Area	5.2×10^3 m^2
Mass	5.0×10^5 kg

[a] Component design parameters obtained from description in Chapter 4.

[b] All areas refer to that directly exposed to 0.004 torr tritium partial pressure.

TABLE 5-4
SOLUBILITY AND DIFFUSION DATA USED IN TRITIUM ANALYSIS

Material	S_o $\frac{g\ T_2}{g\ solid \cdot atm^{\frac{1}{2}}}$	Q_s $\frac{kcal}{mole}$	D_o $\frac{cm^2}{s}$	Q_d $\frac{kcal}{mole}$	Permeation $\frac{Ci \cdot m}{d \cdot m^2 \cdot atm^{\frac{1}{2}}}$	Reference
Al_2O_3	2.9×10^{-3}	18.1	NR[1]	NR	NR	5-4
BeO	NA[2]	NA	1.3×10^{-6}	30.8	NR	5-5
$LiAlO_2$	NA	NA	1.12×10^{-6}	35.8	NR	5-6
SiC[3]	6.6×10^{-10}	-37.0	1.58	73.6	SD[4]	5-7
Stainless	4.8×10^{-5}	2.54	2×10^{-3}	12.5	6.4×10^{-2}[5]	5-8 and 5-9
Aluminum	NA	NA	NA	NA	6.4×10^{-5}[5]	5-9 (700 K)
					6.4×10^{-7}[5]	5-10 (500 K)

[1]NR – not required.

[2]NA – not available.

[3]For temperatures below 1300 K, use results of transport calculations of Ref. 5-11 (see text).

[4]SD – permeation rate obtained from product of solubility and diffusivity, i.e.,

$$Permeation = 2.9\times10^2\ e^{Q_s/RT}\ e^{Q_d/RT}$$

[5]Includes oxide barrier permeation reduction factor of 100.

The results show that the Cascade reactor exhibits a relatively low total tritium inventory of 258 g. This is in addition to the tritium contained in the Fuel Pellet Fabrication Plant. The vulnerable portion of the tritium inventory is 140 g, of which 100 g are contained in the solid $LiAlO_2$ tritium breeder with a characteristic release time of 10 hours. The results for $LiAlO_2$ were obtained using the GA TRIT code as discussed in Ref. 5-12, with the diffusion data of Ref. 5-6. A grain size of 10 μm was used in the calculation. Since the inventory is primarily diffusive and is proportional to the square of the grain size, the incentive exists to produce breeder material with smaller grain size. In fact, a grain size as small as 2 μm was assumed in Ref. 5-13 as representative of a dimension which should be achievable in the near future. Reduced grain size would also reduce the characteristic release time. The decrease in total inventory would have greater impact than the decrease in the characteristic release time.

All of the secure portion of the tritium inventory is contained within the SiC components, with characteristic release times of 100's of years. These components exhibit very low tritium diffusivity and the tritium inventory will not approach the solubility limits within the 40 year lifetime of a Cascade plant. Thus, the calculations for SiC were performed at Sandia Livermore by Rion Causey (Ref. 5-11) using the DIFFUSE 83 tritium transport code (Ref. 5-14) and the solubility and diffusion data of Ref. 5-7. His results show that after 30 years at 1300 K with a tritium overpressure of 0.1 Torr, the tritium inventory in SiC components is 3.3×10^{-6} g/cm^2. At that time, tritium atoms would diffuse just 2 mm into the SiC. Thus, equilibrium calculations of inventory at temperatures below ~1300 K can be overly conservative in that the characteristic diffusion times are long in comparison to the plant lifetime. In the results of Table 5-1, we assumed that the tritium inventory in SiC components below 1300 K was as calculated by Causey, adjusted for the actual tritium pressure of 0.004 Torr. Since the diffusion time is shorter for components above 1300 K, we conservatively calculated the inventory in these using the equilibrium solubility data of Ref. 5-7.

BeO results were obtained using the data of Refs. 5-4 and 5-5. Since no solubility data was found for BeO, we used the data for a comparable ceramic, Al_2O_3. Tritium generation in the Be was not included in the calculation as it is expected to be even smaller than the diffusive inventory. Similarly, data for the solubility and diffusivity of aluminum was not located and the data for steel was used. This results in conservative estimates of the inventory and release rates, since aluminum permeation, the product of solubility and diffusion, is several orders of magnitude lower that of stainless steel.

The tritium inventory in the fuel cleanup system is scaled from data presented in pp. 16-16*ff* of Ref. 5-2. The inventory in the fuel cleanup system of Ref. 5-2 is 3.6 g in the molecular sieves used in the separation process which removes all impurities other than helium, and 22.4 g in the helium separator. The D-T flow rate in the reactor of Ref. 5-2 is 33.6 moles per hour versus Cascade's 8.4. By direct proportionality, the tritium inventory in the molecular sieves is 1 g. The helium mole fraction in

the processing stream of Ref. 5-2 is 25% versus 43% in Cascade. Again by direct proportionality, the tritium inventory in the helium separator is 10 g. The total inventory in the fuel cleanup system is thus 11 g.

5.3. PERMEATION

Tritium permeation across the primary system boundary was calculated as the product of solubility and diffusion (Ref. 5-1) as a function of temperature and tritium overpressure. This product was then multiplied by the surface area exposed and summed to obtain the total permeation rate. The tritium permeation rates into and out of Cascade systems and components are presented in Table 5-5.

TABLE 5-5
TRITIUM PERMEATION RESULTS

Component	Permeation $\frac{Ci}{d}$	Comment
Heat exchanger manifolds and helium piping	23.4	Based on steel at 700 K
SiC tubes in surface layer heat exchanger	1.2	Based on SiC at 1600 K
SiC tubes in all other heat exchangers	0.0	Based on SiC below 1300 K
Vacuum chamber	0.03	Based on aluminum at 700 K
Shield coolant system	0.008	Based on aluminum at 500 K
Total	24.6	

The results were calculated using the design parameters and data in Tables 5-3 and 5-4. The results show that the Cascade reactor has extremely low permeation rates. As shown in Fig. 5-1, the total tritium permeation rate out of the primary tritium containment boundary is 24.6 Ci/d. This tritium permeation rate compares quite favorably with:

- Canadian tritium experience, which shows total fission reactor station tritium release rates of 115 to 170 Ci/d (average from 1978 to 1982), with a low of 50 Ci/d. (Ref. 5-15)

- The guideline adopted in Ref. 5-13 of 100 Ci/d to meet current U.S. regulatory guideline of 5 mrem/y individual dose at a 500 m site boundary (Ref. 5-16) with a 100 m stack.

It is noted that Cascade's 24.6 Ci/d permeation rate is primarily leakage into the helium secondary coolant, which has a tritium recovery system within its own containment, as shown in Fig. 5-1. Due to the very low primary leak rate, actual losses to the environment were not calculated. Negligible permeation rates into the environment are expected.

The primary permeation path for tritium is through the heat exchanger manifolds and helium ducting. Since permeation is a strong function of temperature, the calculations were performed assuming a conservative 700 K metal operating temperature. A factor of 100 reduction in the permeation rate due to the presence of a natural oxide barrier on the helium side was included based on the recommendation of Ref. 5-13. This factor has been observed to vary from 10 to 10^4 (Ref. 5-15). The 2 mm heat exchanger tubes do not permit tritium breakthrough in 30 full power years at temperatures below 1300 K, and only 1.2 Ci/d at 1600 K. Tritium permeation rates through the aluminum vacuum chamber and shield coolant tubes are very low due to the low operating temperatures and the natural Al_2O_3 oxide surface which forms.

5.4. TRITIUM RECOVERY SYSTEMS

The objectives of the tritium recovery systems are to prepare a high-purity DT fuel stream for delivery to the Fuel Pellet Fabrication Plant, maintain tritium concentrations in all fluid streams to below occupational limits, and provide for rapid cleanup of building atmospheres in the event of an accidental release. The tritium-bearing stream characteristics are presented in Table 5-6.

The primary tritium recovery system for Cascade is the vacuum system. Tritium is transported through the vacuum system to a fuel cleanup system. The fuel cleanup system design for Cascade is based on the design developed for fuel recovery from the plasma exhaust of the MARS Tandem Mirror Reactor, pp. 16-16*ff* in Vol. 1-B of Ref. 5-2. The vacuum chamber walls and vacuum ducting provide primary containment of tritium. However, as shown in Fig. 5-1, as tritium permeates out of its primary containment, it permeates into several other systems. These include the

- Secondary coolant (helium working fluid) loop
- Shield coolant loop
- Vacuum chamber coolant loop
- Reactor building atmosphere.

The tritium-bearing stream from any of these systems can be directed to a tritium recovery unit as necessary. Below, we discuss the requirements on each of these.

The chamber exhaust consists principally of unburned D-T fuel, tritium produced in the blanket, the helium produced in fusion events and in the blanket, pellet debris, and vaporized species from the surface layer. As in the fuel cleanup system of Ref. 5-2, this gas stream is routed to columns of type-5A molecular sieves cooled to 77 K, which absorb all impurities except He. When a column is saturated with impurities, it is taken off-line and regenerated at 700 K while the stream is routed to another column. The system is based on a design presently being developed at the Tritium System Test Assembly (TSTA). (Ref. 5-3) Ref. 5-2 states that this design will remove C, N, O, heavy metals, and some He, as well as decompose tritium-bearing hydrocarbons. The impurity gases, containing some tritium are prepared for disposal. Tritium levels are expected to be sufficiently low to allow direct disposal. If the level is too high, the gases are routed to an oxidizing system and the tritium adsorbed on dessicants. The water is then routed to the tritiated water treatment system described below. After passing through the molecular sieves, the chamber exhaust is composed only of D, T,

and He. One technique studied at TSTA for separating helium from hydrogen uses He evaporation from a condensed falling film of hydrogen isotopes. This method was adopted in Ref. 5-2 and will also serve for Cascade.

The largest single tritium permeation rate out of the primary tritium recovery system is leakage into the secondary helium loop. If this tritium were allowed to build up over the full life of the plant, the tritium inventory in the secondary loop would be 27 g. This is less than the 129 g vulnerable inventory in the reactor building. As discussed in Chapter 4, if the entire contents of this loop and the reactor building were released and transported to the site boundary, public exposure would be within present regulatory guidelines. Thus, there is no explicit need to recover tritium from the secondary loop. Tritium removal from the secondary loop is necessary only to maintain tritium inventory as low as possible. A clean-up system for the secondary loop is included to maintain helium purity to proper levels for corrosion and coolant chemistry control. As shown in Table 5-6, slip-stream processing of 136 m^3/min with the Atmosphere Detritiation System discussed below will maintain the tritium inventory in the secondary loop to 8 Ci.

The requirements on tritium recovery from the building atmosphere are dictated by the atmospheric tritium concentration requirements for occupational exposure, 5×10^{-6} Ci/m^3 air, as set forth in regulatory guide 10CFR20. (Ref. 5-17) The building atmosphere is maintained below occupational exposure limits with the Atmosphere Detritiation System (ADS). The unit is sized by the most restrictive of

- Processing of the Reactor Building atmosphere to remove routine vacuum chamber leakage,
- Processing of the Reactor Building or Tritium Building atmosphere to the guidelines on occupational exposure tritium concentrations following an accidental release.

TABLE 5-6
TRITIUM-BEARING STREAM CHARACTERISTICS

Stream	Fluid	*Tritium* In-leakage Rate $\frac{Ci}{d}$	*Tritium* Inventory Ci	Stream Volume $m^3(STP)$	*Tritium* Concentration $\frac{Ci}{m^3}$	*Tritium* Recovery System	*Stream* Reprocessing Flow Rate
Chamber exhaust	(1)	7.2×10^6	9×10^4	2.8×10^4[2]	3.2	FCS[3]	Full flow
Secondary coolant	Helium	25	8	6×10^4	1.3×10^{-4}	ADS[4]	136 m^3/min
Shield coolant	Water	0.008	24	240	0.1	WDS[5]	0.08 m^3/day
Vacuum chamber coolant	Water	0.03[6]	3	30	0.1	WDS	0.3 m^3/day
Reactor Building atmosphere	Air	0.03[6]	0.4	7.5×10^4	5×10^{-6}	ADS	4 m^3/min
Tritium Building atmosphere	Air	–	–	1.4×10^4	–	ADS	–

[1] D + T + He + pellet debris + vaporized surface layer material.

[2] Vacuum chamber volume.

[3] FCS – Fuel Cleanup System.

[4] ADS – Atmosphere Detritiation System.

[5] WDS – Water Detritiation System.

[6] Total permeation through vacuum chamber is 0.03 Ci/d. We've conservatively assumed this leakage into both the vacuum chamber coolant and the Reactor Building atmosphere.

For Cascade, the most restrictive requirement is set by an accidental tritium release into the Reactor Building. The ADS processing rate is governed by economics considerations in that, following a release, the sooner the tritium concentration is below regulatory limits, the sooner that workers can return to the area and the reactor restart. The atmosphere processing rate R, is calculated from

$$C_t = C_o\, e^{-\frac{R}{V}t}$$

where C_t is the desired concentration concentration at time t, 5×10^{-6} Ci/m^3, C_o is the initial concentration following the release, V is the building volume, and t is the time to achieve C_t.

Assuming that the entire 129 g vulnerable inventory in the Reactor Building is instantly released to the 6×10^4 m^3 of available building atmosphere, and that 2 days is an economically acceptable time for tritium recovery, the processing rate required is 150 m^3/min. The atmosphere processing system proposed in Ref. 5-2 consists of individual units of 140 m^3/min capacity. A single unit would thus serve the needs of Cascade, requiring 2.2 days for full cleanup of the Reactor Building. The same unit would require 8.7 h to process a maximum release in the Tritium Building. These scenarios assume that no tritium is released to the public. Since all of the Cascade inventory could be released to the public without exceeding regulatory guidelines, this approach is consistent with a philosophy of maintaining releases to the public as low as possible.

During routine operation, the ADS would be used to process the secondary coolant at a rate of 136 m^3/min to remove the 25 Ci/d inleakage and maintain the tritium inventory in the helium to 8 Ci. The Reactor Building atmosphere would be routinely processed at a rate of 4 m^3/min to remove the 0.03 Ci/d leakage from the vacuum chamber and thus maintain tritium concentrations below 5×10^{-6} Ci/m^3.

The tritium concentrations in water coolants are maintained below 10CFR20 regulatory guidelines with a Water Detritiation System. The low tritium leakage into the shield and vacuum chamber coolants eases the requirements on this system. A

state-of-the-art review of tritium recovery from water coolants is also presented in Ref. 5-2, which concludes that the technologies for tritium removal from water are available on the commercial market. The system selected in Ref. 5-2 uses electrolysis of the tritiated water followed by separation of tritium by cryogenic distillation. Electrolysis of water is well established in industry and is routinely used for hydrogen production. In the present application, the WDS maintains tritium concentration in the water at the 10CFR20 requirement of 0.1 Ci/m^3 with a water processing rate of 0.4 m^3/d, or 16 kg/h. For comparison, the system proposed for Ref. 5-2 processes water at 68 kg/h.

References for Chapter 5

5-1. R. E. Stickney, "Diffusion and Permeation of Hydrogen Isotopes in Fusion Reactors," *The Chemistry of Fusion Technology*, (Plenum Press, New York, D.M. Gruen, ed.), 1972, p. 241.

5-2. B. G. Logan *et al.*, "Mirror Advanced Reactor Study, Final Report," Lawrence Livermore National Laboratory Report UCRL-53480, July 1984.

5-3. J. L. Anderson *et al.*, "Tritium System Test Assembly Design for Major Device Fabrication Review," Los Alamos National Laboratory Report LA-6588-P, June 1977.

5-4. T. S. Elleman, L. R. Zumwalt, and K. Berghese, "Hydrogen Transport and Solubility in Non-Metallic Solids,", *Proceedings of th Third Topical Meeting on the Technology of Controlled Nuclear Fusion*, Santa Fe, NM, Vol. 2, May 1978, p. 763.

5-5. D. Fowler *et al.*, " Tritium Diffusion in Al_2O_3 and BeO," *J. of Am. Ceramic Soc.*, Vol. 60, No. 3-4, March-April 1977, p. 155.

5-6. M. C. Billone and R. G. Clemmer, "Modeling of Tritium Transport in Lithium Aluminate Fusion Breeder Blankets," *Fusion Technology*, to be published, 1985.

5-7. R. A. Causey *et al.*, "Hydrogen Diffusion and Solubility in Silicon Carbide," *J. of Am. Ceramic Soc.*, Vol. 61, No. 5-6, May-June 1978, p. 221.

5-8. P. A. Finn and D. K. Sze, "Tritium Technology Review," *Fusion Technology*, to be published, 1985.

5-9. R. W. Werner *et al.*, "Synfuels From Fusion - Produsing Hydrogen with the Tandem Mirror Reactor and Thermochemical Cycles," Lawrence Livermore National Laboratory Report UCID-18909, Vol. II, January 1981, p. 5.105.

5-10. H. Ihle, U. Kurz, and G. Stocklin, "The Permeation of Tritium Through Aluminum in the Temperature Range of 25 to 250°C," Institut fur Chemie der Kernforschungsanlage Julich Gmbh, Institut 1: Nuklearchemie, D-5170 Julich, FRG.

5-11. R. A. Causey, Physical Research Division, Sandia National Laboratory, Livermore, CA, Letter Communication to I. Maya, April 26, 1985.

5-12. I. Maya, K. R. Schultz *et al.*, "Inertial Confinement Fusion Reaction Chamber and Power Conversion System Study," GA Technologies Report GA-A17267, September 1984; also Lawrence Livermore National Laboratory Report, UCRL-15642.

5-13. D. L. Smith *et al.*, "Blanket Comparison and Selection Study, Final Report," Argonne National Laboratory Report ANL/FPP-84-1, September 1984.

5-14. M. I. Baskes, "DIFFUSE 83," Sandia Report SAND83-8231, June 1983.

5-15. K. Y. Wong *et al.*, *Canadian Tri. ..n Experience*, Canadian Fusion Fuels Technology Project Report, Published by Ontario Hydro, 1984, p. 15.

5-16. U. S. Nuclear Regulatory Commission, Code of Federal Regulations, Title 10, Part 50.

5-17. U. S. Nuclear Regulatory Commission, Code of Federal Regulations, Title 10, Part 20.

6. ACTIVATION ANALYSIS

6.1. INTRODUCTION

The safety characteristics of the Cascade reactor are dominated by the induced radioactivity in the blanket and surrounding material. In this chapter, we present the radioactivity levels in the materials of importance to Cascade. We then design the radiation and biological shields which will allow hands-on maintenance access to the heat exchangers soon after shutdown, and continuous worker occupation of the reactor building during operation.

6.2. RADIOACTIVITY ANALYSIS

6.2.1. Neutron Fluxes and Methods of Calculations

The Cascade reactor concept employs a circulating blanket to transport the nuclear heat to the power conversion system. During reactor operation, part of the blanket is within the reaction chamber and part is in circulation throughout the granule transport system and heat exchangers. The neutron fluxes employed in the radioactivity calculations were thus averaged over the total volumes of BeO and $LiAlO_2$ in the system. Figure 6-1 depicts the neutron spectra in the BeO and $LiAlO_2$ zones within the chamber. In the BeO zone, the averaged total flux is about 5.6×10^{15} n/cm^2/sec, or 1.8×10^{23} n/cm^2 per year of continuous operation. Of this, about 21 and 39% are contributed from neutrons at energies above 0.8 and 0.1 MeV, respectively. In the $LiAlO_2$ zone, the total flux is about 8.9×10^{14} n/cm^2/sec, or 2.8×10^{22} n/cm^2 per year. The fractional contributions from energies above 0.8 and 0.1 MeV are 18 and 42%, respectively. However, the neutron fluences experienced by the BeO and

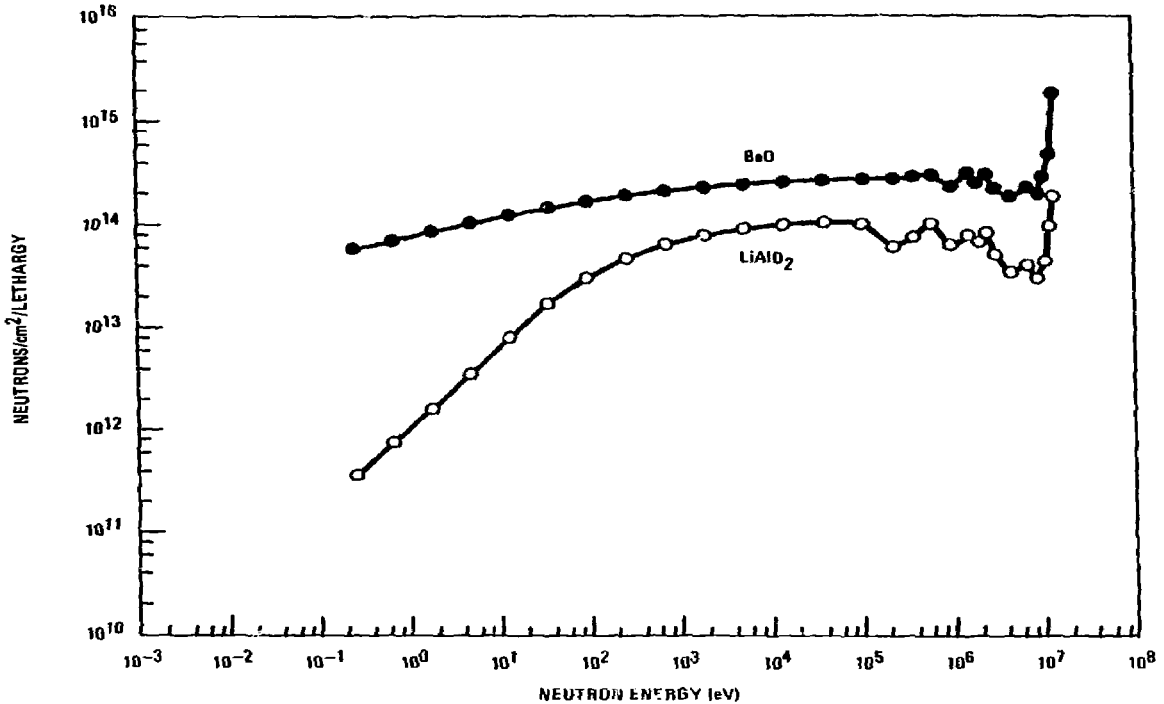

Fig. 6-1. Neutron spectra in BeO and $LiAlO_2$ zones.

$LiAlO_2$ materials must be reduced by the ratios of the total quantities of these materials in the entire reactor to the quantities within the chamber. For the BeO, the total quantity of material is 3.4 times the quantity of BeO just within the chamber. For the $LiAlO_2$, the total is 1.8 times the quantity within the chamber. The diluted total neutron fluences are thus 5.3×10^{22} and 1.6×10^{22} n/cm^2 after one year irradiation in the BeO and $LiAlO_2$ materials, respectively.

Using the above neutron spectra and fluences, the radioactivity calculations were performed with the computer code, REAC, developed by Mann of the Hanford Engineering Development Laboratory (Ref. 6-1). The activation cross sections and decay data were taken from the recent updated libraries compiled by Mann (Ref. 6-2), where the ACTL (Ref. 6-3) activation library is included. The results of these calculations are summarized in Tables 6-1 to 6-4 and are discussed in the following subsections. Note that all results presented in these tables are expressed in terms of activity in full density material.

6.2.2. Radioactivity in BeO and C Materials

Tables 6-1 and 6-2 summarize the shutdown radioactivity in the BeO zone including impurity elements which may be present in the BeO material assuming their levels were mainly carried over from the beryllium metal. The impurity elements and their levels in the beryllium metal were obtained from the Blanket Comparison and Selection Study (BCSS) final report (Ref. 6-4). Table 6-1 presents a detailed breakdown of the shutdown activities, radionuclides resulting from these main and impurity elements, and their half lives after 2 and 30 years of operation, without including the dilution factor due to the inventory out of the reaction chamber. These values were used to estimate the radioactive inventories in the BeO material at times after shutdown when the radioactive decay and the material dilution factor due to the inventory out of the reaction chamber (which is 3.4 in this case) are considered. The dilution factor and the capacity factor are then linearly multiplied to obtain the effective shutdown activity. The methodology to calculate the actual activity in a blanket operated

TABLE 6-1
SHUTDOWN RADIOACTIVITY (Ci/cm^3) in BeO ZONE[a]

Nuclide	Half-Life	Operating Time 2 y	Operating Time 30 y
Element: Be	Content: 50 a/o		
^{11}Be	13.8 s	-	7.92×10^{-3}
^{10}Be	1.6×10^{6} y	7.18×10^{-6}	8.01×10^{-6}
Subtotal:		7.18×10^{-6}	7.92×10^{-3}
Element: C	Content: 0.10 a/o		
^{14}C	5730 y	1.98×10^{-8}	2.77×10^{-7}
^{10}Be	1.6×10^{6} y	5.51×10^{-10}	1.12×10^{-8}
Subtotal:		2.04×10^{-8}	2.88×10^{-7}
Element: N	Content: 0.026 a/o		
^{13}N	10 min	1.96×10^{-3}	7.54×10^{-4}
^{14}C	5730 y	1.97×10^{-4}	1.79×10^{-3}
^{10}Be	1.6×10^{6} y	-	4.53×10^{-8}
Subtotal:		2.16×10^{-3}	2.59×10^{-3}
Element: O	Content: 50 a/o		
^{16}N	7.1 s	29.5	26.1
^{19}O	26.9 s	2.84×10^{-4}	2.45×10^{-4}
^{14}C	5730 y	6.75×10^{-5}	2.29×10^{-3}
^{13}C	9.97 min	-	2.70×10^{-4}
^{10}Be	1.6×10^{6} y	-	1.11×10^{-5}
Subtotal:		29.5	26.1

[a]Not including effect of material dilution factor due to inventory external to reaction chamber. See text in Sections 6.2.1. and 6.2.2. for discussion.

Nuclide	Half-Life	Operating Time 2 y	Operating Time 30 y
Element: Al Content: 0.04 a/o			
^{28}Al	2.24 min	1.63×10^{-1}	1.54×10^{-1}
^{24}Na	15 h	8.41×10^{-2}	7.69×10^{-2}
^{27}Mg	9.46 min	7.47×10^{-2}	6.33×10^{-2}
^{26}Al	7.2×10^{5} y	3.63×10^{-8}	3.72×10^{-7}
Subtotal:		3.22×10^{-1}	2.94×10^{-1}
Element: Ca Content: 0.006 a/o			
^{37}Ar	35 d	2.77×10^{-2}	1.71×10^{-2}
^{45}Ca	164 d	1.63×10^{-3}	1.46×10^{-3}
^{47}Ca	4.54 d	2.79×10^{-4}	2.02×10^{-4}
^{39}Ar	269 y	1.07×10^{-5}	2.94×10^{-4}
^{41}Ca	1.03×10^{5} y	5.67×10^{-7}	1.92×10^{-6}
^{42}K	12.4 h	1.37×10^{-4}	2.40×10^{-2}
^{38}Cl	37.2 min	-	3.75×10^{-3}
^{41}Ar	1.83 h	1.60×10^{-4}	3.25×10^{-3}
Subtotal:		2.97×10^{-2}	5.01×10^{-2}
Element: Cr Content: 0.002 a/o			
^{51}Cr	27.7 d	2.79×10^{-2}	4.57×10^{-4}
^{52}V	3.75 min	2.73×10^{-3}	4.82×10^{-3}
^{49}V	330 d	2.38×10^{-4}	5.44×10^{-6}
^{55}Cr	3.50 min	2.83×10^{-4}	3.60×10^{-3}
^{56}Mn	2.58 h	-	2.67×10^{-3}
^{42}Ar	32.9 y	-	4.50×10^{-11}
^{60}Co	5.27 y	-	1.39×10^{-6}
Subtotal:		3.12×10^{-2}	1.15×10^{-2}

Nuclide	Half-Life	Operating Time 2 y	Operating Time 30 y
Element: Mn	Content: 0.003 a/o		
^{56}Mn	2.58 h	7.88×10^{-1}	9.95×10^{-3}
^{54}Mn	313 d	2.15×10^{-2}	2.88×10^{-4}
^{55}Cr	3.50 min	2.15×10^{-3}	7.34×10^{-4}
^{52}V	3.75 min	1.59×10^{-3}	6.31×10^{-5}
^{55}Fe	2.68 y	-	4.13×10^{-3}
^{59}Fe	44.5 d	-	2.03×10^{-2}
^{60}Co	5.27 y	-	1.27×10^{-2}
^{63}Ni	100 y	-	1.60×10^{-4}
^{60}Fe	1.49×10^{6} y	-	1.29×10^{-8}
^{59}Ni	7.5×10^{4} y	-	4.87×10^{-9}
Subtotal:		8.10×10^{-1}	4.83×10^{-2}
Element: Fe	Content: 0.0013 a/o		
^{55}Fe	2.68 y	4.48×10^{-3}	2.54×10^{-3}
^{56}Mn	2.58 h	2.31×10^{-3}	5.21×10^{-3}
^{54}Mn	313 d	7.05×10^{-4}	4.05×10^{-4}
^{59}Fe	44.5 d	1.04×10^{-4}	9.14×10^{-3}
^{60}Co	5.27 y	-	5.11×10^{-3}
^{63}Ni	100 y	-	1.07×10^{-4}
^{60}Fe	1.49×10^{6} y	-	6.15×10^{-9}
Subtotal:		7.60×10^{-3}	2.25×10^{-2}

Nuclide	Half-Life	Operating Time 2 y	Operating Time 30 y
Element: Ni Content: 0.006 a/o			
^{58}Co	70.9 h	5.73×10^{-2}	1.04×10^{-2}
^{57}Co	271 d	3.07×10^{-2}	5.12×10^{-3}
^{55}Fe	2.68 y	6.23×10^{-3}	5.12×10^{-3}
^{57}Ni	36.1 h	1.73×10^{-3}	2.89×10^{-4}
^{65}Ni	2.52 h	1.47×10^{-3}	4.87×10^{-2}
^{60}Co	5.27 y	9.58×10^{-4}	4.22×10^{-2}
^{63}Ni	100 y	7.49×10^{-4}	1.75×10^{-2}
^{59}Ni	7.5×10^{4} y	6.90×10^{-6}	1.33×10^{-6}
^{60}Fe	1.49×10^{6} y	1.72×10^{-11}	2.75×10^{-8}
^{59}Fe	44.5 d	1.12×10^{-4}	2.02×10^{-2}
Subtotal:		9.75×10^{-2}	1.49×10^{-1}
Element: Cu Content: 0.002 a/o			
^{64}Cu	12.7 h	1.54×10^{-1}	1.17×10^{-2}
^{66}Cu	5.10 min	2.80×10^{-2}	1.68×10^{-2}
^{62}Cu	9.74 min	7.40×10^{-3}	3.88×10^{-4}
^{60}Co	5.27 y	2.69×10^{-4}	2.06×10^{-4}
^{65}Ni	2.52 h	2.37×10^{-4}	1.67×10^{-2}
^{63}Ni	100 y	3.24×10^{-5}	4.28×10^{-4}
^{65}Zn	244 d	-	1.97×10^{-3}
Subtotal:		1.89×10^{-1}	4.72×10^{-2}

Nuclide	Half-Life	Operating Time 2 y	Operating Time 30 y
Element: Co	Content: 0.0001 a/o		
^{60}Co	5.27 y	2.57×10^{-2}	4.93×10^{-4}
^{58}Co	70.9 d	9.01×10^{-4}	7.07×10^{-6}
^{59}Fe	44.5 d	1.11×10^{-4}	1.10×10^{-4}
^{63}Ni	100 y	-	5.95×10^{-4}
^{60}Fe	1.49×10^{6} y	-	4.21×10^{-9}
^{59}Ni	7.5×10^{4} y	-	5.66×10^{-9}
Subtotal:		2.67×10^{-2}	1.21×10^{-3}
Element: Zn	Content: 0.0004 a/o		
^{65}Zn	244 d	5.30×10^{-3}	2.72×10^{-3}
^{69m}Zn	13.8 h	4.18×10^{-3}	3.15×10^{-4}
^{64}Cu	12.7 h	6.55×10^{-4}	1.25×10^{-3}
^{63}Ni	100 y	7.47×10^{-7}	2.16×10^{-5}
^{60}Co	5.27 y	-	7.83×10^{-6}
Subtotal:		1.01×10^{-2}	4.31×10^{-3}
Element: Nb	Content: 0.00026 a/o		
^{94}Nb	2.03×10^{4} y	1.0×10^{-6}	1.99×10^{-7}
^{93}Zr	1.53×10^{6} y	1.76×10^{-10}	8.58×10^{-10}
^{92}Nb	3.5×10^{7} y	1.07×10^{-10}	1.09×10^{-11}
^{90}Sr	28.6 y	-	1.17×10^{-7}
^{93}Mo	3.5×10^{3} y	-	1.17×10^{-7}
^{99}Tc	2.13×10^{5} y	-	2.85×10^{-8}
Subtotal:		1.0×10^{-6}	4.63×10^{-7}

TABLE 6-2A
SUMMARY OF RADIOACTIVE INVENTORIES IN BeO MATERIAL

	Time after shutdown			
	Two Years Operation			30 Years Operation
Total Activity	1 min	1 day	4 weeks	1 min
Ci/cm^3	4.7×10^{-1}	8.4×10^{-2}	5.0×10^{-2}	2.1×10^{-1}
MCi	8.7	1.6	0.93	3.9

TABLE 6-2B
PERCENT CONTRIBUTION BY ELEMENT TO TOTAL OF
RADIOACTIVE INVENTORIES IN BeO MATERIAL

	Time after shutdown			
	Two Years Operation			30 Years Operation
Element (a/o)	1 min	1 day	4 weeks	1 min
	(Dominating Radionuclide given in Parentheses)			
Be (50)	4.5×10^{-4} (^{10}Be)	2.5×10^{-3} (^{10}Be)	4.2×10^{-3} (^{10}Be)	1.1 (^{10}Be)
C (0.1)*	1.3×10^{-6} (^{14}C)	7.2×10^{-6} (^{14}C)	1.2×10^{-5} (^{14}C)	4.0×10^{-5} (^{14}C)
N (0.026)*	1.3×10^{-1} (^{13}N)	6.9×10^{-2} (^{14}C)	1.2×10^{-1} (^{14}C)	3.6×10^{-1} (^{13}N)
O (50)	5.3 (^{16}N)	2.4×10^{-2} (^{14}C)	4.0×10^{-2} (^{14}C)	10.5 (^{16}N)
Al (0.04)*	20.0 (^{28}Al)	9.7 (^{24}Na)	2.1×10^{-5} (^{26}Al)	41.2 (^{28}Al)
Ca (0.006)*	1.9 (^{37}Ar)	10.4 (^{37}Ar)	10.4 (^{37}Ar)	7.0 (^{42}K)
Cr (0.002)*	1.9 (^{51}Cr)	9.9 (^{51}Cr)	8.4 (^{51}Cr)	1.6 (^{52}V)
Mn (0.003)*	50.6 (^{56}Mn)	8.0 (^{54}Mn)	12.0 (^{54}Mn)	6.8 (^{59}Fe)
Fe (0.0013)*	4.7×10^{-1} (^{55}Fe)	1.9 (^{55}Fe)	1.8 (^{55}Fe)	3.2 (^{59}Fe)
Ni (0.006)*	6.1 (^{58}Co)	33.7 (^{58}Co)	48.2 (^{58}Co)	20.9 (^{65}Ni)
Cu (0.002)*	11.8 (^{64}Cu)	14.7 (^{64}Cu)	1.8×10^{-1} (^{60}Co)	6.6 (^{66}Cu)
Co (0.0001)*	1.7 (^{60}Co)	9.4 (^{60}Co)	15.8 (^{60}Co)	1.7×10^{-1} (^{63}Ni)
Zn (0.0004)*	6.3×10^{-1} (^{65}Zn)	2.3 (^{65}Zn)	3.1 (^{65}Zn)	6.0×10^{-1} (^{65}Zn)
Nb (0.00026)*	6.0×10^{-5} (^{94}Nb)	3.5×10^{-4} (^{94}Nb)	6.0×10^{-4} (^{94}Nb)	6.5×10^{-5} (^{94}Nb)

*Impurity.

TABLE 6-3
SHUTDOWN RADIOACTIVITY (Ci/cm^3) in $LiAlO_2$ ZONE[a]

Nuclide	Half-Life	Operating Time 2 y	Operating Time 30 y
Element: O Content: 50 a/o			
^{16}N	7.1 s	1.65	1.63
^{15}C	2.45 s	2.09×10^{-3}	2.56×10^{-3}
^{14}C	5730 y	4.14×10^{-6}	6.64×10^{-5}
^{19}O	26.9 s	1.67×10^{-6}	1.65×10^{-6}
^{13}N	9.97 min	-	1.20×10^{-7}
^{10}Be	1.6×10^{6} y	-	7.60×10^{-8}
Subtotal:		1.65	1.63
Element: Na Content: 0.0036 a/o			
^{24}Na	15.0 h	8.26×10^{-4}	8.14×10^{-4}
^{23}Ne	37.2 s	2.89×10^{-4}	2.83×10^{-4}
^{22}Na	2.60 y	2.23×10^{-5}	5.24×10^{-5}
Subtotal:		9.43×10^{-4}	9.56×10^{-4}
Element: Al Content: 25 a/o			
^{24}Na	15.0 h	3.12	3.12
^{27}Mg	9.46 min	3.03	2.97
^{28}Al	2.24 min	2.03	2.03
^{26}Al	2.03×10^{4} y	1.03×10^{-6}	1.49×10^{-5}
^{22}Na	2.6 y	-	3.09×10^{-5}
Subtotal:		8.18	8.12

[a]Not including effect of material dilution factor due to inventory external to reaction chamber. See text in Sections 6.2.1. and 6.2.2. for discusssion.

Nuclide	Half-Life	Operating Time 2 y	Operating Time 30 y
Element: K	Content: 0.02 a/o		
^{37}Ar	35.0 d	1.97×10^{-3}	1.87×10^{-3}
^{42}K	12.4 h	5.62×10^{-4}	5.55×10^{-4}
^{39}Ar	269 y	6.34×10^{-5}	8.74×10^{-4}
^{36}Cl	3.01×10^{5} y	2.28×10^{-8}	2.96×10^{-7}
Subtotal:		2.60×10^{-3}	3.30×10^{-3}
Element: Ca	Content: 0.01 a/o		
^{37}Ar	35.0 d	3.46×10^{-3}	3.26×10^{-3}
^{47}Ca	4.54 d	2.42×10^{-5}	2.35×10^{-5}
^{45}Ca	1.64 d	1.86×10^{-5}	1.93×10^{-5}
^{39}Ar	269 y	9.73×10^{-7}	1.72×10^{-5}
^{41}Ca	1.03×10^{5} y	1.20×10^{-8}	1.70×10^{-7}
^{42}Ar	32.9 y	2.30×10^{-9}	2.81×10^{-8}
Subtotal:		3.50×10^{-3}	3.30×10^{-3}
Element: Fe	Content: 0.0009 a/o		
^{55}Fe	2.68 y	1.08×10^{-4}	2.52×10^{-4}
^{56}Mn	2.58 h	9.63×10^{-5}	2.02×10^{-4}
^{54}Mn	313 d	3.47×10^{-5}	6.11×10^{-5}
^{60}Co	5.27 y	-	2.68×10^{-6}
Subtotal:		2.39×10^{-4}	5.42×10^{-4}

Nuclide	Half-Life	Operating Time 2 y	Operating Time 30 y
Element: Co	Content: 0.0008 a/o		
^{60}Co	5.27 y	1.05×10^{-2}	6.60×10^{-3}
^{63}Ni	100 y	-	4.05×10^{-6}
Subtotal:		1.05×10^{-2}	6.60×10^{-3}
Element: Ni	Content: 0.0006 a/o		
^{58}Co	70.9 d	4.02×10^{-4}	3.74×10^{-4}
^{57}Co	271 d	1.64×10^{-4}	1.70×10^{-4}
^{55}Fe	2.68 y	3.84×10^{-5}	8.67×10^{-5}
^{57}Ni	36.1 h	7.97×10^{-6}	7.20×10^{-6}
^{60}Co	5.27 y	5.91×10^{-6}	5.77×10^{-5}
^{63}Ni	100 y	7.34×10^{-7}	1.13×10^{-5}
^{59}Fe	44.5 d	6.13×10^{-7}	2.45×10^{-5}
^{59}Ni	7.4×10^{4} y	6.28×10^{-9}	2.99×10^{-8}
Subtotal:		6.18×10^{-4}	7.31×10^{-4}
Element: Cu	Content: 0.0003 a/o		
^{64}Cu	12.7 h	1.12×10^{-3}	9.16×10^{-4}
^{66}Cu	5.1 min	2.28×10^{-4}	2.05×10^{-4}
^{62}Cu	9.74 min	5.63×10^{-5}	4.58×10^{-5}
^{60}Co	5.27 y	2.46×10^{-6}	1.60×10^{-5}
^{63}Ni	100 y	3.74×10^{-7}	6.53×10^{-6}
Subtotal:		1.91×10^{-3}	1.18×10^{-3}

Nuclide	Half-Life	Operating Time 2 y	Operating Time 30 y
Element: Sr Content: 0.055 a/o			
^{89}Sr	50.6 d	2.45×10^{-1}	2.24×10^{-1}
^{85}Sr	64.8 d	4.13×10^{-3}	2.81×10^{-3}
^{86}Rb	18.7 d	4.84×10^{-4}	3.33×10^{-3}
^{85}Kr	10.7 y	1.20×10^{-5}	7.82×10^{-5}
^{90}Sr	28.6 y	-	3.92×10^{-3}
Subtotal:		2.50×10^{-1}	2.34×10^{-1}
Element: Zn Content: 0.013 a/o			
^{65}Zn	244 d	4.56×10^{-3}	5.03×10^{-3}
^{69m}Zn	13.8 h	3.21×10^{-3}	3.07×10^{-3}
^{64}Cu	12.7 h	1.40×10^{-3}	1.68×10^{-3}
^{67}Cu	61.9 h	1.25×10^{-4}	1.31×10^{-4}
^{63}Ni	100 y	1.41×10^{-6}	2.29×10^{-5}
^{60}Co	5.27 y	-	4.47×10^{-6}
Subtotal:		9.30×10^{-3}	9.91×10^{-3}
Element: Ag Content: 0.00015 a/o			
^{110}Ag	24.6 s	1.30×10^{-2}	1.30×10^{-2}
^{110m}Ag	250 d	6.97×10^{-4}	7.60×10^{-5}
^{108}Ag	2.4 min	4.00×10^{-3}	4.00×10^{-3}
^{109m}Ag	39.6 s	3.81×10^{-4}	3.81×10^{-4}
^{107m}Ag	44.3 s	3.77×10^{-4}	3.77×10^{-4}
^{106}Ag	24 min	5.57×10^{-5}	5.57×10^{-5}
^{106m}Ag	8.46 d	2.48×10^{-5}	2.48×10^{-5}
^{108m}Ag	127 y	4.40×10^{-6}	1.57×10^{-5}
^{109}Cd	463 d	-	4.10×10^{-4}
^{113m}Cd	13.7 y	-	4.40×10^{-7}
Subtotal:		1.9×10^{-2}	1.9×10^{-2}

Nuclide	Half-Life	Operating Time 2 y	Operating Time 30 y
Element: Cd Content: 0.0015 a/o			
^{115}Cd	53.5 h	4.96×10^{-3}	
^{115m}Cd	44.6 d	2.48×10^{-3}	
^{109}Cd	463 d	3.37×10^{-4}	
^{113m}Cd	13.7 y	3.22×10^{-4}	
^{111}Ag	7.45 d	1.18×10^{-5}	
^{108m}Ag	127 y	8.11×10^{-9}	
Subtotal:		8.10×10^{-3}	

TABLE 6-4A
SUMMARY OF RADIOACTIVE INVENTORIES IN $LiAlO_2$ MATERIAL

Total Activity	Time After Shutdown: Two Years Operation, 1 min	1 day	4 weeks	30 Years Operation, 1 min
Ci/cc	4.7	7.3×10^{-1}	1.1×10^{-1}	4.6
MCi	730	110	17	720

TABLE 6-4B
PERCENT CONTRIBUTION BY ELEMENT TO TOTAL OF
RADIOACTIVE INVENTORIES IN $LiAlO_2$ MATERIAL

Element (a/o)	Time After Shutdown: Two Years Operation, 1 min	1 day	4 weeks	30 Years Operation, 1 min
	(Dominating Radionuclide given in Parentheses)			
O (50)	5.6×10^{-2} (^{16}N)	3.2×10^{-4} (^{14}C)	2.2×10^{-3} (^{14}C)	5.5×10^{-2} (^{16}N)
Na (0.0036)*	1.1×10^{-2} (^{24}Na)	2.2×10^{-2} (^{24}Na)	1.2×10^{-2} (^{22}Na)	1.1×10^{-2} (^{24}Na)
Al (25)	96.6 (^{24}Na)	78.6 (^{24}Na)	5.4×10^{-4} (^{26}Al)	96.7 (^{24}Na)
K (0.02)*	3.1×10^{-2} (^{37}Ar)	1.7×10^{-1} (^{37}Ar)	5.9×10^{-1} (^{37}Ar)	3.9×10^{-2} (^{37}Ar)
Ca (0.01)*	4.1×10^{-2} (^{37}Ar)	2.7×10^{-1} (^{37}Ar)	1.0 (^{37}Ar)	3.9×10^{-2} (^{37}Ar)
Fe (0.0009)*	2.8×10^{-3} (^{55}Fe)	1.1×10^{-2} (^{55}Fe)	7.3×10^{-2} (^{55}Fe)	6.5×10^{-3} (^{55}Fe)
Co (0.0008)*	1.2×10^{-1} (^{60}Co)	8.0×10^{-1} (^{60}Co)	5.5 (^{60}Co)	7.9×10^{-2} (^{60}Co)
Ni (0.0006)*	7.3×10^{-3} (^{58}Co)	4.7×10^{-2} (^{58}Co)	2.4×10^{-1} (^{58}Co)	8.7×10^{-3} (^{58}Co)
Cu (0.0003)*	2.3×10^{-2} (^{64}Cu)	2.3×10^{-2} (^{64}Cu)	1.3×10^{-3} (^{60}Co)	1.4×10^{-2} (^{64}Cu)
Sr (0.055)*	3.0 (^{89}Sr)	19.1 (^{89}Sr)	88.8 (^{89}Sr)	2.8 (^{89}Sr)
Zn (0.013)*	1.1×10^{-1} (^{65}Zn)	4.4×10^{-1} (^{65}Zn)	2.2 (^{65}Zn)	1.2×10^{-1} (^{65}Zn)
Ag (0.00015)*	8.3×10^{-2} (^{108}Ag)	5.5×10^{-2} (^{110m}Ag)	3.4×10^{-1} (^{110m}Ag)	8.3×10^{-2} (^{108}Ag)
Cd (0.0015)*	9.6×10^{-2} (^{115}Cd)	5.2×10^{-1} (^{115}Cd)	1.2 (^{115}Cd)	9.6×10^{-2} (^{115}Cd)

*Impurity.

in a cyclic mode was discussed previously (Ref. 6-5). The approximation adopted here will, in general, produce accurate long term activities (half-life much greater than the blanket cycle time) if the parent nuclides do not experience very high burnup. The short-term activities (half-lives much less than the blanket material cycle time) will be underestimated because these materials would actually saturate within the chamber, i.e., before the blanket circulates out of the chamber. The activities of materials with half-lives comparable to the cycle time will be slightly higher than the activities calculated using the cycle and capacity-averaged neutron fluxes. Table 6-2 summarizes the estimated radioactivities at 1 min, 1 day and 1 month after shutdown for the case of 2 years operation, and at 1 min after shutdown for 30 years operation. The results after 30 years operation are conservative in that factors such as Be burnup (0.3% per year), and the time required for refabrication or reconstitution of failed granules are not included in the calculation.

From Table 6-2 we see that shortly (1 min) after shutdown the radioactivity in the BeO material is about 0.47 Ci/cm^3 and is mainly contributed by ^{56}Mn ($t_{1/2}$ = 2.58 h) from manganese (0.003 a/o), ^{28}Al ($t_{1/2}$ = 2.24 min) from aluminum (0.04 a/o), ^{64}Cu ($t_{1/2}$ = 12.7 h) from copper (0.002 a/o) and ^{16}N ($t_{1/2}$ = 7.1 s) from oxygen (50 a/o). Among these highest contributing elements, we see that only oxygen is one of the constituent elements of BeO, and its contribution to the total radioactivity is only 5.3% resulting from a very short-lived radionuclide ^{16}N. At times soon after shutdown, the activity in the BeO is thus dominated by that induced from impurity elements.

At 1 day after shutdown, the activity drops by a factor of 5 to about 0.084 Ci/cm^3 where the main contributors are ^{58}Co ($t_{1/2}$ = 70.9 d) from nickel (0.006 a/o), ^{64}Cu from copper, ^{37}Ar ($t_{1/2}$ = 35 d) from calcium (0.006 a/o), ^{51}Cr ($t_{1/2}$ = 27.7 d) from chromium (0.002 a/o), ^{24}Na ($t_{1/2}$ = 15 h) from aluminum, ^{60}Co ($t_{1/2}$ = 5.27 y) from cobalt (0.0001 a/o), and ^{54}Mn ($t_{1/2}$ = 313 d) from manganese, as shown in Table 6-2. Now all dominant radionuclides are resulting from the impurity elements. The main constituting elements, Be and O, give only a combined fraction of about 2.7×10^{-2}%

to the total activity at 1 d after shutdown and the activity is primarily due to long-lived radionuclides, ^{10}Be ($t_{1/2} = 1.6\times10^{6}$ y) and ^{14}C (5730 y). As also shown in Table 6-2, the activity at 4 weeks after shutdown decreases further from the activity at 1 d after shutdown but only by 40%, to about 0.05 Ci/cm^3. The main contributors are, again all from the impurity elements, ^{58}Co from nickel, ^{60}Co from cobalt, ^{54}Mn from manganese, ^{37}Ar from calcium, and ^{51}Cr from chromium. The combined contribution from the constituting elements, Be and O, is only about 0.044%, also due to ^{10}Be and ^{14}C resulting from beryllium and oxygen, respectively.

The activity of the carbon surface layer is dominated by that contributed from the impurity elements. An impurity level on the order of 0.0001 a/o iron is typical in the fabrication of pyrolitic carbon coatings. The shutdown radionuclides in the carbon surface layer are the same as those listed in Table 6-1 under Fe. The shutdown activity is a factor of 100 lower than the activity shown in Table 6-1. This is due to the lower iron impurity level and higher dilution factor of the carbon. The total activity level is 2000 Ci after 2 years operation and 6300 Ci after 30 years. The ^{14}C concentrations are 2.0×10^{-6} and 2.8×10^{-5} Ci/cm^3, contributing 50 Ci and 700 Ci, after 2 and 30 years, respectively. These activity levels do not include the activity that may be deposited on the surface layer from fuel pellet debris.

6.2.3. Radioactivity in $LiAlO_2$ Material

In the same manner, Table 6-3 presents the detailed breakdown of the radionuclides and their half lives which contribute to the shutdown radioactivity from the main and impurity elements in the $LiAlO_2$ compound. The impurity elements and their levels in $LiAlO_2$ material were again taken from the BCSS report. The results are again summarized for two operating times, 2 and 30 years. Table 6-4 further summarizes the resulting activities in $LiAlO_2$ material 1 min, 1 d, and 4 weeks after two years operation taking account of a $LiAlO_2$ dilution factor due to inventory out of the reaction chamber of 1.8. Again, the results after 30 years operation are conservative in that the 5% per year burnup of the ^{6}Li will require some reprocessing of the

blanket, and the calculations do not account for the time required for such operations.

As shown in Table 6-4, the activity in $LiAlO_2$ material shortly (1 min) after shutdown is about 4.7 Ci/cm^3. The main contributor at this time is ^{24}Na from aluminum, which is one of the constituting elements for $LiAlO_2$. The activity at 1 d after shutdown decreases by a factor of 6.4 to about 0.73 Ci/cm^3, and is mainly contributed by ^{24}Na (79%) and ^{89}Sr (19%). Note that ^{89}Sr ($t_{1/2}$ = 50.6 d) is produced from impurity element strontium whose level is about 0.055 atom percent. The activity from strontium-89 then dominates at 4 wk after shutdown together with other less abundant radionuclides, ^{60}Co from cobalt (0.0008 a/o) and ^{65}Zn ($t_{1/2}$ = 244 d) from zinc (0.013 a/o). The activity from the main constituting elements then comprises only about 2.7×10^{-3}% of the total, and is primarily given by long-lived radionuclides, ^{14}C ($t_{1/2}$ = 5730 y) and ^{26}Al ($t_{1/2} = 2.03\times10^4$ y), resulting from oxygen and aluminum, respectively.

6.2.4. Waste Disposal Ratings

One of the important considerations for the development of low activation fusion energy is the waste disposal rating (WDR). It is defined as the sum of the ratios of residual radioactive concentrations from radionuclides in the disposed waste material to the limiting concentrations for these radionuclides according to the U.S. Nuclear Regulatory Commission (NRC) regulations. When the disposal of long-lived radioactive waste is dealt with, it is important to consider shallow land burial waste disposal according to the NRC regulations, 10CFR61. (*Ref.* 6-6) Tables 6-5 and 6-6 summarize the 10CFR61 Class C waste disposal ratings of the BeO and $LiAlO_2$ materials in the ICF reactor after two operating times, 2 and 30 years. The limiting radioactive concentrations are mainly obtained from the 10CFR61 regulations, namely ^{14}C (80 Ci/m^3), ^{63}Ni (7000 Ci/m^3), ^{59}Ni (220 Ci/m^3), ^{94}Nb (0.2 Ci/m^3), ^{90}Sr (7000 Ci/m^3), and ^{99}Tc (3 Ci/m^3), assuming the radionuclides are contained within a metal matrix. For those long-lived radionuclides whose concentration limits for Class C waste disposal are not available, the recent estimates by Maninger (Refs. 6-7 and 6-8) were

TABLE 6-5
SUMMARY OF IMPORTANT LONG TERM ACTIVATION PRODUCTS (Ci/cm^3)
AND RELATED WASTE DISPOSAL RATINGS IN BeO MATERIAL
INCLUDING IMPURITY ELEMENTS AND EFFECTS OF
MATERIAL DILUTION FROM INVENTORY EXTERNAL TO REACTION CHAMBER

Element	a/o	Long Term Nuclide	Half-Life	Operating Time 2y	30 y
O	50	^{14}C	5730 y	2.0×10^{-5} (0.25)[a]	6.8×10^{-4} (8.5)
N*	0.026	^{14}C	5730 y	5.9×10^{-5} (0.74)	5.0×10^{-4} (6.2)
Al*	0.04	^{26}Al	7.2×10^{5} y	1.1×10^{-8} (0.11)	1.1×10^{-7} (1.1)
Ca*	0.006	^{39}Ar	269 y	3.2×10^{-6} (0.04)	8.5×10^{-5} (1.1)
		^{42}Ar	32.9 y	-	1.9×10^{-7} (0.24)
Mn*	0.003	^{60}Fe	1.49×10^{6} y	-	3.8×10^{-9} (0.38)
Fe*	0.0013	^{63}Ni	100 y	-	3.2x10-4 (0.05)
		^{60}Fe	1.49×10^{6} y	-	1.8×10^{-9} (0.18)
Ni*	0.006	^{63}Ni	100 y	2.2×10^{-4} (0.03)	5.0×10^{-3} (0.70)
		^{60}Fe	1.49×10^{6} y	5.1×10^{-12} (-)	7.9×10^{-9} (0.79)
Cu*	0.002	^{60}Fe	1.49×10^{6} y	-	3.2×10^{-10}(0.05)
Nb*	0.00026	^{94}Nb	2.03×10^{4} y	2.9×10^{-7} (1.45)	5.9×10^{-8} (0.30)
Co*	0.0001	^{60}Fe	1.49×10^{6} y	-	1.2×10^{-9} (0.12)
Total Waste Disposal Rating				2.6	19.7

[a]Waste disposal ratings are given in parentheses for shallow land burial (Class C) waste disposal.

*From impurities.

TABLE 6-6
SUMMARY OF IMPORTANT LONG TERM ACTIVATION PRODUCTS (Ci/cm^3)
AND RELATED WASTE DISPOSAL RATINGS IN $LiAlO_2$ MATERIAL
INCLUDING IMPURITY ELEMENTS

Element	a/o	Long Term Nuclide	Half-Life	Operating Time 2y	Operating Time 30 y
O	50	^{14}C	5730 y	2.3×10^{-6} (0.03)[a]	3.7×10^{-5} (0.46)
Al	25	^{26}Al	7.2×10^{5} y	5.7×10^{-7} (5.7)	8.3×10^{-6} (83.3)
K*	0.02	^{39}Ar	269 y	3.5×10^{-5} (0.44)	4.8×10^{-4} (6.0)
Ca*	0.01	^{39}Ar	269 y	5.4×10^{-7} (0.01)	9.4×10^{-5} (1.18)
Sr*	0.055	^{90}Sr	28.6 y	-	2.2×10^{-3} (0.31)
Ag*	0.00015	^{108m}Ag	127 y	2.4×10^{-6} (0.80)	8.9×10^{-6} (2.97)
Total Waste Disposal Rating:				7.0	94.2

[a]Waste disposal ratings are given in parentheses for shallow land burial (Class C) waste disposal.

*From impurities.

used. These radionuclides and their limiting concentrations are: ^{26}Al (0.1 Ci/m^3), ^{92}Nb (0.3 Ci/m^3), ^{108m}Ag (3 Ci/m^3), ^{42}Ar (0.8 Ci/m^3), and ^{60}Fe (0.01 Ci/m^3). For the radionuclide whose Class C waste disposal limiting concentration is not available in the regulations or in the literature, the available lowest limit for the radionuclide with similar radioactive characteristics should be employed. Under the above criteria, the concentration limit, 80 Ci/m^3, for ^{14}C ($t_{1/2}$ = 5730 y) is then used for ^{39}Ar ($t_{1/2}$ = 269 y) although there is another β-emitting only radionuclide, ^{63}Ni ($t_{1/2}$ = 100 y), which has a higher concentration limit, 7000 Ci/m^3.

Table 6-5 gives the radioactive concentrations and corresponding Class C waste disposal ratings for each long-lived radionuclide in the BeO material after 2 and 30 years operation. As shown in this table, the total waste disposal ratings are about 3 and 20, respectively, after 2 and 30 years operations. The dominating radionuclides at 2 years operating time are primarily ^{94}Nb and ^{14}C, resulting from the impurity elements, Nb (0.00026 a/o) and nitrogen (0.026 a/o), respectively. The waste disposal rating from all other elements, including the main constituting elements Be and O, is less than 0.5. Thus if the niobium and nitrogen levels in the BeO material can be lowered by one order of magnitude, namely 0.003 a/o for nitrogen and 0.00003 a/o for niobium, then the Beo irradiated for 2 years should be qualify for Class C waste disposal. However, if the operating time is 30 years, the dominating radionuclides for waste disposal consideration are ^{14}C from oxygen (WDR=8.5) and nitrogen (WDR=6.2), ^{26}Al from aluminum (WDR=1.1), and ^{39}Ar ($t_{1/2}$=269 y) from calcium (WDR=1.1). Among these, the waste disposal rating from the main constituting element, oxygen, is no less than 8.5. This implies that for the BeO material to qualify as Class C waste with operating times greater than 2 years, the waste must be diluted before disposal regardless of the purity level achieved. The surface layer waste disposal rating is dominated by the ^{14}C concentration. The carbon's WDR is 0.35 after 30 years operation and thus does not require dilution for shallow land burial.

For the $LiAlO_2$ material, impurity elements do not play a significant role. Table 6-6 presents the Class C waste disposal ratings for the elements contained in this

material, again, after two operating times, 2 and 30 years. The total waste disposal ratings are 7 and 94, respectively, as given in Table 6-6. The dominating radioactivity comes primarily from ^{26}Al ($T_{1/2} = 2.03\times10^{4}$ y) resulting from n,2n reactions with the main element aluminum. To satisfy the Class C waste disposal requirement, it is necessary to either limit the operating time of the $LiAlO_2$ material to less than 2 months or dilute the waste material before disposal.

6.3. SHIELDING ANALYSIS

6.3.1. Introduction

The shield system for Cascade consists of the radiation shield, biological shield, and cooling system. A schematic representation of the shield configuration is shown in Fig. 6-2. The radiation shield provides attenuation of the neutron and gamma fluxes during operation to levels consistent with materials considerations, such as damage and activation levels. One of the important considerations for the radiation shield design of an ICF reactor is to estimate the required shield thickness such that direct access behind the shield is allowable shortly after shutdown. In the Cascade concept, this consideration is vital in allowing hands-on access to the heat exchanger and vacuum chamber located external to the shield. The design of the radiation shield is described in Section 6.3.2. The biological shield provides the final attenuation of the neutron and gamma fluxes to levels dictated by worker occupational exposure limits. The design of the biological shield is presented in Section 6.3.3.

6.3.2. Radiation Shield

Two materials were considered for the radiation shield of the Cascade reactor: boronated graphite and borated water. The structure is aluminum, 10% by volume, and the coolant for the solid shield is water, also 10% by volume. Three design arrangements were studied here:

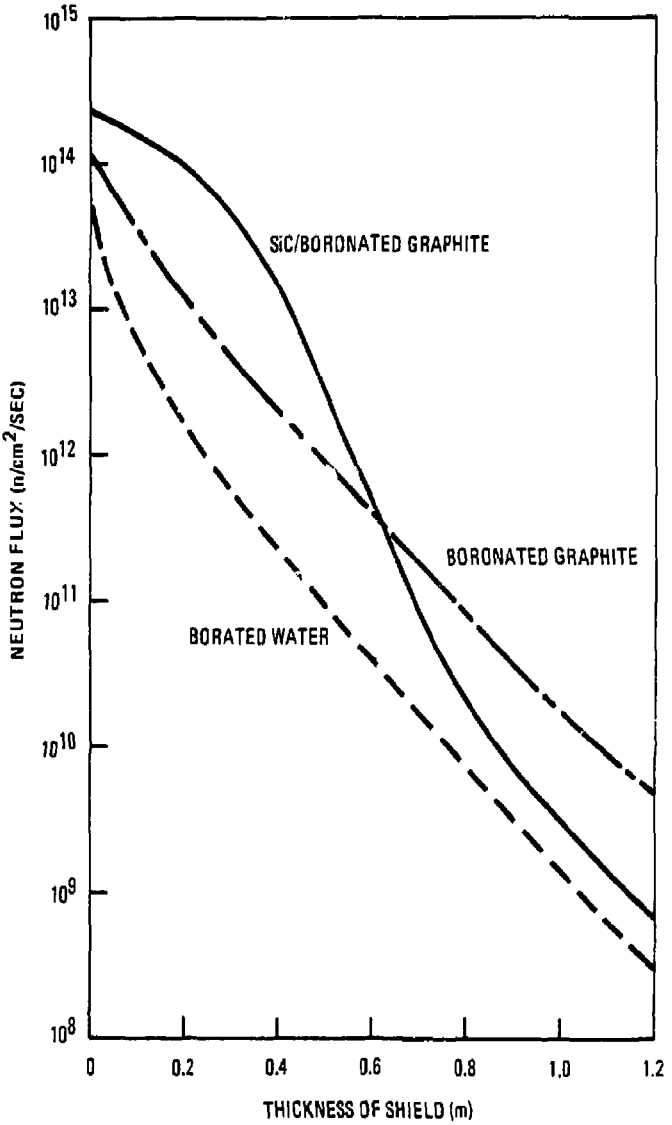

Fig. 6-2. Schematic of the Cascade shield system.

Case A. Borated water shield behind the blanket.

Case B. Boronated graphite shield behind the blanket.

Case C. Boronated graphite shield behind a 0.5 m SiC reflector which is placed behind the blanket.

The Case C design is introduced primarily due to the concern that the tritium breeding ratio in the reactor will be reduced due to the immediate presence of neutron absorbing materials behind the blanket. This reduction of tritium breeding ratio in Case A and Case B designs is about 5%. With these shields, the tritium breeding ratio would be marginal for the reference blanket design. An adequate tritium breeding ratio can be restored by increasing the thickness of the blanket BeO zone by 2 to 3 cm, enriching the lithium in ^{6}Li, or modifying the shields to provide neutron reflection by removing the boron from the front 30 to 50 cm of the Case A and Case B designs.

Neutronics calculations were performed for these shield arrangements. Figure 6-3 displays the neutron flux distribution in the shield. From this figure, it appears that borated water has the best flux attenuation capability, followed by the SiC/boronated graphite arrangement. The boronated graphite shield alone shows the poorest attenuation capability among all shield designs compared here.

Shutdown dose rates were estimated behind a 1.0 meter shield based on Case C, SiC/boronated graphite design, for metallic alloys which may be needed for the vacuum chamber and the heat exchanger. This was initially the reference shield based on perceived difficulties with tritium permeation into the borated water shield. The borated water shield, Case A, was adopted as the reference shield after the tritium analysis of Chapter 5 indicated tritium permeation would not be a problem. The neutron flux at the location immediately behind the 1 m shield is about $3.7\times10^{9}n/cm^{2}/sec$. Table 6-7 summarizes the shutdown dose rates resulting from iron, nickel and chromium materials assumed to be in place behind the shield. As seen in Table 6-7, the shutdown dose rate from iron is about 2.2 rem/h. Of this, about 71% is due to ^{56}Mn whose half-life is 2.58 hours. Hence, at one day after shutdown, it drops to about 0.62 rem/h and is primarily due to ^{54}Mn whose half-life is 313 days.

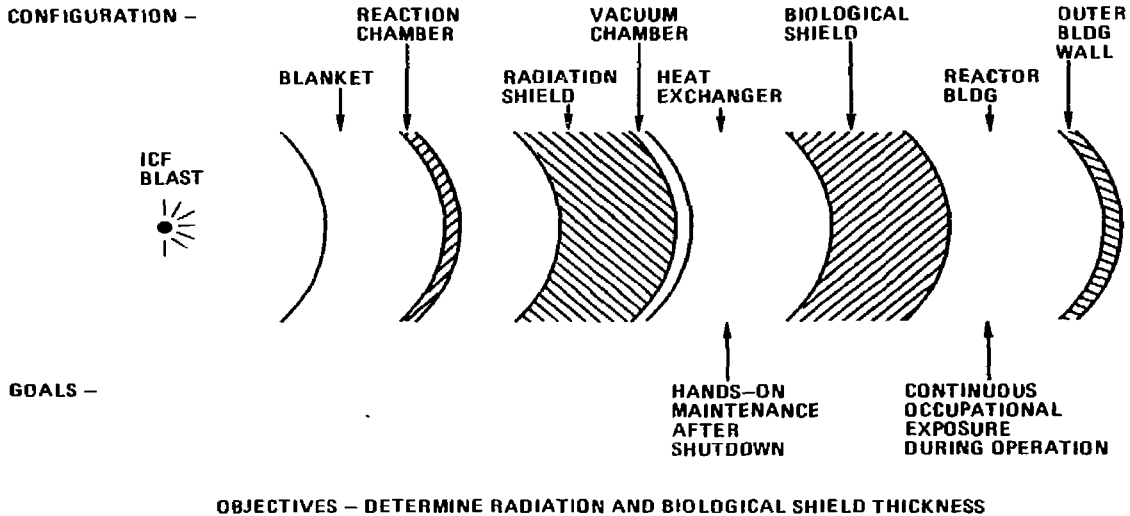

Fig. 6-3. Neutron flux distribution in three radiation shields: Case A – Borated water; Case B – Boronated graphite; Case C – SiC/Boronated graphite.

TABLE 6-7
SHUTDOWN DOSE RATES FROM Fe, Ni and Cr
BEHIND A 0.5 m SiC + 0.5 BORONATED GRAPHITE SHIELD
(After 30 Years Operation)

Radionuclide	Half-Life	Contributing Dose Rate (Rem/Hour)	Radioactive Concentration at First cm (Ci/cm^3)
Element: Fe (0.08×10^{24} atoms/cm^3)			
^{56}Mn	2.58 h	1.54	1.07×10^{-5}
^{54}Mn	313 d	0.57	1.53×10^{-5}
^{59}Fe	44.5 d	0.05	6.12×10^{-7}
Sum		2.16	2.66×10^{-5}
Element: Ni (0.08×10^{24} atoms/cm^3)			
^{58}Co	70.9 d	20.3	1.46×10^{-4}
^{57}Co	271 d	0.07	2.78×10^{-5}
^{60}Co	5.27 y	3.23	9.43×10^{-6}
Sum		23.6	1.83×10^{-4}
Element: Cr (0.08×10^{24} atoms/cm^3)			
^{51}Cr	27.7 d	0.047	1.72×10^{-5}
^{48}V	15.9 d	0.006	1.59×10^{-8}
Sum		0.053	1.72×10^{-5}

The shutdown dose rate from nickel, as also shown in Table 6-7, is about 24 rem/h which is a factor of 10 higher than that from iron. The dose rate at one day after shutdown is about the same level as at shutdown because the dominating radionuclides ^{58}Co and ^{60}Co are of medium half-lives, 70.9 days and 5.27 years, respectively. The dose rate from chromium is the lowest among these three elements. It is about 0.053 rem/h at shutdown and remains at this level for a few months after shutdown since ^{51}Cr (half-life = 27.7 d) is mainly responsible for the gamma-ray activity, as also shown in Table 6-7.

Assuming the dose rate is linearly proportional to the neutron flux level, we estimated the allowable maximum neutron flux level in the metallic materials behind the shield for direct access at one day after shutdown during the entire 30 years operational lifetime. As presented in Section 4.4, continuous direct access is possible for a dose rate of 2.5 mrem/h, assuming a 40 h work week. The allowable neutron flux levels were estimated to be about 4×10^5 and 1.4×10^7 n/cm^2/sec, respectively, for nickel and iron-based alloys. The chromium activity in both iron- and nickel-based alloys is not significant compared to the iron and nickel activites as shown in Table 6-7. Note that the attenuation effectiveness of these shields at thicknesses greater than ~0.9 m are very similar, as shown in Fig. 6-3. We extrapolated the results of Fig. 6-3 to the required limiting flux levels using the neutron attenuation coefficient of 0.078 cm^{-1} for all shield materials as shown in Fig. 6-3, and we estimated the required shield thicknesses for these two alloys. Table 6-8 summarizes the results of this calculation. As shown in the table, the required shield thicknesses are 1.58, 1.91 and 1.70 meters, respectively, for the iron-based alloy behind borated water, boronated graphite, and SiC/boronated graphite shield materials. An additional 0.46 m shield will be required for all these shield materials if a nickel-based alloy is employed behind the shield, as seen in Table 6-8. The 2.0 m borated water shield was thus adopted for the reference design to provide flexibility in materials selection for components in this location. Note that two coolant loops will be required to provide

TABLE 6-8
REQUIRED SHIELD THICKNESSES (METERS) FOR
DIRECT ACCESS AT ONE DAY AFTER SHUTDOWN

Shield Design[a]	Fe-based Alloy (1.5×10^{7})[b]	Ni-based Alloy (4.0×10^{5})[b]
Borated Water	1.58	2.04
Boronated Graphite	1.91	2.37
SiC/Boronated Graphite	1.70	2.16

[a]A flux attenuation coefficient of 0.078 cm^{-1} is employed for all shield designs beyond 1.2 m.

[b]Corresponding maximum allowable neutron flux in units of $n/cm^2/sec$.

unborated water to the portion of the shield closest to the reaction chamber and borated water to the rear of the shield to ensure a tritium breeding ratio greater than 1.0.

At the location behind the blanket and in front of the shield the shutdown biological dose rate is primarily due to ^{24}Na ($t_{1/2} = 15h$) resulting from aluminum in the Al/SiC composite tendon material, support girders, or structure in the shield. This is estimated to be about 1×10^6 rem/h which will decay to 2.5 mrem/h within 18 days. However, the dose rate due to ^{26}Al ($t_{1/2} = 7.2 \times 10^5 y$) becomes significant after the ^{24}Na activity decays away. It is about 0.8 rem/h. after 2 years of operation and increases to about 2.4 rem/h at the end of reactor lifetime, 30 years of continuous operation. The biological dose rate due to iron impurity element which may be present in aluminum or SiC was also estimated. It is about 0.26 rem/h at one day after two years of operation assuming a 1 appm impurity level in the main materials. At the end of the reactor lifetime it will be about 0.4 rem/h. The main contributors to the dose rate are ^{54}Mn ($t_{1/2} = 313\ d$) and ^{59}Fe ($t_{1/2} = 44.5\ d$) at 2 years after shutdown. After 30 years of operation, ^{60}Co ($t_{1/2} = 5.27\ y$) also contributes significantly to the decay dose rate, up to about 35%. The total shutdown maintenance dose rate directly outside the reaction chamber thus rises quickly to 1 rem/h after 2 years of operation, and continues to increase to 3 rem/h after the full lifetime of 30 full power years. Limited access with local shielding may be possible to the reaction chamber and other components within the radiation shield. Access time would be severely limited (<1 h per person per calendar quarter) unless fairly thick local shielding were used. Thus contact maintenance should not be part of the planned maintenance activities except for a brief shakedown period during initial operation.

6.3.3. Biological Shield

In the design of the biological shield, the operating neutron flux level outside the biological shield should be attenuated to below about 0.1 n/cm^2/sec in order to limit the dose rate below 1 mrem/hour. As shown in Ref. 6-9, the attenuation coefficient of

concrete on the operating biological dose is estimated to be about 0.0617 cm^{-1}. Using this attenuation coefficient and the allowable neutron flux levels for shutdown dose rate consideration mentioned previously in Section 6.3.2 (4×10^5 and 1.4×10^7 $n/cm^2/s$ for nickel and iron-based alloys), we estimated the required additional concrete thicknesses for biological shielding. These concrete biological shields are estimated to be about 2.5 and 3.1 meters for the designs employing nickel and iron-based alloy components outside the radiation shield but inside the biological shield. In conjuction with the 2.0 m borated water shield, a 2.5 m concrete biological shield thickness was thus adopted for the baseline design. Table 6-9 summarizes all the required shield thicknesses.

6.4. CONCLUSIONS

The Cascade reactor design incorporates low activation materials in all the regions of high neutron fluence. The result is relatively low activation (700 MCi one minute after shutdown after 30 full power continuous years of operation versus 3000 MCi for a MARS tandem mirror reactor of comparable power, Ref. 6-10, after 2 years operation), and greatly reduced safety, waste management and maintenance dose rate concerns caused by radioactivity. The waste disposal characteristics of Cascade are dominated by the inherent constituents of the reactor materials (oxygen and aluminum). Shallow land disposal as low level waste under 10CFR61 is possible, but will require dilution of the reactor materials with inert materials by a factor of 10 to 100, depending on the exposure lifetime.

A 2.0 m thick radiation shield of borated water is used outside the reaction chamber to reduce the operating neutron fluence to low enough levels to allow conventional iron and nickel alloys to be used in the heat exchanger region and outside the vacuum boundary. Contact maintenance of these components is possible 1 day after reactor shutdown. Only very limited access will be possible inside the radiation shield, and at least 3 weeks of cooldown time would be needed prior to this very limited access.

TABLE 6-9
SUMMARY OF REQUIRED SHIELD THICKNESSES (METERS) FOR THE ICF CASCADE REACTOR

Shield Design	Structural Material Behind the Radiation Shield: Fe-Based Alloy Radiation[a]	Fe-Based Alloy Biological[b] (Concrete)	Fe-Based Alloy Total	Nickel-Based Alloy Radiation[a]	Nickel-Based Alloy Biological[b] (Concrete)	Nickel-Based Alloy Total
Borated Water	1.58	3.09	4.67	2.04	2.46	4.50
Boronated Graphite	1.91	3.09	5.00	2.37	2.46	4.83
SiC/Boronated Graphite	1.70	3.09	4.79	2.16	2.46	4.62

[a] 2.5 m Rem/h one day after shutdown during 30-year plant life.

[b] 1.0 mRem/h during reactor operation.

A 2.5 m thick concrete biological shield is employed exterior to the radiation shield, heat exchangers and vacuum vessel. The dose rate exterior to this biological shield is less than 1 mrem/h during reactor operation, permitting unrestricted occupational access.

References for Chapter 6.

6-1. F. M. Mann, "Transmutation of Alloys in MFE Facilities as Calculated by REAC (A Computer Code System for Activation and Transmutation)," HEDL-TME 81-37, Hanford Engineering Development Laboratory report, Aug. 1982.

6-2. F. M. Mann, *et al.*, "HEDL Reduced Activation Analysis: Status Report," Trans. Am. Nucl. Soc., 49, 66 (1985).

6-3. M. A. Gardner and R. J. Howerton, "ACTL: Evaluated Neutron Activation Cross Section Library—Evaluation Techniques and Reaction Index," WCRL-50400, Vol. 18, Lawrence Livermore National Laboratory report, October 1978. Updated versions available.

6-4. D. L. Smith, *et al.*, "Blanket Comparison and Selection Study, Final Report," ANL/FPP-84-1, Argonne National Laboratory report, September 1984.

6-5. U. S. Nuclear Regulatory Commission, "Licensing Requirements for Land Disposal of Radioactive Waste," Code of Federal Regulations, 10CFR61, Dec. 1982.

6-6. G. R. Hopkins and E. T. Cheng, "Decay Heat Properties of Fusion-Fission Hybrid Mobile Blankets," Proceedings of the 8^{th} Symposium on Engineering Problems of Fusion Research, IEEE Publication Number 79CH1441-5 NPS, 1979, p. 623.

6-7. R. C. Maninger, D. W. Dorn, "Radiation Safety Criteria for Maintenance and Waste Management in the Mirror Advanced Reactor Study," Fusion Technology, 6, 616 (1984).

6-8. R. C. Maninger, "Impact of Long-Lived Radionuclides on Waste Classification for Fusion," Trans. Am. Nucl. Soc., 49, 65 (1985).

6-9. R. Conn, *et al.*, "SOLASE, A Conceptual Laser Fusion Reactor Design," UWFDM-220, University of Wisconsin report, Dec. 1977, Vol. II, Section XIII-D.

6-10. B. G. Logan *et al.*., "Mirror Advanced Reactor Study, Final Report," Lawrence Livermore National Laboratory Report UCRL-53480, July 1984.